2018

Analyzing a Shopper's Visual Experience in a Retail Store and the Impact on Impulse Profit

Bradley Robert Guthrie
Wright State University

Analyzing a Shopper's Visual Experience in a Retail Store and the Impact on Impulse Profit

A dissertation submitted in partial fulfillment of the
Requirements for the degree of
Doctor of Philosophy

By

BRADLEY ROBERT GUTHRIE
B.S.I.S.E., Wright State University, 2013
M.S.E.G., Wright State University, 2015

2018
Wright State University

WRIGHT STATE UNIVERSITY

GRADUATE SCHOOL

August 30, 2018

I HEREBY RECOMMEND THAT THE DISSERTATION PREPARED UNDER MY SUPERVISION BY Bradley Robert Guthrie ENTITLED Analyzing a Shopper's Visual Experience in a Retail Store and the Impact on Impulse Profit BE ACCEPTED IN PARTIAL FULFILLMENT OF THE REQUIREMENTS FOR THE DEGREE OF Doctor of Philosophy.

_____

Pratik Parikh, Ph.D.
Dissertation Director

_____

Brian Rigling, Ph.D
Interim Director of Ph.D. in Engineering Program

_____

Barry Milligan, Ph.D.
Interim Dean of the Graduate School

Committee on Final Examination

_____
Pratik Parikh, Ph.D.

_____
Xinhui Zhang, Ph.D.

_____
James Munch, Ph.D.

_____
Frank Ciarallo, Ph.D.

_____
Nan Kong, Ph.D.

ABSTRACT

Guthrie, Bradley Robert Ph.D., Engineering Ph.D. program, Wright State University, 2018. Analyzing a Shopper's Visual Experience in a Retail Store and the Impact on Impulse Profit

The retail industry in the U.S. contributed 1.14 trillion in value added (or 5.9%) to the GDP in 2017, an increase of 3.7% from the previous year. While store closures have dominated the news in the recent past (e.g., Toys-R-Us, Sears, and Bon-Ton) due to ineffective supply chain practices, inadequate in-store experiences, and competition from e-tailers, other retailers such as Ross, T. J. Maxx, Burlington Coat Factory, and Kroger have been expanding their footprint. Brick-and-mortar stores are unique as they allow shoppers the ability to see, touch, and try products, in addition to exploring new products. Kohl's CEO has even indicated that 90% of their revenue is still generated in brick-and-mortar stores. Besides reducing supply chain costs, retailers have been paying considerable attention to redesigning their stores by varying layouts and displays to improve shopping experience and remain profitable. However, a lack of scientific methods that correlate layout changes to improved experience has often led to time-consuming and expensive trial-and-error approaches for the retailers.

This research focuses on the design of such brick-and-mortar stores by developing a quantitative approach that models the visual interaction between a 3D shopper's field of view and the rack layout. This visual interaction has been shown to influence shopper purchasing habits and their overall experience. While some metrics for visual experience have been proposed in the literature, they have been limited in many ways. The objective of this research is to develop new models to quantify visual experience and employ them in layout design models.

Our *first* contribution consists of quantifying exposure (which rack locations are seen) and the intensity of exposure (how long they are seen) by accounting for the dynamic interaction between the human 3D field of regard with a 3D rack layout. We consider several rack designs/layouts that we noticed at nearby retail stores, ranging from the typical rectangular racks placed orthogonal to the main aisle to racks with varying orientations,

curvatures, and heights. We model this 3D layout problem as a series of 2D problems while accounting for obstructions faced by shoppers during their travel path (both uni- and bi-directional). We also validate our approach through a human subjects study in a Virtual Environment. Our findings suggest that curving racks in a layout with racks oriented at 90° could increase exposure by 3-121% over straight racks. Further, several layout designs could increase exposure by over 500% with only a 20% increase in floor space.

In our *second* contribution, we introduce the Rack Orientation and Curvature Problem (ROCP) for a retail store, which determines the best rack orientation and curvature that maximizes marginal impulse profit (after discounting for floor space cost). We derive impulse profit considering the probability a shopper will see a product category, the probability the shopper will purchase a product from that category if seen, and the product category's unit profit. We estimate the probability that a shopper will see a location through a novel approach that considers (i) the effective area of that location, (ii) probability distribution of a shopper's head position based on real shopper head movements, and (iii) exposure estimates from our approach in Contribution 1. To solve the ROCP, we design a particle swarm optimization approach and conduct a comprehensive experimental study using realistic data. Our findings suggest that layouts with either high-acute and straight-to-medium-curved racks or high-obtuse and high-curved racks tend to maximize marginal impulse profit. Profit increases ranging from 70-233% over common rack layouts (orthogonal and straight racks) can be realized depending on the location policy of product categories. The sensitivity of these solutions to shopper volume, cost of floor space, travel direction, and maximum aspect ratio is also evaluated.

The implications of our proposed models and findings are wide-ranging to retailers. *First*, they provide retailers with insights on how design parameters affect both exposure and marginal impulse profit; this can help avoid expensive experiments with layout changes. *Second*, they reveal hot-warm-cold spots for specific layout designs, allowing for effective product location assignments. *Finally*, these insights can help enhance shopper interactions with products (i.e., ability to see more products, find products faster), which can improve their shopping experience and drive up sales.

TABLE OF CONTENTS

1 Introduction 1

1.1 Retail Design 2

1.2 Measures to Evaluate Retail Layouts 4

1.3 Exposure 4

1.4 Motivation of our Research 5

1.5 Research Questions 7

1.6 Research Contributions 8

1.7 Research Implications 11

1.8 Dissertation Outline 12

2 Evaluating Exposure of a Retail Rack Layout in 3D 13

2.1. Introduction 13

2.2 Literature Review 16

2.3 Modeling Exposure in a 3D Rack Layout 18

2.3.1 Modeling the Human FoR in 3D 19

2.3.2 Modeling a Curved Rack in 3D 21

2.3.3 Modeling a Layout of Racks 22

2.3.4 A Quantitative Model for Exposure and Intensity 23

2.4 Experimental Study 27

2.4.1 Dynamics of Obstruction and Exposure 27

2.4.2 Determining Best Orientation (θ) and Curvature (α) 30

2.4.3 Rack Height Sensitivity 34

2.4.4 Relative Influence of θ, α, and H on Exposure 35

2.5 Implications on Floor Space 36

2.6 Validation Study 40

2.7 Conclusions 44

3 Optimizing Rack Orientation and Curvature to Maximize Marginal Impulse Profit 46

3.1 Introduction 46
3.2 Literature Review 50
3.3 Modeling Marginal Impulse Profit 53
3.3.1 Layout Design 53
3.3.2 A Mathematical Model for Marginal Impulse Profit 55
3.3.3 Estimating the Probability, v_p 57
3.4 A Particle Swarm Optimization Algorithm for the ROCP 63
3.4.1 PSO Description 63
3.4.2 Solution Representation 64
3.4.3 Solution Updating 65
3.5 Experimental Study 66
3.5.1 Data 66
3.5.2 Product Category Location Policies 67
3.5.3 PSO Evaluation 69
3.5.6 Sensitivity to Space Cost and Shopper Volume 80
3.6 Conclusions 83
4 Conclusions and Future Research 85
4.1 Summary of Contribution 1 85
4.2 Summary of Contribution 2 86
4.3 Future Research 88
References 90
Appendices 97
Appendix A. Determining the Distance l_r 97
Appendix B. Estimating 3D Exposure of Top Faces. 102
Appendix C: Estimating Exposure in 2D 105
Appendix C.1: Approximation Algorithm for Vertical Tangent Curves 110
Appendix C.2: Approximation Algorithm for Dead Zone Curve 114

Appendix C.3: Additional Considerations for Estimating 3D Exposure 118
Appendix C.4. An Example of Illustrating our Proposed Approach 119
Appendix D. Models for Space and Aspect Ratio 129
Appendix E. Validation Study Conference Paper 133
Appendix F. Product Category Assortment Data 148

List of Figures

Figure 1: Different types of store layouts 3
Figure 2. Racks oriented at 45°. 6
Figure 3. Curved racks. 6
Figure 4. Low rack heights. 6
Figure 5. Curved endcaps. 6
Figure 6. Modeling 3D FoR 20
Figure 7. Modeling 3D curved racks 21
Figure 8. Example rack orientations 22
Figure 9. Designing a layout of racks 22
Figure 10. Decomposing by height 23
Figure 11. 3D Exposure Algorithm 23
Figure 12. Exposure/intensity at step y 25
Figure 13. Riemann Sum Approximations for side (a) and top (b) faces 26
Figure 14. Rack layouts with overlaid intensity 27
Figure 15. Analyzing the obstruction phenomenon with varying θ and α 29
Figure 16. Heat maps of exposure for combinations of θ and α for H =7. 32
Figure 17. Sensitivity of exposure to rack height; 35
Figure 18. Impact of layout parameters (a) uni-directional traffic and (b) bi-directional traffic 36
Figure 19. Exposure vs. layout area with small head rotations; 38
Figure 20. Virtual Environment 40
Figure 21. Sensitivity and Specificity of model performance. 42
Figure 22. Rack layouts with (a) curved racks (b) curved endcaps (c) non-orthogonally oriented racks. 47
Figure 23. Layout design for ROCP 54
Figure 24. (a) v_l for locations; (b) v_p for products 59
Figure 25. Determining angles for vertices of location l 60
Figure 26. Probability distribution of shopper focal point direction; 61
Figure 27. Overlaying shopper head position distribution with location l 63
Figure 28. Probability v_l of layout with θ=90°, α=90°;. Red areas indicate locations with higher values of v_l. 63
Figure 29. Illustration of location policies. 69
Figure 30. Top performing layouts from PSO. Darker squares indicate higher values of v_l. 72

Figure 31. Sensitivity of the solutions to the Ar_{MAX} constraint. 79
Figure 32. Sensitivity of floor space cost and shopper volume (uni-directional traffic). 81
Figure 33. Sensitivity of floor space cost and shopper volume (bi-directional traffic). 81
Figure A1. Determining combination that produces minimum distance between racks (a) 7 possible combinations (b) feasible combination for this example 98
Figure A2. Layout with additional feasibility checks to determine l_r 100
Figure A3. Illustration of parameters to determine l_r for combination (D_n, A_{n+1}) 100
Figure B1. Approximated exposed area on face F 103
Figure B2. Reimann Sum approximation of exposure of face F 103
Figure B3. Calculations steps to determine exposure of face F 104
Figure B4. Procedure for approximating the exposure of face F 104
Figure C1. Estimating Exposure in 2D 105
Figure C2. Classifications of obstruction where black shaded areas are obstructed 107
Figure C3. Illustration of example candidate points 107
Figure C4. Pairing of feasible points 109
Figure C5. Vertical tangent curves. (a) Self, (b) Preceding, and (c) Succeeding. 110
Figure C6. Illustration of vertical tangent lines 112
Figure C7. Analytical expressions to determine vertical tangent lines 113
Figure C8. Illustration of dead zone curve (a) top view (b) front view (c) side view 114
Figure C9. Changing *DOV* with changes in height 118
Figure C10. Changing angular limits with changes in height 118
Figure C11. 3D view of select candidate points at shopper step *y* 119
Figure C12. Finding candidate points 1 and 2 at height $h = S_{E.}$ 121
Figure C13. Finding candidate point 3 at height $h = S_{E.}$ 123
Figure C14. Finding obstruction points to candidate point 3. 124
Figure C15. Finding candidate point 6 at height $h = 0$. 126
Figure C16. Determining if candidate point 6 is in dead zone 128
Figure D1. Exact procedure to estimate L and W of the layout 129
Figure D2. Dimensions of L and W for example layouts with $N = 3$ 130
Figure D3. Change in floor space (ft^2) for various rack orientations and curvatures 131
Figure D4. Change in Aspect Ratio with varying values of θ and α 132

List of Tables

Table 1. Values for moderate eye and head movements 20
Table 2. Input parameters for experiments. 28
Table 3. Sensitivity experiments for exposure. 31
Table 4. Parameters used in model 56
Table 5. Decision variables in the model 56
Table 6. Location policies. 67
Table 7. Example product category assignments. 69
Table 8. Baseline (realistic) parameters of a store section 69
Table 9. Best solutions from PSO and Grid Search. 70
Table 10. Comparing the distribution of v_l of top performing layouts against {90°,0°}. 74
Table A1. Expressions to calculate l_r 101
Table C1. Candidate points to determine exposure. 105
Table C2. Feasibility checks for candidate points. 106
Table C3. Explanation of example feasible candidate points 108
Table C4. Explanation of example non-feasible candidate points 108
Table C5. Design values for rack layout. 120
Table C6. Eye and head movement parameters. 120
Table F1. Data from U.S grocery store 148

ACKNOWLEDGEMENTS

- I first would like to thank my wife, Ellen, for all of her love and support during this process. I cannot thank you enough for everything you have done.
- To my parents, Bob and Nancy, I thank for being wonderful parents, being excellent role models, and all your support through my education journey.
- To my brothers, Alex and Ethan, thanks guys for all the love.
- To my wife Ellen's family, thank you for all the love and support, and welcoming me into your family.
- To all my friends, thanks a whole heap.
- To my cats, Anna and Elsa, thank your comfort and support as I worked from home.
- To Dr. Corinne Mowrey, thank you for all your assistance, expertise, and previous research in the retail layout domain.
- To current and former members of DAOL, thank you for joining me on this ride.
- To my committee members, thank you for your time spent with me through this process. Your ideas, comments, and suggestions all proved to be valuable.
- To the faculty and staff of the BIE department at Wright State, I humbly thank you for all of your guidance and assistance toward my degree.
- Finally, I want to thank my life-long advisor, Dr. Pratik Parikh, who has been overseeing my work. for the past 6 years. I have learned so much from you as a researcher, manager, and person. Thank you for everything.

This research was partially supported by the National Science Foundation grant CMMI #1548394.

1 Introduction

The retail industry in the U.S. contributed 1.14 trillion in value added (or 5.9%) to the GDP in 2017, an increase of 3.7% from the previous year (Bureau of Economic Analysis, 2018). Typically, retail shoppers make purchases by either visiting 'brick-and-mortar' stores or through online shopping environments (i.e., e-commerce). Some retailers even offer the option for customers to order online, then come to the store to pick up their purchases. There are varying reasons for customers favoring online shopping. According to a recent study, top reasons include the ability to shop 24/7, opportunity to compare prices, and overall lower prices (Leadem, 2017). Although these factors have contributed to the recent growth of e-commerce (14% increase in revenue from 2016 to 2017), *92% of retail sales still occur in brick and mortar stores* (US Census Bureau, 2016). In fact, in 2017, *in-store revenue from retail purchases increased by 5%* (from 2016), and *more stores opened than closed* (IHL Group). Even Amazon, a world leader in online retail sales, recently purchased 460 stores from Whole Foods in 2017, and has opened 13 bookstores since 2015 (Bloomberg News, 2018).

This begs the question, why do shoppers continue to visit stores when they can achieve the same goal at their fingertips from home? Three of the most popular reasons include (i) the ability to see and/or touch products, (ii) trying items (apparel) on, and (iii) enjoying the experience of going to the shops (Leadem, 2017). Further, physical stores support *impulse* buying, where customers not intending to purchase an item may be reminded by seeing that item or be enticed to purchase it for self-gratification (Piron, 1991). Essentially, brick-

and-mortar stores give shoppers the opportunity to interact with the retailer's products, which can therefore make or break a retailer (Underhill, 1999). It is thus the retailer's job to best present their products to customers. This is the basis of retail design, and the topic of this research.

1.1 Retail Design

There are many facets of retail design. These include visual communications (e.g., signage, commercials), merchandising (e.g., fixture selection and product presentation), store design (e.g., ambiance, lighting), and store planning (e.g., layout, space allocation), all of which contribute to the overall shopping experience by customers, and therefore the success of the retailer (Dunne et. al., 1995). Clear, visible, navigational cues facilitate customer flow through the store and, therefore, spending habits (Burke, 2006; Wang and Hsiao, 2012). Practical organization of products and transparent communication of their features bears less stress on customers allowing for a smooth shopping experience (Burke, 2006). Longer travel paths by shoppers are associated with larger basket sizes (Hui et. al. 2009). Further, designing a shopping environment that adheres to the comfort of shoppers, by means of sight, smell, feel, etc., allows shoppers to become more accessible to the store, easing their purchasing behavior (Gladwell, 1996; Spies et. al. 1997).

Store planning, more specifically, refers to the decisions concerning the physical store area. In particular, the *layout of a store* is considered the backbone, as it serves as the organizational structure to how products are presented to customers. *Layout decisions* typically consist of department allocation/location decisions (e.g., allocation of facility space to different departments) and layout type/circulation decisions (e.g., aisle configuration to dictate a certain traffic pattern) (Dunne et. al., 1995). Four general layout

types are typically used in the retail stores: grid, free flow, serpentine, and racetrack (Peters et al., 2004; Kizer and Bender, 2007). The *grid layout* is usually found in grocery stores, where fixtures (usually rectangular gondolas) are placed in long rows parallel to each other, allowing shoppers to walk through each aisle (Dunne et al., 1995) (Figure 5a). *Racetrack layouts* are popular with mass merchandisers (e.g., Kohl's, Target) where a main aisle loops around the store, leading shoppers quickly to their desired departments (Figure 5b). The less-organized *free-flow layout* often appears in specialty stores, where fixtures, usually in the form of clothing stands or glass display cases, are placed sporadically around the store. (Figure 5c). The *serpentine layout* is constructed to only allow shoppers to walk along a single path throughout the store, usually in a single direction (e.g., IKEA) (Peters et al., 2004) (Figure 5d).

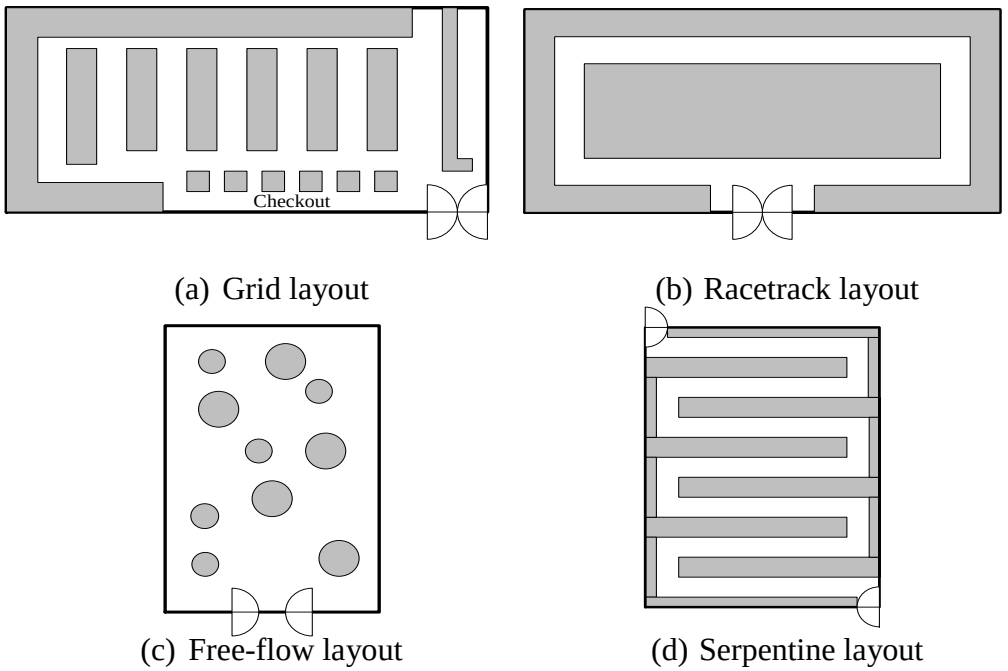

Figure 1: Different types of store layouts

1.2 Measures to Evaluate Retail Layouts

There are numerous measures used in both literature and industry to evaluate retail layouts. Generally, layouts in the retail sector are measured by the amount of revenue that the store is pulling in (Peters et. al., 2004). Substantial literature supports the influence of layout design on total sales (Bitner, 1992; Turley and Milliman, 2000; Burke, 2006; Shankar et. al.., 2011; Lu and Seo, 2015). Simply relying on this high-level measure, however, gives little insight into (i) *why* a specific store layout results in a certain amount of sales and (ii) *how* sales could be increased by varying layout design parameters. Researchers and practitioners, therefore, have adopted many metrics specific to retailing. Sorensen (2009) defines *aisleness* as the percentage of store area that is occupied by all structures, products, and staff; in other words, the remaining area would be available for customers to walk upon. *Shopper efficiency*, he further defines, is the length of time it takes a shopper to spend a dollar in the store. *Path length, travel deviations* (i.e., shopper not following optimal path between products), and *order deviations* (i.e., shopper picking out products in non-optimal order) have been analyzed by Hui et al. (2009). *Store coverage* (i.e., how much of the store area a shopper covers), *trip length* (i.e., time in store), and *basket size* have also been observed (Sorensen, 2017).

1.3 Exposure

One measure that has recently gained momentum in the literature is *exposure* (or *visibility*). While there are many variations on specific definitions, essentially exposure refers to the degree to which products, or a layout, is seen by shoppers. Many empirical studies in retail literature have supported the significance of exposure, most notably its effect on unplanned or *impulse* purchases (Cairns, 1962; Anderson, 1979; Dreze et al.,

1994; Chen et al., 1999). In fact, *Sorensen (2009) suggests that placing impulse products along a shopper's already-intended path can potentially entice them to make 1-5 additional purchases on impulse*; this could increase sales by more than 30%. Improving product exposure not only benefits the retailer, however. When shoppers are able to efficiently locate their planned purchases and experience the positive sensation associated with impulse purchases, their shopping experience is benefited (Piron, 1991; Yoo et al., 1998).

Nevertheless, studies have found that shoppers are only exposed to a small percentage of a store's products on a given shopping trip. Sorensen (2009) found that most shoppers will be exposed to only 11%-41% of products in a store depending on the type of shopping trip. In a later study, Sorensen (2016) observed that shoppers will only visit 16% of the store in hypermarkets (e.g., Walmart, Kroger), and 30% in smaller supermarkets (e.g., Whole Foods, Food Lion), thus limiting their exposure to products. It is, therefore, critical to effectively design stores that increase exposure, thus improving shopper satisfaction and retailer revenue. In this research, we focus on *layout* design decisions.

1.4 Motivation of our Research

While there are many ways to increase exposure in a retail store (e.g., circulation design, aisleness, number of entrances), a common practice among retailers has been to vary their design of rack layouts. Recently, retailers have begun to implement designs that have varied from the typical straight rack, placed orthogonal to a main aisle; see Figure 1. Figure 2 shows racks at an acute angle; shoppers walking by can potentially see both sides of the rack without having to make large head turns. Similarly, racks at low heights (i.e., under eye-height) allow shoppers to see *over* racks, in addition to the top surfaces; see

Figure 4. Figures 3 and 5 meanwhile demonstrate that racks or endcaps can be *curved;* these designs can potentially better synchronize with a shopper's natural scanning pattern to increase exposure and are visually appealing. While it is possible to evaluate such rack designs based on intuition and qualitative studies, a quantitative analytical-based approach would prove valuable to both research (e.g., more precise, robust models) and retail communities (e.g., more informed decision making).

Figure 2. Racks oriented at 45°.

Figure 4. Low rack heights.

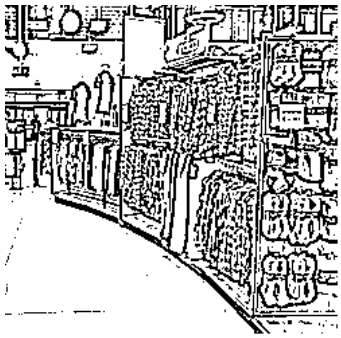

Figure 3. Curved racks.

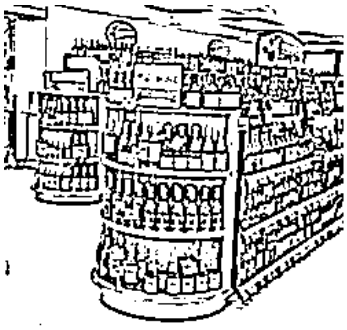

Figure 5. Curved endcaps.

Recently, Mowrey et al. (2017) suggest utilizing the shopper's field of regard (i.e., the visual sector for where their line of sight may fall on) to quantitatively evaluate exposure of varying rack orientations. They estimate exposure of a rack layout (with a specific orientation) considering a shopper walking along a main aisle in a 2D setting. In a more recent work, they use these models to optimize the rack layout to maximize exposure given a constrained floor space (Mowrey et al., 2018). While their contributions offer a refined model of exposure, *there are several limitations*; (i) they rely on a 2D approximation of the 3D environment, (ii) their focus on layout design is limited to straight

racks, (iii) rack heights are all assumed to be above eye-height and identical, and (iv) exposure is not linked to sales.

The focus of our research is to quantify exposure in 3D by considering racks of varying orientations, curvatures, and heights. We further seek to link exposure to sales (via marginal impulse profit) for prespecified product assortment and shelf space allocation decisions, and various product category location policies. We also take into consideration the cost of floor space and aspect ratio (i.e., length/width). We summarize below the research questions and contributions.

1.5 Research Questions

We now summarize the research questions we address in this research, followed by our research contributions.

Q1. How can exposure be quantified in 3D considering human field of regard?

Q2. What effect does rack orientation, curvature, and height have on exposure?

Q3. How sensitive are these findings to shopper traffic and scanning patterns?

Q4. What is the trade-off between exposure and floor space?

Q5. How can increases in exposure quantitatively be connected to gains in impulse profit?

Q6. What is the optimal rack configuration that maximizes impulse profit?

Q7. How sensitive is the optimal solution to the product location strategy, shopper volume, travel direction, floor space cost, and maximum aspect ratio?

We address research questions 1-4 with contribution 1, and questions 5-7 with contribution 2. These are both described below.

1.6 Research Contributions

Contribution 1. Quantifying and Analyzing Exposure in 3D

Our first contribution adds to the limited literature in retail layout design in several ways. To address Q1, we present a model for a human field of regard (FoR) as the extent to which the human head and eye movements occur in *3D* (substantially extending previous research that considered only 2D). We do so by considering both head and eye movements in horizontal and vertical directions. *Second*, we develop a model for a generic *curved* rack in *3D* (generalizing prior research conducted with straight racks). We develop an approach to design a layout of such generic curved racks oriented at a specific angle along the shopper pathway (similar to Figures 1 and 4), and at a specific height (similar to Figure 2). *Third*, we then propose a quantitative approach to model the dynamic interaction of a walking shopper's FoR and layout of racks (both uni- and bi-directionally). We quantify this interaction using two measures, exposure and intensity. Whereas *exposure is a binary value* indicating whether or not a certain location on a rack face is visible anytime during the shopper travel, *intensity indicates the time a location is exposed* to the shopper. In so doing, we can estimate not only the rack area that may be exposed to the walking shopper, but also identify 'hot-warm-cold spots' on each of the rack faces based on how long they were exposed to the walking shopper. To address Q2, we evaluate various orientation, curvature, and rack height values to determine the best designs and their improvements over a 90º layout of rectangular racks. The relative impact of rack height against orientation and curvature is also explored. For Q3, we do sensitivity analysis on shopper traffic patterns (uni-directional vs. bi-directional) and shopper scanning patterns (small vs. large).

Finally (Q4), we present analytical models for space and shape of the rack layout and evaluate the impact of increasing exposure against space.

There are several insights revealed in our study. They are summarized in the bullets below.

- When the racks are required to be oriented orthogonally to the shopper travel (i.e., θ=90°), use of curved racks in the layout could increase exposure (by 3-121%) over straight racks (α=0°).
- If such curved racks can be placed at any orientation, then there exist layouts that would further increase exposure (by 18-321%) over straight racks at 90º. If curved racks are not viable, then there exist orientations that allow achieving nearly this same increase in exposure.
- If the rack height (*H)* can be changed, then it trumps both orientation (θ) and curvature (α) in impacting exposure; rack heights just below eye-height appear to maximize exposure when the top of the rack is allowed for product allocation.
- The increase in exposure comes with a floor space tradeoff. Depending on the system parameters, it is possible to achieve nearly 530% increase in exposure with 18% floor space increase; 48% increase in exposure with a modest increase in space (<5%).

Contribution 2. Optimizing Rack Layout for Impulse Profit

In our second contribution, we utilize the model for exposure we developed in Contribution 1 to optimize marginal impulse profit. *First*, to address Q5, we derive a probabilistic measure for a product being seen, referred to as *visibility*, based on the effective area of locations, distribution of actual shopper head positions (from a prior

human subjects study), and exposure estimates from Contribution 1. This measure will help estimate the impulse profit. To then address *Q6*, we propose a non-linear optimization model, which we refer to as the Rack Orientation and Curvature Problem (ROCP), that determines the optimal rack orientation and curvature to maximize marginal impulse profit (after discounting for floor space) for a given location strategy of product categories. Impulse profit is estimated based on the probability that a product category on the shelf is seen, impulse purchase rate of that product category, and its average unit profit. We consider four different product location policies commonly found in either practice or literature*;* assortment and shelf space allocation decisions (i.e., number of facings) are assumed to be known. Given the difficulty in solving the proposed optimization model using commercial solvers, we propose an effective heuristic based on particle swam optimization framework and demonstrate this heuristic's performance against a grid search technique. *Finally*, for Q7, we evaluate the sensitivity of the optimal rack variables (orientation and curvature) to shelf location strategy, maximum aspect ratio, floor space cost, and shopper volume.

There are several insights revealed in our study. They are summarized in the bullets below.

- Varying rack orientation (θ) and curvature (α) from orthogonal and straight racks can improve marginal impulse profit by 70-233% depending on the location policy for product categories.
- The values of orientation (θ) and curvature (α) that resulted in the best marginal impulse profits were either high-acute and straight-to-medium-curved (i.e., θ = [25°,35°] and α = [0°,90°]), or high-obtuse and high-curved (i.e., θ =160° and

$\alpha=180°$). These layouts either contained a relatively large percentage of highly visible locations (ideal when using the Impulse Ordering Rule), or racks with a relatively large percentage of moderately visible (ideal when using the Demand Ordering Rule).

- The Impulse Rule generally leads to higher absolute marginal profit, while the Demand Rule demonstrated a higher relative increase in marginal profit compared to a layout with orthogonal and straight racks.
- The best values of θ trend toward either high-acute or high-obtuse as the tolerable aspect ratio increases; this increases the time a shopper can see locations on racks. The best values of α meanwhile generally increase.
- As shopper volume increases and floor space cost decreases, orienting (i.e., to acute or obtuse) and curving (i.e., $\alpha>0°$) racks lead to increased benefits over a {90°,0°} layout.

1.7 Research Implications

The implications of our research are worth mentioning. Our model and findings, we believe, would provide a store designer many benefits. *First*, retailers will gain insights into how key rack design parameters (e.g., orientation, curvature, height) affect exposure and impulse profit. *Second*, retailers can use our models to derive hot-warm-cold spots on racks to better locate products; i.e., more efficiently showcase novel and high impulse products. *Third*, top performing designs (based on exposure, impulse profit, space) can quickly be identified that adhere to unique design constraints of retailers; this can help avoid expensive experiments with layout changes. *Finally*, improved decision making by

retailers will facilitate better experiences for shoppers via improved shop-ability and increased impulse purchases.

Researchers, meanwhile, would experience a similar level of benefits from our research. *First*, the ROCP can be used as a baseline for developing more detailed models in store or category planning; incorporating additional decision variables such as product location and assortment would be viable options. *Second*, researchers interested in analyzing a wider variety of rack designs (e.g.., inverted pyramid, slanted racks) can adapt pieces from our models to understand the impact these designs have on exposure. *Finally*, our models to estimate exposure (and visibility) could be used as a reference to analyze layouts in other domains (i.e., airports, libraries, museums) where understanding the relationship between human visibility and layout design would be valuable.

1.8 Dissertation Outline

The remainder of this dissertation is organized as follows. Chapter 2 presents details of Contribution 1, while Chapter 3 presents details of Contribution 2. Chapter 4 summarizes conclusions from this research, and ideas for future research.

2 Evaluating Exposure of a Retail Rack Layout in 3D

2.1. Introduction

In chapter 1 we introduced the importance of exposure as a measure for retail layout design. Exposure, to reiterate, quantifies how well a layout presents its products to customers. Increasing a shopper's exposure to products, as well as knowing exposure levels of specific fixture locations in a layout, can be beneficial to both shoppers and store managers. Shoppers would potentially experience less time searching for already planned purchases, as well as make more unplanned purchases, thus boosting their shopping experience. Managers meanwhile would benefit by strategically placing their products, while being better equipped to negotiate rack space with manufacturers. Considering that 92% of retail sales still occur in brick and mortar stores, plus the fact that shoppers will typically only see around 11% - 41% of products (depending on the length of shopping trip), there is great potential and motivation to improve the customer shopping experience (Sorensen, 2009; US Census Bureau, 2016).

While some major retailers have implemented newer rack designs as discussed in Chapter 1 (i.e., curved racks, oriented racks, rack of varying heights), these designs lack supporting quantitative studies; their implementation is often based on intuition and/or qualitative findings. In that case, this research aims to fill this gap. Specifically, we question *what is the best orientation of racks to increase exposure? Can such increases be quantified? Would curving a rack increase or decrease exposure? How does the height of a rack affect exposure?*

To address these questions, this paper contributes to the limited literature in retail layout design in several ways. *First*, we present a model for a human field of regard (FoR) as the extent to which the human head and eye movements occur in *3D* (substantially extending previous research that considered only 2D). *Second*, we develop a model for a generic *curved* rack in *3D* (generalizing prior research conducted with straight racks). We extend this single-rack model to a layout of such racks oriented at a specific angle along the shopper pathway (similar to Figures 1 and 4), and at a specific height (similar to Figure 2). *Third*, we then propose a quantitative approach to model the dynamic interaction of a walking shopper's FoR and layout of racks (both uni- and bi-directionally). We quantify this interaction using two measures, exposure and intensity. Whereas exposure is a binary value indicating whether or not a certain location on a rack face is visible anytime during the shopper travel, intensity indicates the time a location is exposed to the shopper. In so doing, we can estimate not only the rack area that may be exposed to the walking shopper, but also identify 'hot-warm-cold spots' on each of the rack faces based on how long they were exposed to the walking shopper. *Fourth*, we conduct comprehensive experiments to illustrate the obstruction phenomenon that plays a vital role in altering the exposure and intensity values across designs. We then evaluate various orientation and curvature values to determine the best designs and their improvements over 90º layout of rectangular racks. The relative impact of rack height against orientation and curvature is also explored. *Finally*, we present analytical models for space and shape of the rack layout, and evaluate the impact of increasing exposure against space.

The key insights from our study include: (i) curving racks alleviates preceding obstruction (racks are visibly blocked to shoppers by racks *earlier* on a shopper's path),

yet increases self-obstruction (sections of a rack are visibly blocked by other sections of the *same* rack); (ii) either curving racks at an orientation of 90° *or* orienting straight racks to a more acute angle can provide a higher layout exposure (relative to straight racks at an orientation of 90°); (iii) racks with a height just below shopper eye-height can provide for increased exposure over racks just above eye-height due to top surfaces being potentially exposed; (iv) the height of racks is the most influential parameter on exposure, followed by orientation and then curvature; and (v) considering the floor space of layout, when head rotations are small, variations in θ and α from traditional racks become more beneficial in terms of exposure and space as the number of racks N increases.

Our model and findings, we believe, would provide a store designer a more realistic and comprehensive understanding of the relationship between rack layout design and exposure. There are numerous potential benefits: (i) top performing designs (based on exposure and space) can quickly be identified that adhere to unique design constraints, (ii) the shopping experience of customers (e.g., navigation, searching) would potentially benefit with designs catered to visibility metrics, resulting in increased loyalty, (iii) our models would serve as an input to shelf-space allocation models to estimate revenue, where hot and cold spots on racks (based on intensity of exposure) can be appropriately allocated to high and low impulse products respectively.

The remainder of this section is outlined as follows: 2.2 provides a review of related literature. In 2.3 we present our modeling approach. 2.4 presents our experimental study, while 2.5 discusses the impact on space. In 2.6, we present a human subjects study to validate our models. Finally, 2.7 discusses implications of our work for the retailers.

2.2 Literature Review

Prior research has revealed a strong relationship between exposure and sales (Applebaum, 1951; Cairns, 1962; Granbois, 1968; Dreze et al., 1994; Dunne et al., 1995; Knox et al., 2011; Hui et al., 2013). However, Sorensen (2016) observed that shoppers will only visit 16% of the store in hypermarkets (e.g., Walmart, Kroger), and 30% in smaller supermarkets (e.g., Whole Foods, Food Lion), thus limiting their exposure to products. Clearly, there is a need and potential for improved layout designs in terms of product exposure.

The IE/OR research community has recently begun incorperated some form of a visibility measure into retail layout evaulations. Peters et al. (2004) proposed a mathematical model to maximize expected store revenue by finding a balance between the time a customer spends in the store and the number of products they are exposed to along their path. Botsali and Peters (2005) extend this work to formulate a network-based model where they specifically focus on the serpantine layout, again to maximize expected revenue. They found that implementing "shortcuts" into the serpentine path allows for increased exposure of products on the corners of the shortcut. Li (2010) proposed an optimization model considering the aisle structure design, department allocation, as well as department layout in a sequential design process with the objective of maximizing expected profit. To model exposure, they suggest a decay function in terms of a product's distance from the main aisle, considering surrounding shopper traffic as well. Further, Yapicioglu and Smith (2012) develop a bi-optimization model considering the design of a retail store, where they seek to maximize revenue and adjacency scores of department locations by determining the size and location of each department. They assume exposure

to be a function of the department location with respect to pre-defined store traffic zones, as well as the department size. (i.e., high departmental exposure would coincide with a large area, and its location within a zone that has a high traffic density). Recently, Mowrey et al. (2017) suggest that evaluating layouts for exposure must account for the shopper's field of regard (i.e., the visual sector for where their line of sight may fall on). They estimate exposure of a layout with racks oriented at varying angles considering a shopper walking along a main aisle in a 2D setting. In a recent work, they use these models to optimize the rack layout to maximize exposure (Mowrey et al., 2018). While their contribution offers a refined model of exposure, there are three key limitations; (i), they rely on a 2D approximation of a 3D environment, (ii), their focus on layout design is limited to rectangular racks and (iii), rack heights are all assumed to be above eye-height and identical.

There has also been a recent growth in human visibility research in the urban planning domain. However, while 3D environments have been extensively covered (Bartie et al., 2010; Suleiman et al., 2011; Koltsova et al., 2013; Kim and Jung, 2014; Fisher-Gewirtzman, 2016), to our knowledge there has been no literature that provides an analytical framework, as all human visibility approximations rely on some form of a ray-shooting algorithm. Further, they do not account for head movements distinctly, nor human scanning patterns.

Eye-tracking measurements have often been used to understand human visibility. Specifically in the retail domain, Phillips and Bradshaw (1993) explored the simplicity (i.e., variety of product groups, geometric positioning) of shelf space with regards to attracting customer exposure, finding the simpler, the better. Both Pieters and Warlop

(1999) and Janiszewski et al. (1998) found a significant relationship between the time customers were exposed to certain products and the selection of those products. Chandon et al. (2006) model and empirically support the phenomenon that increased number of product fixations increases the probability the shopper will consider that product for purchase. Considering the layout of a retail setting, Sorensen (2009) utilized eye tracking to find a substantial drop-off in exposure from end-aisle displays and free-standing racks to all other fixture types. Further, Hendrickson and Ailawadi (2014) use eye-tracking to uncover several shopper habits relating to vertical eye fixation patterns, attention span, product consideration set, and reading patterns. While the above research supports the notion that visibility plays a key role in the shopping experience, none consider the implications on the design of a layout. With the emergence of a variety of rack layouts (some with curved racks), many of which can be found in stores of top U.S. retailers as highlighted in Section 1, it is imperative to characterize these layouts in terms of their effect on product visibility to shoppers.

Realizing the above gaps in the literature, we reiterate the contributions of this paper: (i) a quantitative approach to model the dynamic interaction between a shopper's 3D field of regard (FoR) and a layout of racks, (ii) analysis of the effect of rack orientation, curvature, and height on exposure and intensity, (iii) evaluating the implications of floor space and aspect ratio, and (iv) generating managerial insights to aid the retailer in identifying promising rack layouts that tradeoff the exposure and space effectively.

2.3 Modeling Exposure in a 3D Rack Layout

Studies have shown that it is common for shoppers to recognize what the product is based on its distinct shape, size, color, or symbol on the package without necessarily

reading all the letters on that package (Wedel and Pieters, 2008). With this in mind, we define exposure as the visual connection between a shopper and area of rack space (on which a certain product may be placed). To evaluate if a rack location is exposed or not, we must first model the dynamics that ensue from the interaction of the traveling shopper's 3D FoR and the static racks. Our approach considers a shopper walking along a main aisle in a retail setting with racks on either side. Accordingly, we first present models for (i) the human FoR in 3D, (ii) a generic curved rack in 3D, and (iii) a layout of curved racks placed at a prespecified orientation before presenting our quantitative approach to estimate both exposure and intensity.

2.3.1 Modeling the Human FoR in 3D

The human FoR in 3D is an angular volume of possible viewing angles for a fixation point (line of sight) to fall on; approximately 2º immediately surrounding the center of a human's fixation point perceives details necessary for information extraction (Monty and Senders, 1976; Wickens and Hollands, 2000; Ware, 2004). We model the 3D human (FoR) considering the angular limits of vision in both horizontal and vertical directions (Figures 6(a) and (b)), along with the depth of vision (*DOV*). The combination of both horizontal and vertical limits can be modeled as an elliptical sector of a sphere; see Figure 6(c), where we further break down these limits by head (Ω) and eye (Φ) rotations. Our parameters (Figure 6(d)) are based on those presented by Parker and West (1972). Typical values considering moderate movements are shown in Table 1.

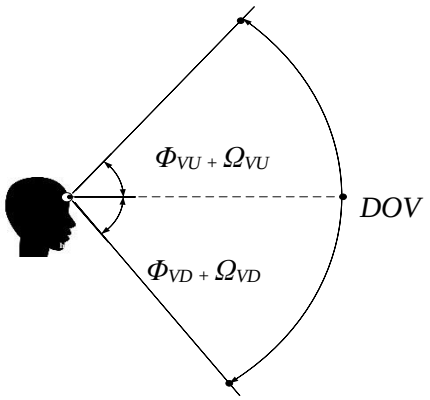

(a) Side view

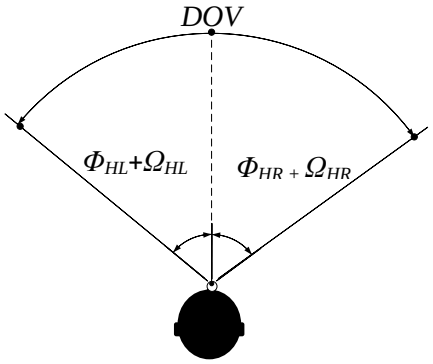

(b) Top view

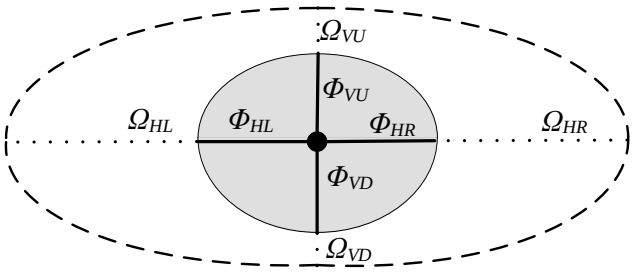

(c) Front View

Movements

Eye	Head	**Direction**
Φ_{HL}	Ω_H	*Horizontal Left*
Φ_{HR}	Ω_{HR}	*Horizontal Right*
Φ_{VU}	Ω_{VU}	*Vertical Up*
Φ_{VD}	Ω_V	*Vertical Down*

(d) Parameters for angular limits of vision.

Figure 6. Modeling 3D FoR

Table 1. Values for moderate eye and head movements (Parker and West, 1972)

Eye Movements				*Head Movements*			
Φ_H	Φ_{HR}	Φ_{VU}	Φ_{VD}	Ω_{HL}	Ω_{HR}	Ω_{VU}	Ω_{VD}
15°	15°	15°	15°	30°	30°	30°	30°

To determine *DOV*, we utilize the visual angle (v) notated as $v = 2\arctan\left(\frac{h}{2d}\right)$; h represents the height of the object and d is the distance from the optical center of the eye to the object (Ware, 2004). Assuming a recognizable package label on a retail shelf to be at least 1 inch tall (e.g., the Nike swoosh or *K* on Kellogg's cereal) or simply the color of the product package (e.g., orange on Tide detergent or blue on Oreos cookies) and a

shopper to have 20/20 vision (v = 5 arcmin), we can estimate the approximate *DOV* for a shopper to be approximately 50 ft.

2.3.2 Modeling a Curved Rack in 3D

Although a wide variety of racks can be found in retail stores, we focus on gondolas, which are the type of racks most prominent in grocery stores and mass retailers. We model a generic curved gondola (referred to as a rack from here on) in 3D as a combination of angle of curvature (α), perimeter (p), width (w), height (H), and curved end caps; see Figure 7 (a-b). Each of the four rack faces (f) are denoted as A-D (see Figure 7 (c)).

For such a curved rack, using the expression for arc length (i.e., $L_f = \frac{\alpha\pi r}{180}$), the arc lengths of faces A – D (L_A, L_B, L_C, L_D) can be calculated as $\frac{\alpha\pi}{180}\left(\frac{w}{2}\right)$, $\frac{\alpha\pi}{180}\left(r - \frac{w}{2}\right)$, $\frac{\alpha\pi}{180}\left(\frac{w}{2}\right)$, and $\frac{\alpha\pi}{180}\left(r + \frac{w}{2}\right)$ respectively, where r represents the radius of curvature to the midline of the rack. Radius r can be obtained as $r=\frac{90*(p-\pi w)}{\alpha\pi}$, where p is the prespecified perimeter of the rack (which ensures that the total rack display remains the same across -180°≤α≤180°). The corresponding chord length (c) is given by $2r\sin\left(\frac{\alpha}{2}\right)$. For instance,

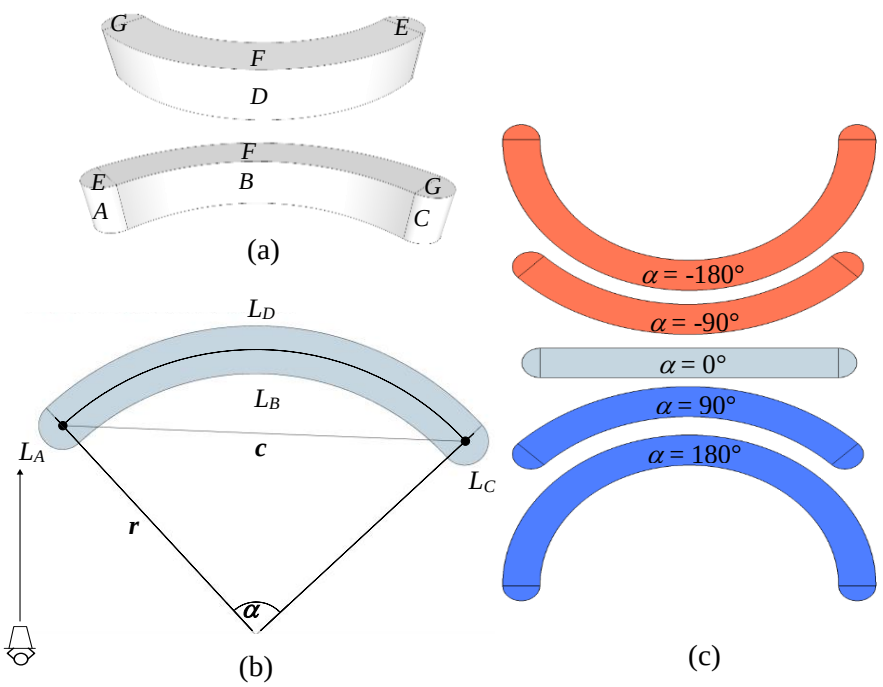

Figure 7. Modeling 3D curved racks

given values of p=110 ft, α=90° and w=5 ft, we compute r=30.01 ft, c=42.45 ft, L_A= L_B=7.85 ft, L_C = 43.22 ft, and L_D=51.07 ft.

Note that a straight, rectangular rack typically found in retail stores is a special case of a curved rack. That is, as $\alpha \rightarrow 0$, r approaches, $\lim_{\alpha \to 0} \frac{90*(p-\pi w)}{\alpha \pi} = \infty$, which is a straight rack. We, therefore, refer to such racks as racks with α=0° in our experiments later.

2.3.3 Modeling a Layout of Racks

Having now modeled a generic curved rack in 3D, we illustrate how we model a layout of such racks on both sides along the shopper pathway, each identically oriented at a prespecified angle ($0 \leq \theta < 180^o$) (see Figure 8). We designate the minimum distance between racks as a_c and the width of the main walking aisle as a_w; the distance from the shopper to the nearest part of the racks is notated as a_m (Figure 9). For a given number of curved racks (n) with curvature (α) and orientation (θ), we ensure that the minimum cross-aisle (perpendicular) distance between the racks (a_c) is maintained. Depending on the values of θ and α, the minimum perpendicular distance

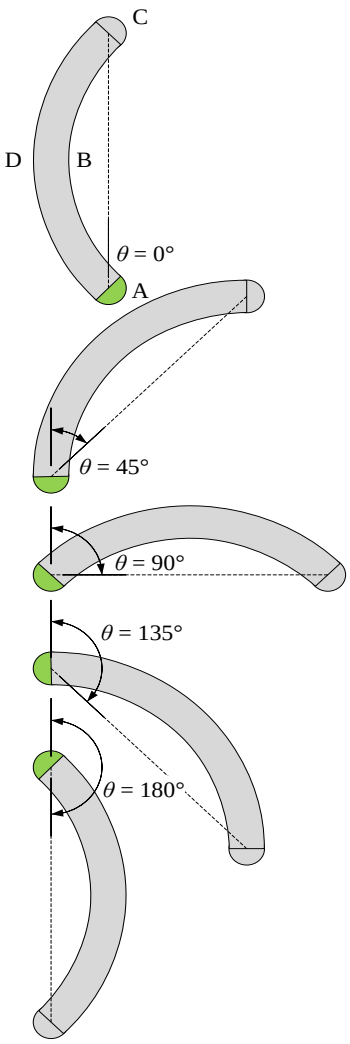

Figure 8. Example rack orientations

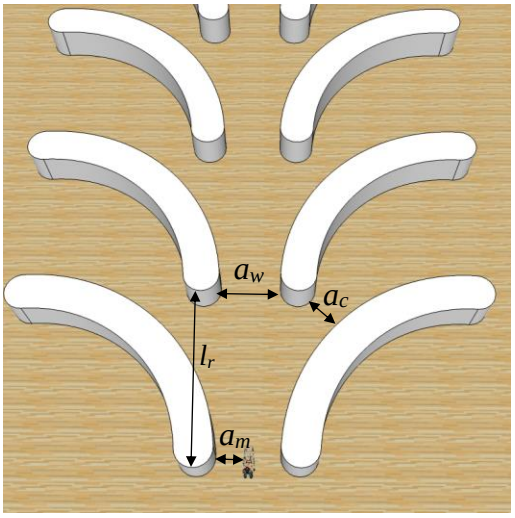

Figure 9. Designing a layout of racks

between the racks may occur along either endcap (faces A and C), or face D. See Appendix A for details on determining l_r. All ensuing racks are accordingly placed a distance l following each previous rack**.** With these preliminaries (i.e.., models for human FoR, generic rack, and corresponding rack layout), we now present our proposed approach to quantify exposure and intensity of a given rack layout

2.3.4 A Quantitative Model for Exposure and Intensity

Our proposed approach to estimate exposure (seen or not) and intensity (time of exposure) in 3D considers a shopper walking along a path through a layout of racks while perpetually scanning. It is quite challenging to directly derive an analytical model of exposure in 3D given the complex and dynamic interaction of the FoR of a moving shopper with a layout of static racks. Consequently, we decompose this 3D problem into a set of 2D problems by discretizing the FoR by height (h) within the range of the vertical angular limits from the shopper's eye-height (S_E). Each height h is spaced k ft apart (depending on the average

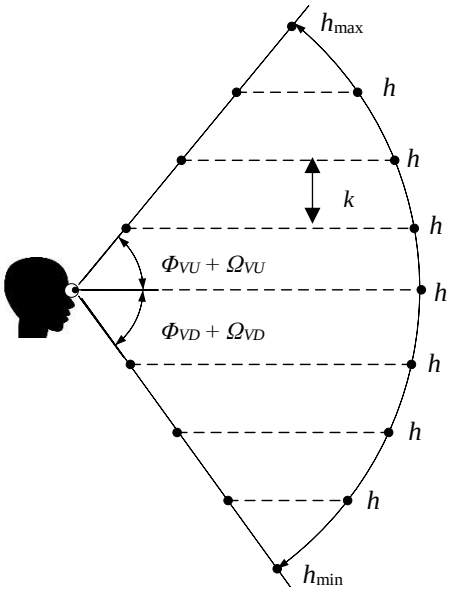

Figure 10. Decomposing by height

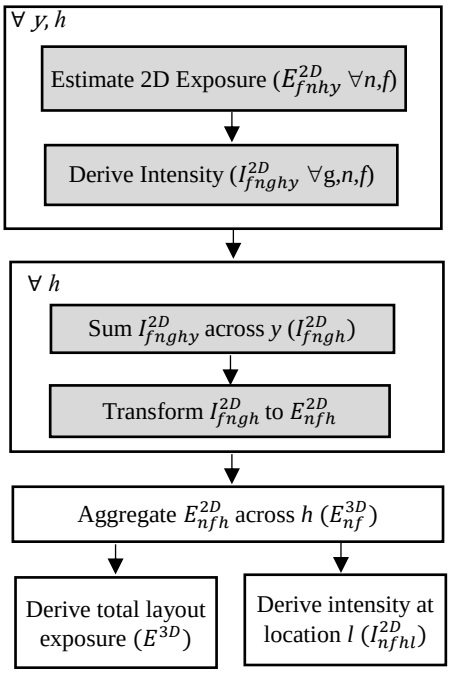

Figure 11. 3D Exposure Algorithm

height of the products). We consider $h \in [h_{\min}, h_{\max}]$, where $h_{\max}$ (i.e., maximum height of FoR) $= S_E + DOV * \sin(\Phi_{VU} + \Phi_{VU})$ and $h_{\min}$ (i.e., minimum height of FoR) $= S_E - DOV * \sin(\Phi_{VD} + \Phi_{VD})$ (see Figure 9).

To estimate exposure in 2D, we first discretize the shopper path into a set of steps Y (ρ ft apart), where each step $y \in Y$. At each discrete step y, we estimate 2D exposure, E^{2D}_{fnhy}, as one or more continuous arc(s) in ft on each face (f) of rack (n) for all discrete heights (h) in the 3D FoR that fall within $[0, H_n]$, where H_n is the height of rack n. That is, if $H_{\max} > H_n$ then we only find exposure up to H_n; if $H_{\min} < 0$ then we find exposure beginning at h=0. Specific details on how we estimate E^{2D}_{fnhy} are found in section 3.3.2. While our approach allows for estimating exposure of racks in 2D in a continuous space (i.e., as exposed arcs), to estimate intensity (i.e., time of exposure), we discretize racks into arc segments $g \in G$ (of length l_w) at each height h. The values of l_w will depend on the average width of products placed on the rack faces. Intensity (I^{2D}_{fnhyg}) at a step y is assigned either a 1 or 0 depending if any portion of arc segment g falls within the continuous exposed arc(s). For instance, consider Figure 12 (a), which illustrates exposure of a rack at a single shopper step y; the red arcs represent *exposed* arcs at each height h. Figure 12(b) shows the overlay of the discretized arc segments over the rack face and exposed arcs. In this specific case, for the exposed arc across h=4, arc segments g=0 through g=5 are considered as exposed, and thus their intensity values, I^{2D}_{fnhyg}, are set to 1 (see Figure 12(c)). Following the completion of a shopper's pathway, we sum I^{2D}_{fnhyg} across all y to find I^{2D}_{fnhg}.

Now to estimate the *total* exposure of a layout (i.e., the rack segments that a shopper will see for at least one step *y*), we separate the segments that were exposed (i.e., with non-zero intensity value) from those never exposed (i.e., intensity value of 0). Let $\hat{I}^{2D}_{fnhg}$ be a 0-1 indicator such that $\hat{I}^{2D}_{fnhg}$=1, if the intensity I^{2D}_{fnhg}>0, and 0 otherwise. Then, total 2D exposure is given by $E^{2D}_{nfh} = l_w * \sum_{l=1}^{L} \hat{I}^{2D}_{nfhg}$. We then use the trapezoidal rule to aggregate these arcs (E^{2D}_{nfh}) across all heights (h) to estimate 3D exposure (E^{3D}_{nf}, in ft^2) of face f on rack n; i.e., $E^{3D}_{nf} = \frac{k}{2}[E^{2D}_{nfa_s} + 2E^{2D}_{nf(a_s+k)} + 2E^{2D}_{nf(a_s+2k)} + \ldots + E^{2D}_{nfb_s}]$, where a_s and b_s represent the lowest and highest points of a rack face, respectively (see Figure 13(a)). The final step is to sum these 3D exposure estimates across each face f and each rack n; i.e., $E^{3D} = \sum_{n,f} E^{3D}_{nf}$, which is provides an estimate of the total exposed rack area (in ft^2) of a given layout of n racks. Finally, the intensity of a location (l) on a rack (i.e., the bounded area between segment (g) and height (h)) can be estimated as $I^{2D}_{nfhl} = \left(\frac{I^{2D}_{nfhg} + I^{2D}_{nf(h+1)g}}{2}\right)$; see Figure 12(d).

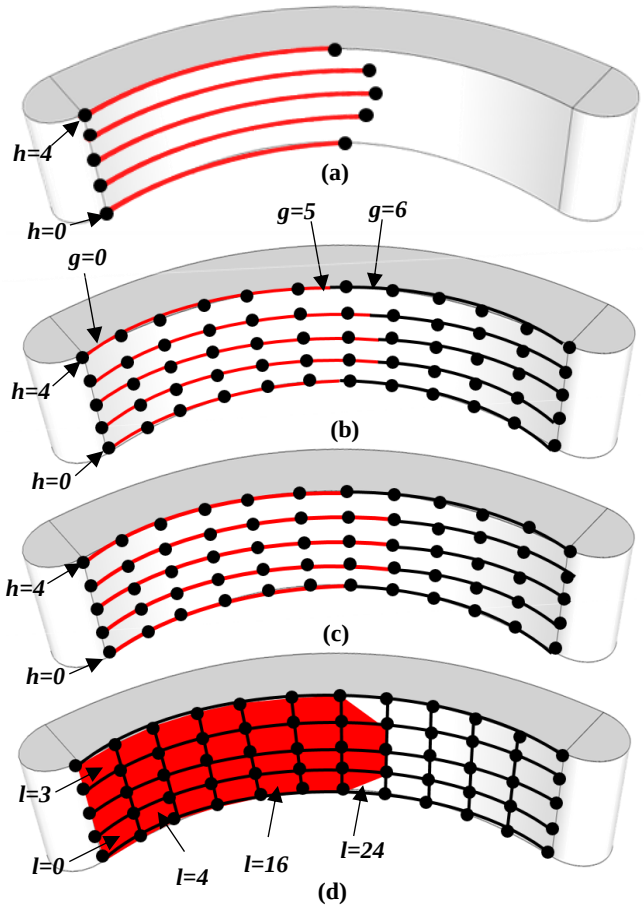

Figure 12. Exposure/intensity at step *y*

Recall that racks in a layout may be of different heights. If the height of a rack (H_n; $1 \leq n \leq N$) is below the eye height of the shopper (S_E), the top faces can potentially be exposed. In order to incorporate these faces (i.e., E, F, and G) into our 3D exposure and intensity estimations, we discretize the top face into arcs spaced γ_d apart. At each shopper step (y) and each height (h), if h is equal to the height of any rack (H_n) in the layout, then we simply repeat the 2D algorithm at that height for $\left(\frac{w}{\gamma_d}\right) + 1$ steps to estimate exposure at each discretized curve. To then estimate 3D exposure of the top faces, we again use the trapezoidal rule (see Figure 13(b)). The expressions for this calculation are presented in Appendix B. Details of our 2D approach to estimate continuous exposed arc(s) on a rack face at each height are found in Appendix C.

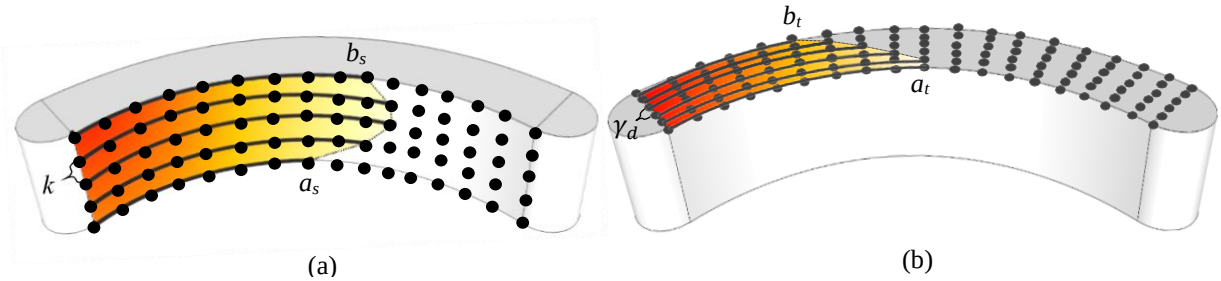

(a) (b)

Figure 13. Riemann Sum Approximations for side (a) and top (b) faces

To first illustrate the use of our approach to obtain exposure and intensity, we present four different designs with varying combinations of θ and α. Figure 14 shows these designs with overlaid intensity profiles (red=longest exposed, yellow=shortest exposed, and white=not exposed).

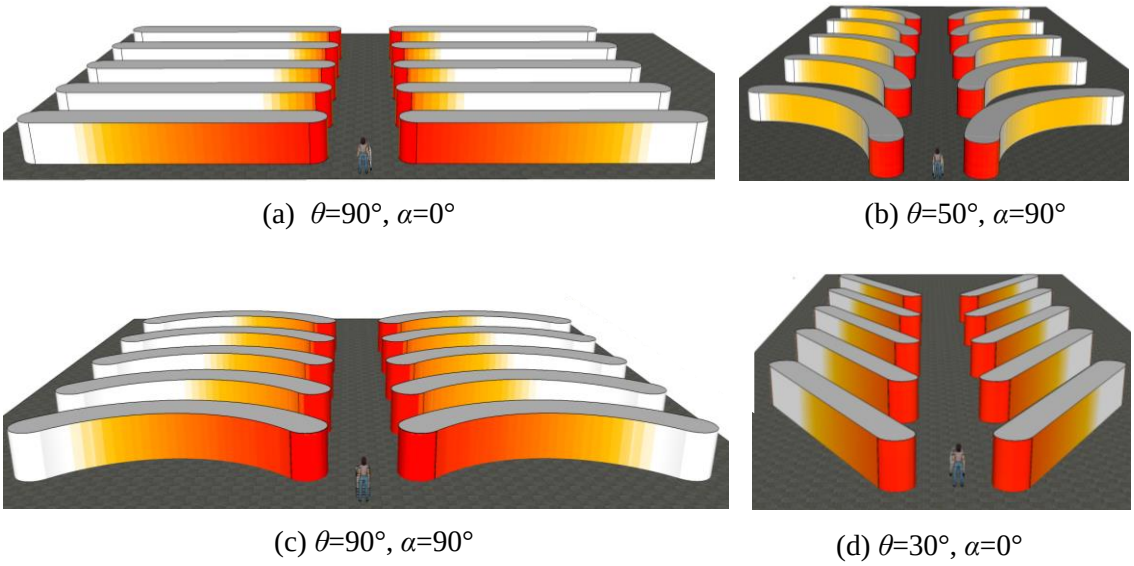

(a) θ=90°, α=0° (b) θ=50°, α=90°

(c) θ=90°, α=90° (d) θ=30°, α=0°

Figure 14. Rack layouts with overlaid intensity

Observing these layouts, there are many questions that arise: *Which layouts have the highest amount exposure? Which layouts experience obstruction? How do varying θ, α, and H affect exposure?* To answer the above questions, and subsequently derive managerial insights, we conducted a comprehensive experimental study, as discussed below.

2.4 Experimental Study

The experimental study was conducted in 3 phases. First, we generated the intensity profiles of several layouts and analyzed the obstruction phenomenon. Second, we expanded our experiments to a range of values for rack orientation (θ), curvature (α), and height (H) to find combinations that provide the highest exposure. Third, we explore the effect of H, and the relative influence of θ, α, and H.

2.4.1 Dynamics of Obstruction and Exposure

As discussed in section 3.3.2, for a candidate point on a rack to be visible to the shopper, it must be mathematically feasible, be within the FoR, and not be obstructed. In

this section we visually examine the effect of varying of θ and α on the obstruction phenomenon. Specifically, we evaluate 6 different rack layouts considering 2 angles of curvature (α) and 3 angles of orientation (θ). Table 2 summarizes the system parameters. Unidirectional shopper travel (i.e., κ=1, where κ represents the proportion of traffic one-way) is considered. Shopper FoR parameters are based on moderate eye (horizontal and vertical) and head (horizontal) movements. Figure 15 shows the intensity profiles (red = longest exposed and yellow = shortest exposed; white = not exposed) for each of the 6 rack layouts.

Table 2. Input parameters for experiments.

Notatio	**Definition**	**Value**
N	Number of full length racks (right	3
a_c, a_w	Width of cross aisle, main aisle	8,10 ft
a_m	Shopper distance to racks	5 ft
c,w,H	Chord length, width, height of rack	40, 5, 7 ft
DOV	Depth of focused vision	50 ft
S_E	Shopper Eye Height	5 ft
ρ	Step size of shopper path	0.25 ft
l_w, k	3D rack location	1 ft

Field of Regard Parameter Values							
Φ_H	Φ_{HR}	Φ_{VU}	Φ_{VD}	Ω_{HL}	Ω_{HR}	Ω_{VU}	Ω_{VD}
15°	15°	15°	15°	30°	30°	30°	30°

We first discuss the effect of *preceding-obstruction* (i.e., degree of rack area that lies within FoR, but is blocked by parts of the *previous* rack), which we found is *less prevalent* in racks with *higher* degrees of curvature or *acute* orientations; e.g., examine illustrations (a) and (i) in Figure 15. Notice the substantial difference in exposure between rack 1 (unobstructed) and rack 2 obstructed by rack 1 (and rack 3 obstructed by rack 2) in each layout.

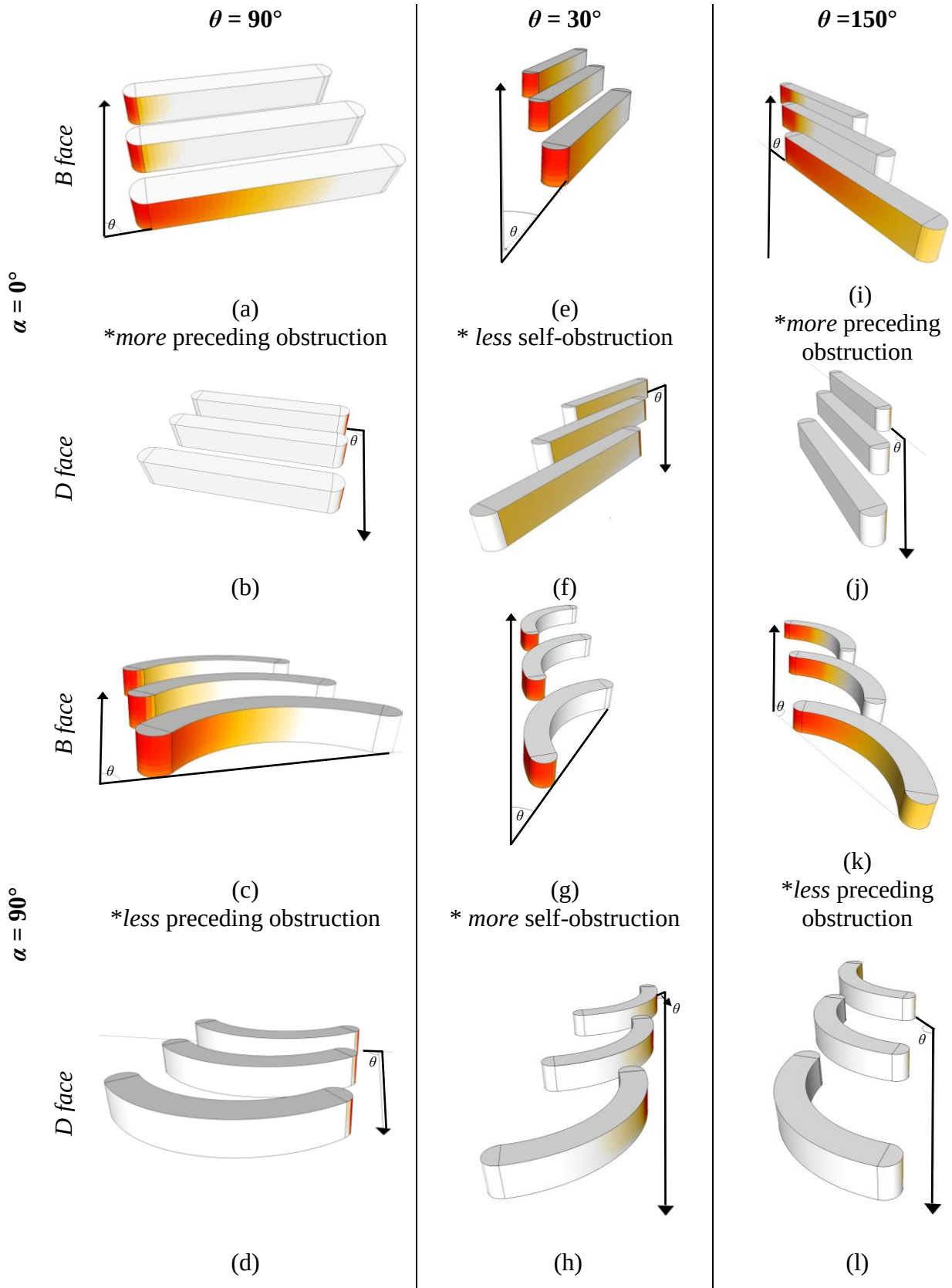

Figure 15. Analyzing the obstruction phenomenon with varying θ and α.

Now consider illustrations (c) and (k) and notice how racks 2 and 3 have an increased amount of exposure compared to illustrations (a) and (i), respectively. We attribute this to the ability of the human eye to see more around the curved (α = 90°) face D of preceeding racks, leading to increased exposure of face B on succeeding racks compared to when α = 0°. Considering the effect of θ, notice how exposure on face B for all 3 racks in illustration (e) is identical; this is contrary to orthogonal and obtuse orientations in illustrations (a) and (i) where preceding obstruction is evident.

Further, we found *self-obstruction* (i.e., degree of rack area that lies within FoR, but is blocked by other parts of the *same* rack) is *more prevalent* in racks with higher degrees of curvature and *acute* orientations. For instance, compare the level of exposure on each face B in illustrations (e) and (g). As can be seen, when curving the rack at this orientation, there is no longer exposure on face B due to obstruction from face A (endcap).

2.4.2 Determining Best Orientation (θ) and Curvature (α)

Realizing how obstruction varies with θ and α, eventually affecting exposure and intensity, we then sought to determine the *best* values of θ and α corresponding to highest exposure. We considered a variety of combinations of shopper head movement, traffic pattern, and rack height. For each parameter combination, Table 3 summarizes the following: (i) the best combination of θ and α (θ*, α*), (ii) the improvement that this best design provides over the design with *straight racks at their best orientation* (θ*, α=0°) and *straight racks at 90°* (θ=90°, α=0°), (iii) the best curvature for racks oriented at θ=90°, and (iv) the improvement of this design over *straight racks at 90°*. We tested for 0°≤ θ<180° in increments of 10° and for -180°≤α<180° in increments of 10°. A small shopper scanning pattern (horizontal) was modeled as head and eye movement values $\Phi_{HR} + \Omega_{HR} = 45°$, while

a large pattern as $\Phi_{HR} + \Omega_{HR} = 90°$. A uni-directional traffic pattern, again, refers to one-way traffic (κ =1), while a bi-directional traffic pattern models two-way traffic (equal proportion of shoppers travelling in each direction, i.e., κ =0.5); exposure is calculated in both directions and subsequently averaged. Further, we consider racks at heights 3 ft, 5ft, and 7 ft, for a shopper eye-height at 5 ft (corresponding to average female eye-height). All additional parameter values are identical to those in Table 2.

Table 3. Sensitivity experiments for exposure.

Shopper scanning pattern	**Traffic pattern**	**Rack height**	**Best curvature for racks oriented at θ=90°**		**Best combination of orientation (θ*) and curvature (α*)**			
			α*	**% better than straight rack (α =0°) at θ=90°**	**θ***	**α***	**% better than straight rack (α =0°) at θ=90°**	**% better than best straight rack (θ*, α =0°)**
Small (Φ_{HR} + Ω_{HR} = 45°)	Uni-directional	3 ft	180°	59%	30°	20°	120%	4.46% 30°
		5 ft	180°	121%	30°	10°	321%	1.54% 30°
		7 ft	180°	121%	30°	10°	320%	1.60% 30°
	Bi-directional	3 ft	180°	55%	30°	20°	89%	3.55% 20°
		5 ft	180°	80%	30°	20°	195%	2.04% 20°
		7 ft	180°	80%	30°	20°	193%	2.09% 20°
Large (Φ_{HR} + Ω_{HR} = 90°)	Uni-directional	3 ft	150°	15%	50°	60°	37%	4.24% 60°
		5 ft	150°	38%	60°	20°	81%	1.36% 60°
		7 ft	150°	38%	60°	20°	82%	1.18% 60°
	Bi-directional	3 ft	150°	10%	50°	60°	18%	4.88% 60°
		5 ft	150°	3%	50°	70°	23%	1.66% 60°
		7 ft	150°	3%	50°	70°	23%	1.33% 60°

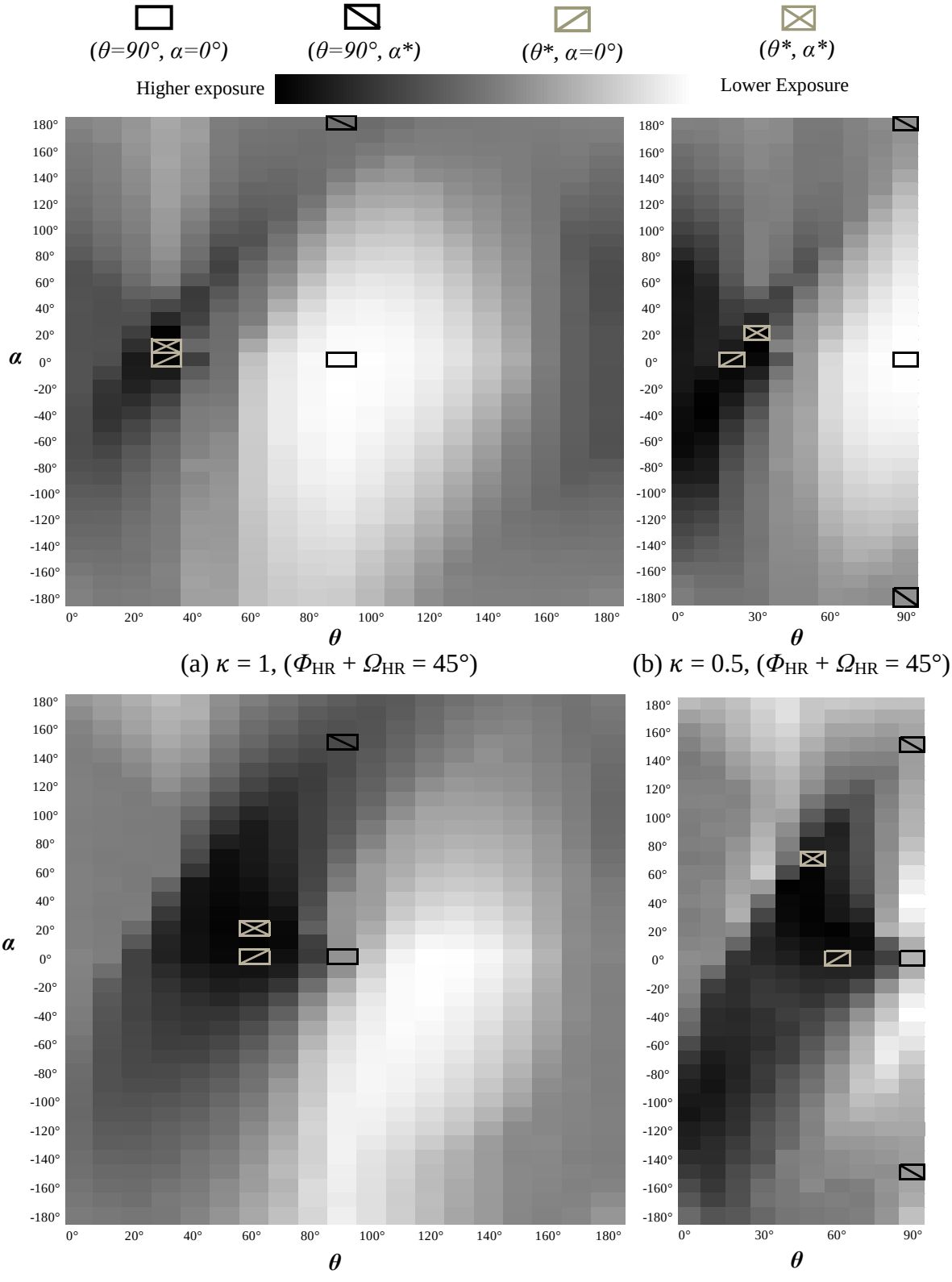

(a) κ = 1, (Φ_{HR} + Ω_{HR} = 45°)

(b) κ = 0.5, (Φ_{HR} + Ω_{HR} = 45°)

(c) κ = 1, (Φ_{HR} + Ω_{HR} = 90°)

(d) κ = 0.5, (Φ_{HR} + Ω_{HR} = 90°)

Figure 16. Heat maps of exposure for combinations of θ and α for H =7.

These results indicate the following:

i. For designs with racks oriented at 90°, the best curved racks (θ=90°, α*) appear to exhibit higher exposure than traditional racks (θ=90°, α=0°) for all parameter combinations considered in our study; i.e., if θ=90°, then α* > α=0°. The magnitude of this improvement is higher for (i) rack heights at, or above the shopper eye height (except for large head rotations with bi-directional traffic), (ii) uni-directional traffic and (iii) small eye/head rotations.

ii. The best curved racks (θ*, α*) appear to exhibit higher exposure than traditional racks (θ=90°, α=0°) for all parameter combinations considered in our study; i.e., (θ*, α*) > (θ=90°, α=0°). The magnitude of this improvement is higher for (i) rack heights at, or above the shopper eye height (ii) uni-directional traffic and (iii) small eye/head rotations.

iii. The best curved racks (θ*, α*) appear to exhibit approximately equal exposure to the best straight racks (θ*, α=0°) for all considered combinations; i.e., (θ*, α*) ≈ (θ*, α=0°).

These insights can visually be validated by observing heat maps of exposure in Figure 16 for rack heights of 7 ft (above eye-height). The darker shades indicate higher exposure improvement from the minimum exposure across all combinations of θ and α, whereas lighter shades represent the lowest exposure values. We mark each (θ, α) combination shown in Table 3. For instance, considering uni-directional traffic and small head movements (Figure 16 (a)), we mark the best combination of θ and α (θ=30°, α=10°), best straight rack (θ=30°), best rack oriented at θ=90° (α=180°), and a rack (θ=90°, α=0°).

2.4.3 Rack Height Sensitivity

We further explored what rack heights provide the highest exposure values. To evaluate this, we selected a few of the top performing layouts from Table 3 and examined the effect of varying the rack height from 3 ft to 7 ft in 1 ft increments (maintaining an eye-height of 5ft). Based on Figure 17(a), where we assume small head rotations ($\Phi_{HR} + \Omega_{HR} = 45°$) and uni-directional traffic (κ=1), we make note of an increasing trend in exposure with a discontinuity at the shopper eye-height; we present results of rack height just below 5 ft (i.e., 4.95 ft) to better depict this. This discontinuity occurs due to the shopper being able to see the top surface of racks, and *over* racks onto succeeding racks when racks are below the eye-height. However, when the racks are equal to the eye-height or above, the top surfaces are no longer visible. Further, we notice that heights *just below* eye-height result in the highest exposure (considering the 3 – 7 ft range), while heights *at* eye-height result in the lowest exposures. These observations are robust to large head movements as well, and for both uni- and bi-directional traffic (Figure 17(b-d)).

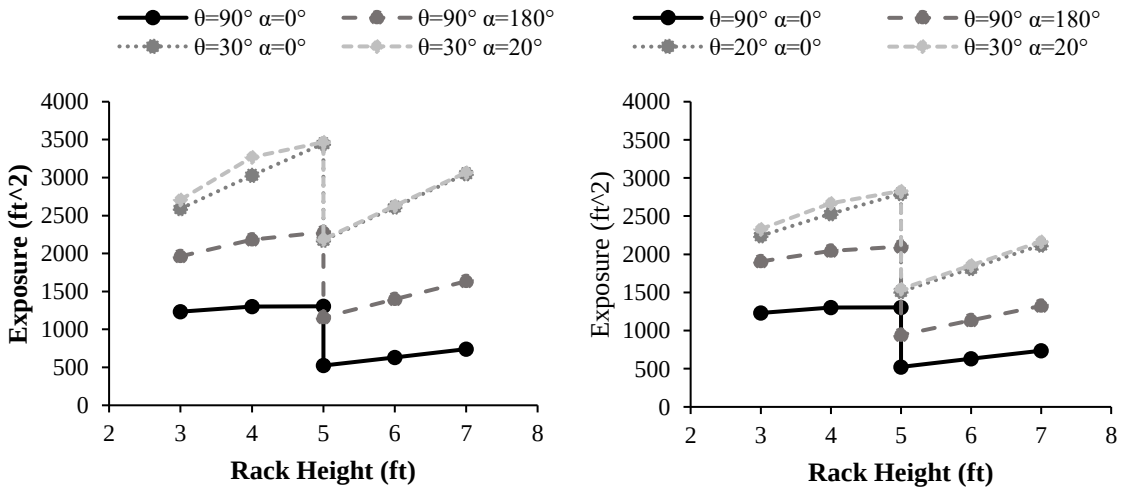

(a) κ=1, $\Phi_{HR} + \Omega_{HR} = 45°$

(b) κ=0.5, $\Phi_{HR} + \Omega_{HR} = 45°$

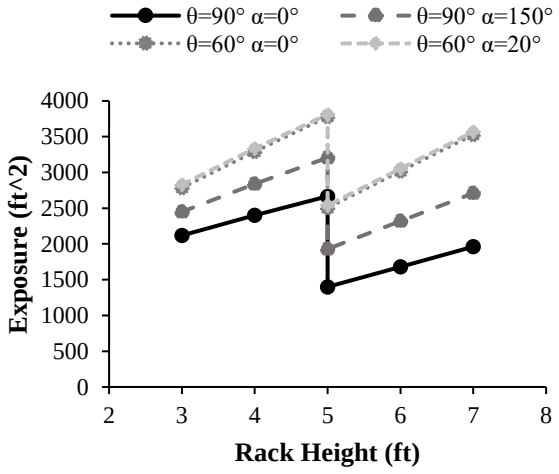

(c) κ=1, $\Phi_{HR} + \Omega_{HR} = 90°$

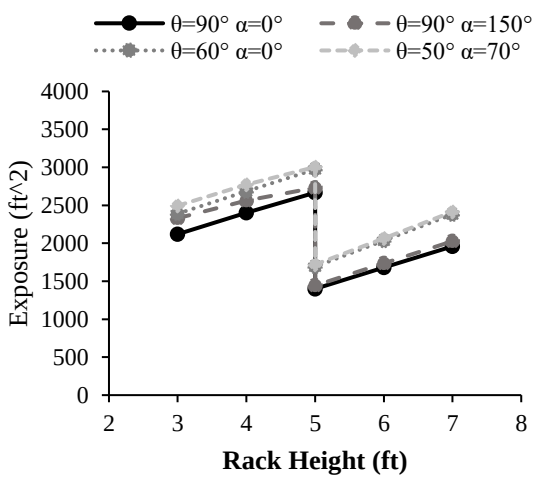

(d) κ=0.5, $\Phi_{HR} + \Omega_{HR} = 90°$

Figure 17. Sensitivity of exposure to rack height;
$\Phi_{HR} + \Omega_{HR} = 90°$ refers to small head movements and $\Phi_{HR} + \Omega_{HR} = 90°$ refers to large head movements.

2.4.4 Relative Influence of θ, α, and H on Exposure

To check the relative influence of θ, α and H, we developed a statistical model that uses all of our experimental data (across $0^o \leq \theta \leq 180^o$, $-180^o \leq \alpha \leq 180^o$, and $H \in \{3,5,7\}$) with exposure as the dependent variable and θ, α, and H as the independent variables. Preliminary analysis suggested that the exposure errors from a simple linear regression model were not normally distributed (per the quantile-quantile plot). Thus, we chose a non-parametric modeling approach, such as a decision tree. We developed four decision tree models (in JMP, a SAS product) considering each combination of head movement (small and large) and traffic pattern (uni-directional and bi-directional). Splits were determined based on chi-square values for each variable (i.e., largest ones were split at each level).

The relative importance of each variable is based on the error sum of squares; i.e. the sum of squared difference between each observation and the mean for each respective variable. The higher the error sum of squares for a decision tree model, the higher variation

within a group (corresponding to a variable's relative influence of the response variable). As illustrated in Figure 18(a) (uni-directional traffic) and Figure 18(b) (bi-directional traffic), we observe *H* to be the most influential parameter in terms of impacting exposure, followed by θ, and then α. The impact of *H* is pronounced when the rack height is closer to eye-height; as indicated in Section 4.4., just below eye-height exposes the top surface that adds additional exposure. We noticed that the first split in the decision trees was always at *H*=5 ft (eye-height). In contrast, between θ and α, θ (rack orientation) was much more influential as it affected the alignment of the rack faces to the human FoR much more than α (rack curvature); better alignment lead to better exposure.

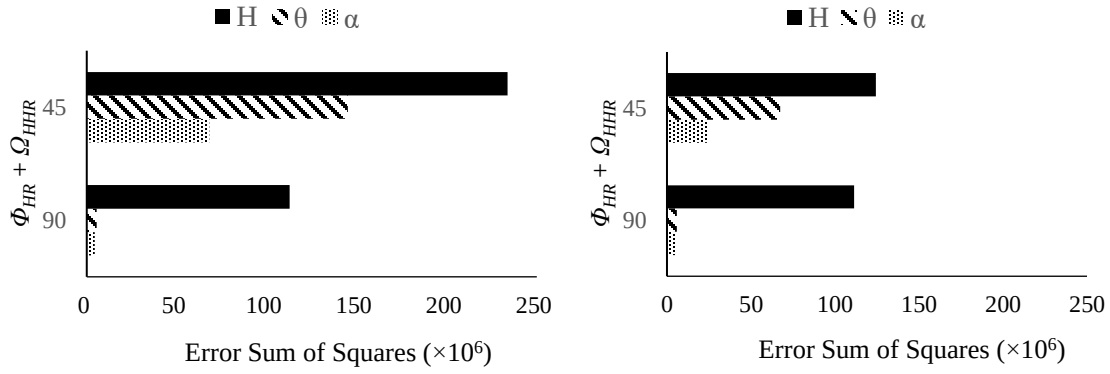

(a) κ=1 (b) κ=0.5

Figure 18. Impact of layout parameters for (a) uni-directional traffic and (b) bi-directional traffic

2.5 Implications on Floor Space

While the focus until now was on analyzing the impact of rack orientation (θ), curvature (α), and height (*H*) on exposure compared to straight racks oriented orthogonally (i.e., θ=90°, α=0°), we acknowledge that both θ and α could impact floor space and aspect ratio of the layout. To analyze these effects, we developed analytical models for space and

aspect ratio; see Appendix D for details. Below we compare and contrast a variety of rack layouts against their exposure and required floor space.

With the layout (θ=90º, α=0°) as a baseline, we illustrate the % increase in exposure along the vertical axis and the resulting % increase in floor space along the horizontal axis (Figures 19 (a-d)). Thus, the best designs have relatively high increases in exposure with low increases in floor space (i.e., upper left corner). We present results for designs with θ=30º, θ=60º, and θ=90º and values of α ranging from 0° (indicated by smaller markers) to 180° (indicated by larger markers) in increments of 10°. Graphs are shown considering rack heights above eye-height (7 ft) and small head rotations ($\Phi_{HR} + \Omega_{HR} = 45°$), for small ($N$=3) and medium-to-large (N=20) layouts, across both uni-directional (κ=1) and bi-directional (κ=0.5) shopper traffic.

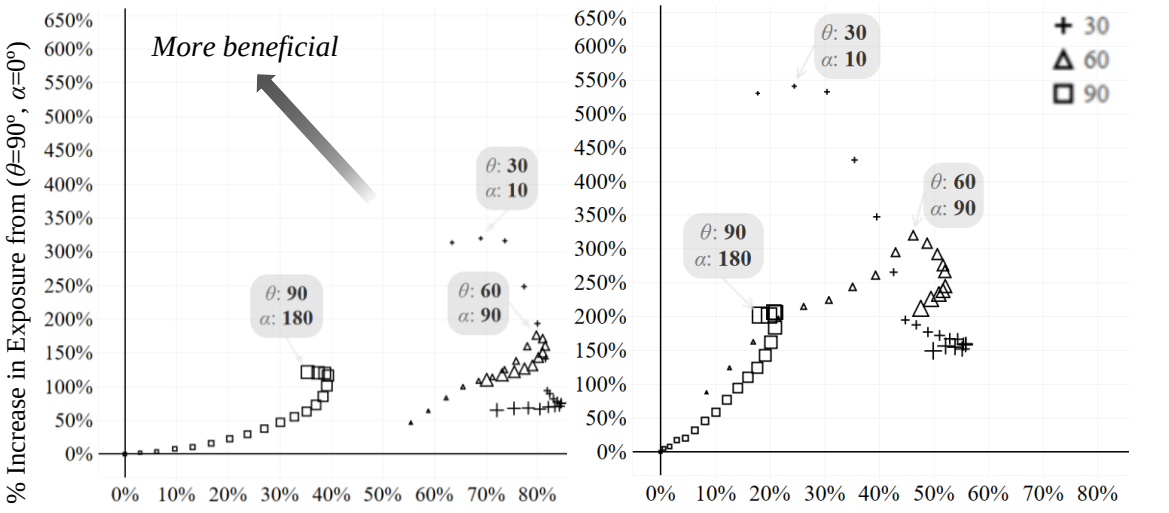

(a) N=3, κ=1 (b) N=20, κ=1

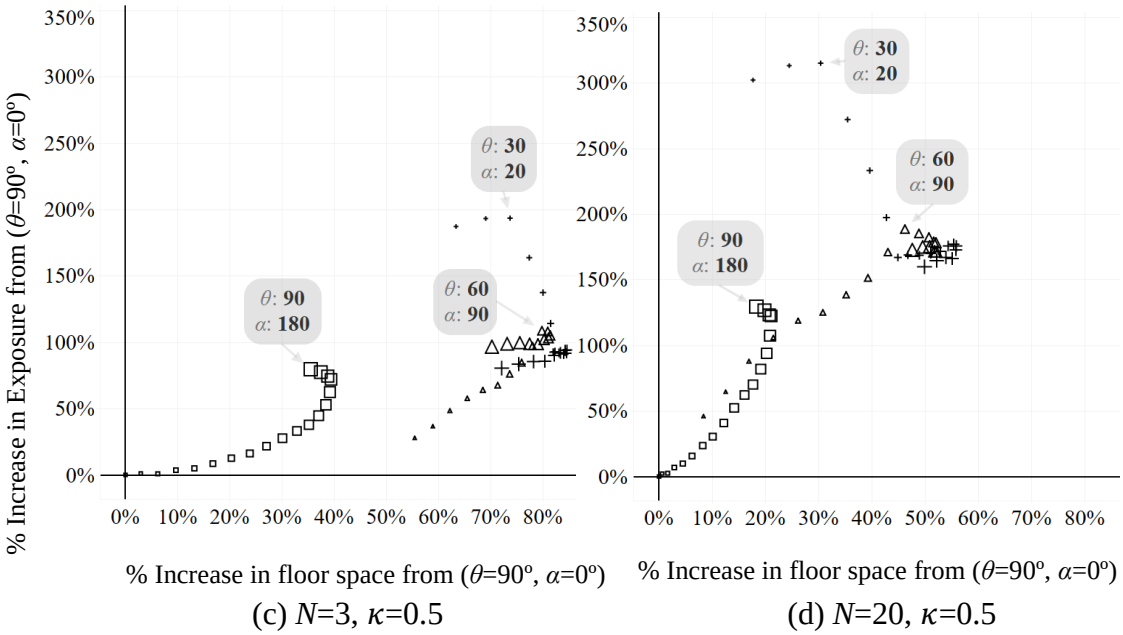

(c) N=3, κ=0.5 (d) N=20, κ=0.5

Figure 19. Exposure vs. layout area with small head rotations;
(a)-(b) = unidirectional and (c)-(d) = bidirectional

While in Section 4.2 we observed that varying both orientation (θ) and curvature (α) can increase exposure compared to layout with θ=90° and α =0°, Figure 22 illustrates that these benefits come with an increase in floor space. In Figure 19(a), where we assume small head rotations (Φ_{HR} + Ω_{HR} = 45°), unidirectional traffic (κ=1), and a layout of N=3 racks, we observe that the best design (θ=30°, α=10°) could result in nearly 320% increase in exposure over the (θ=90º, α=0°) design, but with a 69% increase in space. Similarly, the best designs for other values of θ (e.g., θ=60°, α=90° and θ=90°, α=180°), could increase exposure by 176% and 121%, but with floor space increases of 80% and 35%, respectively.

While the patterns between designs across the two layout sizes (N=3 vs. 20; Figures 19(a) and 19(b)) stay consistent, both the level of exposure and floor space requirements (compared to θ=90° and α=0°) become more favorable for medium-to-large rack layouts (i.e., N=20). That is, the % increase in exposure (relative to θ=90º, α=0°) *increases* and the

% increase in floor space *decreases*. For instance, the (θ=30°, α=10°) design with N=20 now could increase exposure by 540% with a 24% increase in floor space. We attribute the increased benefit of exposure to exposure patterns among the interior racks (i.e., not the first or last racks in a layout). Rack designs with (θ=90°, α=0°) appeared to result in low exposure on among such racks due to a high level of succeeding obstruction. In contrast, interior racks in alternate designs provided at maximum 605% higher exposure. Since increasing N from 3 to 20 increases the number of interior racks in a layout, the overall exposure difference increases. So considering a limit of floor space increase of, say, 10%, two feasible designs for N=20 would be (θ=60º, α=0°) and (θ=90º, α=70°), which would increase exposure by 88% and 58%, respectively (compared to θ=90º, α=0°).

When considering bi-directional traffic, we observed similar patterns as uni-directional traffic, however to a lesser extent (notice the scaling of the vertical axes in Figure 19 (c,d)). The best combination of θ and α (θ=30°, α=20°) appears to provide exposure increases of 193% (N=3) and 315% (N=20), but again with considerable increases in the required floor space of 74% (N=3) and 30% (N=20). Since bi-directional traffic essentially averages supplementary acute and obtuse orientations together, the exposure benefits obtained with acute orientations are diffused when paired with their respective obtuse orientation.

We also compared exposure and floor space considering large head rotations and observed that the % increase in exposure when increasing N from 3 to 20 remained rather stable (graphs not shown). Again, considering a 10% limit on floor space increase, the designs (θ=80°, α=0°) and (θ=60°, α=0°) can provide 80% and 48% increases in exposure for only 8% and 3% increases in floor space when N=20. We attribute the stable exposure

increase for an increasing N to the fact that the exposure values for all N racks (in designs where $\theta \leq 90°$) are nearly similar; there is no substantial increase in succeeding or preceding obstruction between the first and last racks, and the interior racks given the large head movement.

In summary, the tradeoff between exposure and floor space appears to be favorable to the retailer in situations where the expected shopper head movement is smaller compared to larger, and for larger sized layouts than smaller. The increase in exposure would likely offset the increase in space if products with high impulse purchase rates, high seasonality, or even promotional pricing were allocated to these prime, exposed locations.

2.6 Validation Study

To validate our proposed quantitative models presented above, we conducted a human subjects study in a virtual environment (VE); a high level summary will be presented in this section with additional details provided in Appendix E. The VE utilizes 27 LCD screens with LED backlight (each 55" in size) to achieve a 12x12 sq. ft. of walkable area at a height of 87 inches (Wischgoll et al., 2017). This provides a three-walled CAVE-type immersive display (see Figure 20). The optical head tracking system is composed of 11 cameras to provide maximal redundancy and accuracy. Using the head position, the system is able to recreate the user's perspective on all 27 displays in such a way that the user feels completely immersed in the scenario. The head

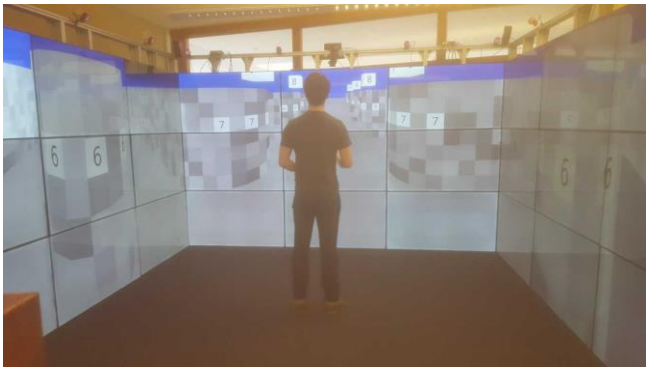

Figure 20. Virtual Environment

tracker also calculates both horizontal (x-axis) and vertical (z-axis) head movements for each human subject.

For our study, the scenario we developed in the VE corresponded to a rack layout of 10 racks on either side (a total of 20 racks in the layout), each placed at a prespecified orientation (θ) and with curvature (α). We recruited 27 participants between the ages of 19-26 who have had several years of prior shopping experience. We evaluated 9 rack layouts; 3 values each of θ and α (i.e., θ=45°,90°,135° and α=0°, 30°, 90°). Each participant evaluated all 9 layouts. For each layout, a participant was asked to identify targets (12, 1″x1″ red colored squares) strategically placed on the faces of the racks. The shopper travel was simulated by configuring the VE to move past the stationary participant at a speed of 3.33 fps (similar to 3.41 fps in Daamen (2004)). We simulated the typical bidirectional travel in a store by first letting the shopper experience the environment in one direction (forward), and then reversing the environment to let them experience the other direction (reverse) in the same layout, each time calling out the aisle number and side (left or right) when they saw a target.

To compare the actual human performance in these layouts with our model, we first predicted whether or not a target would be seen for a given layout (with identical placements of the targets). For this binary classification problem (target seen vs. not seen), we used several metrics; e.g., *true positive* (TP, model predicts participant will see, participant actually sees), *false positive* (FP, model predicts participant will see, participant does not see), *true negative* (TN, model predicts participant will not see, participant does not see) and *false negative* (FN, model predicts participant will not see, but participant sees). We then calculated the sensitivity and specificity, where sensitivity = $\frac{TP}{TP+FN}$, and

specificity = $\frac{TN}{TN+FP}$. In our problem, sensitivity refers to, 'among the targets the participant saw (TP+FN), what proportion did our model predict would be seen (TP)?' Contrarily, specificity refers to 'among the targets the participant *did not* see (TN+FP), what proportion of our model predicted *not to be seen* (TN)?' In other words, values of sensitivity lower than 1.0 suggest our proposed model underestimated human performance (for specific targets) and values of specificity lower than 1.0 suggest our model overestimated human performance (for specific targets). Figure 21 displays values of these three measures for each of the 9 different layouts (forward and reverse).

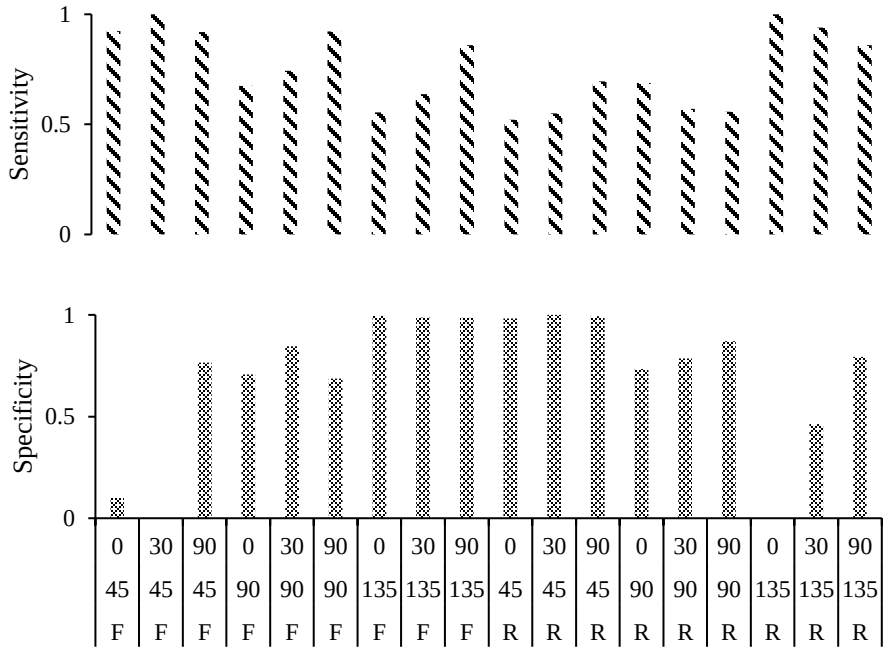

Figure 21. Sensitivity and Specificity of model performance.

Notice from Figure 21 that the sensitivity and specificity values seemed to have opposite trends in the forward and reverse directions; recall, a θ=135˚ (α=0˚) rack in the forward direction will appear as θ=45˚(α=0˚) in the reverse direction. We, therefore, will discuss results only for forward direction in detail. Considering sensitivity, notice that it is

high for acute orientations (average=0.95 across α=0˚, 30˚, 90˚ when θ=45˚) compared to obtuse orientations (average=0.68 across α=0˚, 30˚, 90˚ when θ=135˚). One explanation, is for acute orientations, the average participant head movement ranged from 8°-55° (we assumed 75˚ in our model, plus 15˚ eye rotation) causing nearly all of the targets that were predicted by the model actually being seen by the participants. We further noticed variations in scanning patterns by participants (i.e., how fast the head moved). This likely resulted in some participants seeing additional targets not predicted by the model (FN), causing the sensitivity to not equal 1.0. In contrast, for obtuse orientations in the forward direction, the average participant head movement ranged from 14-95, resulting in some participants seeing more targets that were not predicted to be seen by the model (FN) besides the predicted ones (TP); this reduced the sensitivity.

We further noticed a general trend of increasing sensitivity with an increase in rack curvature (α), as the number of FN decreased, and TP increased. An explanation for this outcome could be that the increased curvature creates sections of Face D that are impossible to see no matter how a participant turned their head, resulting in a more bounded environment.

In contrast, our proposed model's specificity had a noticeable increasing trend (forward direction) as the orientation changed from acute to obtuse, primarily because of the similar reasons discussed earlier. Note that the specificity values were relatively low for layouts θ=45˚, α=0, 30˚ (forward direction). This was because our model predicted that there would be 1 and 0 targets respectively not seen by the participants. This resulted low TN values, and hence low specificity values. Discounting these two layouts, we obtained a specificity of .85 across the remaining layouts.

In summary, we believe our model has reasonably high sensitivity and specificity across a majority of the layouts (barring extreme cases) to allow a retail designer to narrow down the search space to a set of promising layouts among myriad choices.

2.7 Conclusions

Exposure has been recognized as a key metric in designing retail layouts, but to date no quantitative model exists that effectively utilizes the shopper's 3D FoR (field of regard) to estimate exposure of a rack layout. Such a model would aid the retailer in comparing various layout designs and trading the corresponding exposure with floor space requirements.

As a key contribution of this paper, we propose such a quantitative model based on first principles to model the dynamics of a moving shopper's 3D FoR across a given rack design in order to estimate exposure and intensity. This model was used to analyze the impact of three primary parameters of a layout; i.e., rack orientation (θ), rack curvature (α) and rack height (H), considering uni- and bi-directional travel, small and large head movements, and small and medium-to-large layouts. The key managerial insights from our study include the following:

- When the racks are required to be oriented orthogonally to the shopper travel (i.e., θ=90°), use of curved racks in the layout could increase exposure (by 3-121%) over straight racks (α=0°).
- If such curved racks can be placed at any orientation, then there exist layouts that would further increase exposure (by 18-321%) over straight racks at 90º. If curved racks are not viable, then there exist orientations that allow achieving nearly this same increase in exposure.

- If the rack height (*H)* can be changed, then it trumps both orientation (θ) and curvature (α) in impacting exposure; rack heights just below eye-height appear to maximize exposure when the top of the rack is allowed for product allocation.
- The increase in exposure comes with a floor space tradeoff. Depending on the system parameters, it is possible to achieve nearly 530% increase in exposure with 18% floor space increase; 48% increase in exposure with a modest increase in space (<5%).

The implications of our model and findings can be critical to the retailers. Knowing how long specific locations on racks will potentially be exposed to the shopper could allow retailers to better allocate products to the racks, effectively showcase novel and high impulse products, and better match the expectations of a shopper with their shopping needs. The ability to quantitatively compare and contrast alternate layouts against exposure and space requirements could help avoid expensive experiments with layout changes, which would not only reduce their retail facility costs, but also help them meet their objectives (of increased sales and better shopper experience) promptly.

Future work in this area could include extending our approach to model other fixtures used in retail stores and estimate the resulting exposure. For instance, how do the presence of clothing racks or other unique rack designs affect overall exposure? How can we estimate exposure at an intersection of multiple aisles? How do different orientations effect shopper traffic and congestion through cross-aisles? Quantitatively linking exposure to expected sales and then maximizing it through an appropriate optimization approach is an interesting research endeavor. We expect this research to trigger many more questions and solutions for retail store design that not only benefit the retailers, but also the shoppers.

3 Optimizing Rack Orientation and Curvature to Maximize Marginal Impulse Profit

3.1 Introduction

Retail stores encompass many supporting features that lead to a suitable environment for shoppers. Dunne et al. (1995) suggest visual communications (e.g., signage, commercials), merchandising (e.g., product presentation), store design (e.g., ambiance, lighting), and store planning (e.g., layout, category planning) as the four primary factors. Among these, store planning is considered the organizational structure of the store, effectively dictating the way shoppers interact with the products during their shopping trip.

Layout design, the vital backbone of store planning, includes decisions such as department location, aisle arrangement, and shelf orientation. These decisions affect shopper traffic density along the aisles, trip length, and what products shoppers will be exposed to (i.e., product *exposure*) (Dunne et al., 1995; Peters et al., 2004). Exposure has long been observed to have a significant relationship with revenue, as shoppers will ultimately only buy what they see (Suher and Sorensen, 2010; Ebster and Garaus, 2015). Since shoppers only visit 16% of the store in hypermarkets (e.g., Walmart, Kroger) and 30% in smaller supermarkets (e.g., Whole Foods, Food Lion), it becomes imperative to consider exposure when designing a layout (Sorensen, 2017).

The limited retail layout design approaches that consider exposure as a metric, however, have used approximations under narrow criteria. Such approximations include prespecified deterministic functions of (i) customer traffic (i.e., frequency of visits, density) and product shelf length (Botsali and Peters, 2005; Flamand et al., 2016) (ii) customer

traffic and department size (Yapicioglu and Smith, 2012) (iii) distance from the shopper (Li, 2010) or (iv) walking past a department (Ozgormus, 2015). These approximations are further limiting as they assume the environment to be fixed (i.e., rectangular racks orthogonal or parallel to the shopper). Since humans have a constrained field of regard (i.e., horizontal and vertical eye and head movements) through which they see, simply walking past a rack location may not be sufficient for the shopper to actually see it. For instance, a location on the bottom shelf, or one on the back side of a rack facing *away* from a walking shopper could be challenging or impossible to see.

Only recently have models for exposure been proposed that account for the dynamic interaction between a traveling shopper's field of regard and a rack layout, as specified by rack orientation and curvature (Mowery et al., 2017; Guthrie and Parikh, 2018). The approach in the latter study estimated which locations were exposed, and for how long, for both standard straight racks and newer curved rack designs currently in use at a wide variety of retailers (see Figure 22). They also show that a location's time of exposure is dependent on the *visual* distance (based on shopper's depth of view) and alignment (based on shopper's field of regard)

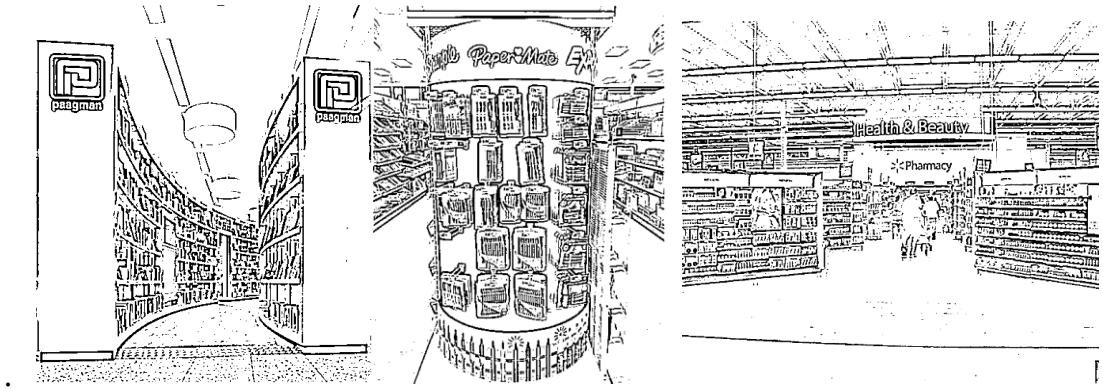

(a) (b) (c)

Figure 22. Rack layouts with (a) curved racks (b) curved endcaps (c) non-orthogonally oriented racks.

It is vital, however, to quantify increases in exposure of products using a measure that retailers can act on, such as increases in revenue or profit, to evaluate layout changes or explore new rack designs. While planned purchases are primarily independent of layout (shoppers will search for them), unplanned, or 'impulse' purchases have been shown to be highly dependent on how well products are exposed to shoppers (Iyer, 1989; Abratt and Goodey, 1990; Peck and Childers, 2006). That being said, we do not know of an approach that translates exposure to impulse purchases considering the human FoR. Our research attempts to fill this void by incorporating the dynamic interaction between a traveling shopper's FoR and a rack layout to directly estimate the probability of a shopper visually connecting with products (from here on, product *categories*) on racks This helps us address the following questions: *How do specific layout design factors (e.g., rack orientation and curvature) affect expected impulse purchases? How sensitive is the best rack design to the product category location policy, traffic direction, maximum layout aspect ratio, cost of floor space, and shopper volume?*

We make the following contributions in addressing these questions. *First*, we propose a non-linear optimization model, referred to as the Rack Orientation and Curvature Problem (ROCP), that determines the optimal rack orientation and curvature to maximize marginal impulse profit (after discounting for floor space) for a given location policy (i.e., within aisles) of product categories. Impulse profit is estimated based on the probability that a product category on the shelf is seen, impulse purchase rate of that product category, and its average unit profit. We consider four different location policies commonly found in either practice or literature for given product assortment and shelf space allocation decisions (i.e., number of facings). *Second*, to help estimate impulse profit, we derive a

probabilistic measure for a product category being seen, referred to as *visibility*, based on the effective area of locations, distribution of actual shopper head positions (from a prior human subjects study), and exposure estimates from our prior work (Guthrie and Parikh, 2018). *Third*, because the derivation of exposure estimates is algorithmic and cannot be expressed in closed-form, we propose an effective heuristic based on particle swam optimization framework and demonstrate its performance against a grid search approach. *Finally*, we derive several insights related to layouts that maximize marginal impulse profit and evaluate the sensitivity of these solutions to product category location policy, maximum aspect ratio, floor space cost, and shopper volume.

Based on our experimental study, we observed that variations in rack orientation (θ) and rack curvature (α) from orthogonal and straight racks can increase marginal impulse profit as much as 70% or 233% depending on the product category location policy. Further, the best layouts consisted of racks that were generally high-acute and low-to-medium-curved or high-obtuse and high-curved. These layouts exhibit a relatively large percentage of locations with either high or moderate visibility. Considering the location policies of product categories, we found the Impulse Rule to outperform the Demand Rule for *absolute* marginal profit; this ranking is reversed considering the *relative* improvement of the best layouts compared to orthogonal and straight racks. We also analyzed the sensitivity of maximum aspect ratio, shopper volume, and floor space cost. Relaxing the aspect ratio constraint allowed the best orientation (θ) to become more acute or obtuse; curvature (α) also generally increased. Further, the best combinations of θ and α (high-acute and low-to-medium-curved or high-obtuse and high-curved) were generally robust to variations in

shopper volume and floor space cost. Only for low shopper volumes and high floor space costs did orthogonal and straight racks become more attractive.

We now present details of our research with the following outline. Section 2 summarizes relevant literature in the areas of retail layout and shelf space allocation. Section 3 presents our proposed optimization model for ROCP and an approach to estimate the probabilistic visibility measure required to solve this model. Section 4 discusses a particle swarm optimization approach to solve the ROCP model. Section 5 discusses the performance of this approach and presents key insights derived from our experimental study. Finally, we summarize the implications of our research and discuss potential future endeavors in Section 6.

3.2 Literature Review

Many studies have alluded to a strong relationship between exposure and revenue (Applebaum, 1951; Cairns, 1962; Granbois, 1968; Dreze et al., 1994; Dunne et al., 1995; Knox et al., 2011; Hui et al., 2013). Several eye-tracking studies have investigated this phenomenon further by analyzing how shoppers interact with retail layouts and products. Janiszewski et al. (1998) and Pieters and Warlop (1999) found a significant relationship between the time customers were exposed to certain products and the selection decisions of those products. Chandon et al. (2006) found that the number of product fixations increases the probability that a shopper will consider that product for purchase. Sorensen (2009) utilize eye tracking to find a substantial drop-off in exposure from end-aisle displays and free-standing racks to all other display types. Further, Hendrickson and Ailawadi (2014) use eye-tracking to discover several shopper habits related to vertical eye fixation patterns, attention span, product consideration set, and reading patterns.

While marketing literature has provided ample evidence for the significance of exposure, only a few studies in the IE/OR domain have incorporated exposure into retail layout problems. Peters et al. (2004) propose a mathematical model to maximize expected store revenue by finding a balance between the time a customer spends in the store and the number of products they are exposed to along their path. In this study, if a shopper simply walks past a product, it is considered 'exposed.' Botsali and Peters (2005) extend this work to formulate a network-based model where they maximize expected store revenue in a serpentine layout. They use a visibility measure that is a function of a product's shelf length and number of shopper visits. Li (2010) proposes a sequential design process for a retail layout; the dimensions of the racetrack layout are found that maximizes exposure in the first stage. To model exposure, they suggest a decay function in terms of distance from the main aisle, considering surrounding shopper traffic as well. Yapicioglu and Smith (2012) develop a bi-objective optimization model to determine the size and location of each department in order to maximize revenue and department adjacency scores. They assume exposure to be a function of the department location with respect to *pre-defined* traffic zones in the store as well as the department size; i.e., high departmental exposure is associated with a large area and its location within a high traffic zone. Recently, Mowrey et al. (2018) propose a non-linear optimization model to maximize exposure of a rack layout in 2D under space constraints. This model determines the number of rack columns in the layout and the angle of orientation for each column using a metaheuristic approach. Although their exposure estimates account for the shopper's field of regard, as proposed in their prior work (Mowrey et al., 2017), they are limited to rectangular racks, each above shopper eye-height. Guthrie and Parikh (2018) address these limitations in evaluating the

effect of rack orientation, curvature, and height on exposure in 3D and suggest there are benefits to gain through non-orthogonal orientations and curvature of racks.

Another area of research in store planning is category planning. Literature in this area has focused on product assortment, shelf space planning, and replenishment decisions (Hubner and Kuhn, 2012). Shelf space planning specifically determines *how much* shelf-space (i.e., shelf space allocation) each product requires, and specifically *where* products should be placed (i.e., shelf location). Similar to layout design, shelf space planning also directly affects the level of visual interaction a shopper has with specific products; it has been shown to be directly linked to revenue through several empirical studies (Curhan, 1972; Desmet and Renaudin, 1998).

Many optimization approaches have addressed aspects of shelf space planning; see Hübner and Kuhn (2012) for in-depth review. More recently, Bai et al. (2013) present a 2D (height and length) shelf-space allocation model and solve using a hyper-heuristic approach. Geismar et al. (2015) further consider a similar 2D problem by allowing product displays to extend multiple shelves. Further, Flamand et al. (2016) formulate an optimization approach to maximize profit from impulse purchases considering location and space allocation decisions for product categories. Flamand et al., (2017) extend this work to include assortment decisions and considerations for product affinities.

Our review of literature in these two domains reveals the following gaps. *First*, a model to estimate visibility directly from the shopper's FoR, shopper head movement, and effective area of rack locations has not been explored. *Second,* the impact of location policies that modify visibility of product categories for a given layout has not been fully addressed. *Third*, an optimization approach that combines the above features, while

considering floor space, to determine the rack layout that maximizes marginal impulse profit is lacking. And *finally*, the impact of traffic direction, shopper volume, floor space cost, and maximum aspect ratio on the best layouts is yet to be studied. Through this research, we address these gaps in an effort to better connect retail layout and category planning literature. In the sections that follows, we present details of our modeling approach.

3.3 Modeling Marginal Impulse Profit

We define marginal impulse profit as the expected annual profit from impulse purchases (discounting cost of floorspace). Our proposed mathematical model determines the optimal values of rack orientation and curvature to maximize marginal impulse profit, accounting for the visibility of a specific layout. For a given product assortment (with known number of facings), we consider several policies to locate product categories on the racks. In the subsections that follow, we present the following: (i) a procedure for layout design (ii) a mathematical model for marginal impulse profit, and (iii) an approach to estimate visibility.

3.3.1 Layout Design

The layouts we consider consist of a series of generic curved gondolas (referred to as racks) on both sides of a main aisle (see Figure 23). The racks are identical, each with width (W), perimeter (M) measured along the top face of the rack, height (H), curvature (α) and curved endcaps. Each rack is further represented in terms of 4 faces; i.e., inner face (B), outer face (D), and two endcaps (A and C). Because we fix shelf space (or total display area), the radius of curvature (R) for a rack varies with angle of curvature (α); i.e., $R=\frac{90*(M-\pi W)}{\alpha\pi}$. Observe that when $\alpha \rightarrow 0^{\circ}$, $R = \lim_{\alpha\to 0} \frac{90*(M-\pi W)}{\alpha\pi} \rightarrow \infty$.

To then design the layout, we place each rack at a prespecified orientation ($0^o \leq \theta \leq 180^o$) ensuring a minimum distance between racks (*Ac*) and a width of the main walking aisle (*Aw*). The distance of the shopper to the nearest part of the racks is represented as *Am*.

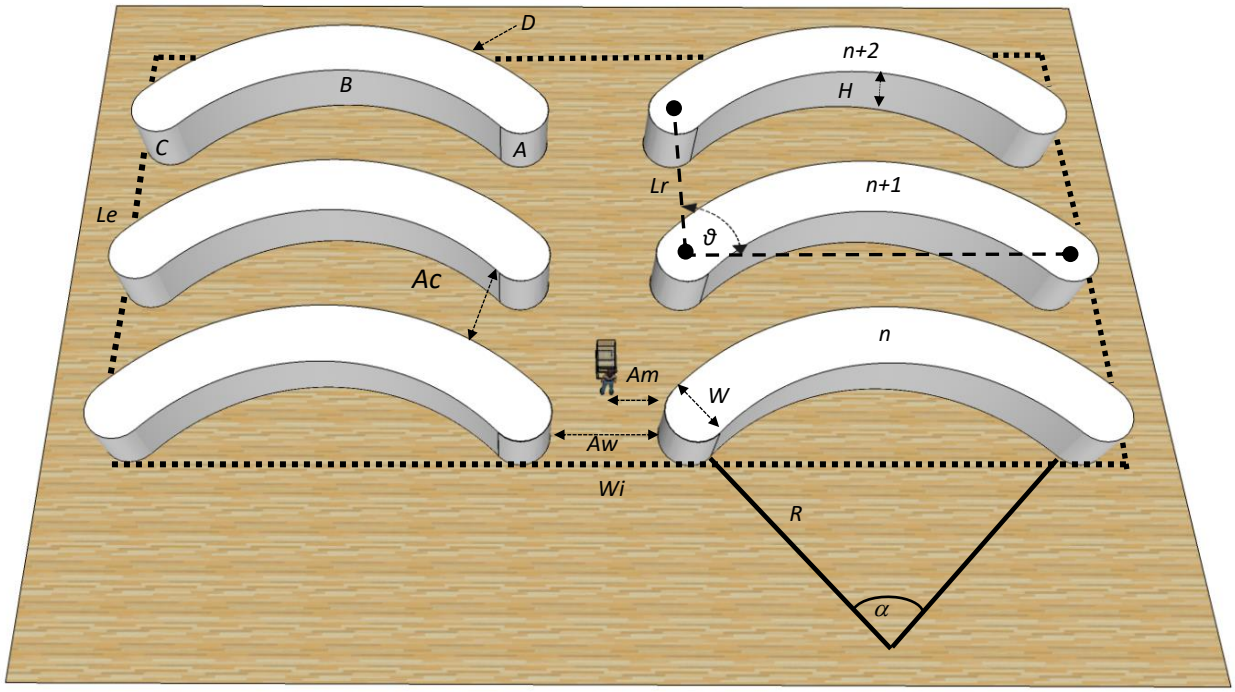

Figure 23. Layout design for ROCP

The procedure to design a feasible layout (i.e., determine the distance between successive racks (*Lr*) to ensure *Ac* is achieved) with a given set of parameters is discussed in Guthrie and Parikh (2018). To derive the area (*al*) and aspect ratio (*ar*) of our layout, we find the smallest bounding box that encapsulates the layout (both sides). Area is then simply the length × width (i.e., *Le* × *Wi*) of this bounding box, while the aspect ratio is length ⁄ width (i.e., *Le*/*Wi*)

With this representation of the layout, we now present a mathematical model to maximize marginal impulse profit.

3.3.2 A Mathematical Model for Marginal Impulse Profit

We define the Rack Orientation and Curvature Problem (ROCP) as the determination of optimal rack orientation and curvature for a layout that maximizes expected marginal impulse profit (after discounting cost of space). We assume that:

- All racks are identical (in terms design parameters) and are placed at the same orientation.
- Shoppers walk down the main aisle (in discrete steps) past the racks on route to a location specific to a planned purchase.
- Planned purchases remain unchanged with changes in the layout, since the total display area in the layout is unchanged resulting in identical product types and inventories.
- We consider *dynamic* product location decisions; i.e., product location decisions are dependent of the layout.

Below we present our mathematical model, followed by Tables 4 and 5 that summarize the parameters and decision variables, respectively, used in our model.

Maximize: $D*S*(\sum_p^P P_p\, T_p \nu_p) - (C*al)$

Subject to:

$$\nu_p = f(z_{pl}, \nu_l, F_p) \quad (1)$$

$$\nu_l = f_1(W, R, Ac, Am, Aw, \alpha, \theta, H, N, DOV, \Upsilon, \omega, S_E, Lh, Lw, g(\Omega_H, \Omega_V)) \quad (2)$$

$$a_l = f_2\,(W, R, Ac, Am, Aw, \alpha, \theta, H, N, Lh, Lw) \quad (3)$$

$$a_r = f_3\,(W, R, Ac, Am, Aw, \alpha, \theta, H, N, Lh, Lw) \leq Ar_{MAX} \quad (4)$$

$$\alpha \in [-180°, 180°] \quad (5)$$

$$\theta \in [0°, 180°] \quad (6)$$

Table 4. Parameters used in model

Notation	Definition
p	Index for product category; p = 1, 2. …, P
l	Index for location; l = 1, 2, …, L
P_p	Average unit profit of products in category p ($/unit)
T_p	Probability of purchasing a product from category p if seen (i.e., impulse purchase rate)
F_p	Number of locations l allocated to product category p
C	Annualized cost of floor space for the layout ($/ft^2)
D	Number of days a retail store is open per year
Ar_{MAX}	Maximum allowable aspect ratio for the layout
H, W, M	Height, width, and perimeter of racks (ft)
Ac	Minimum distance between successive racks (ft)
Aw	Width of main aisle (ft)
Am	Perpendicular distance of shopper from the rack endcaps (ft)
Lh, Lw	Height and width (ft) of a discrete product location on rack
S	Daily number of shoppers
S_E	Shopper's eye height (ft)
ω	Shopper's walking speed (fps)
ρ	Eye fixations per second (fps)
DOV	Shopper depth of vision (ft)

Table 5. Decision variables in the model

Notation	Definition
v_p	Probability of visibility for product p during the shopping path
v_l	Probability of visibility for location l during the shopping path
z_{pl}	Assignment of product p to location l; 1, assigned; 0, unassigned
al	Rectangular area of layout (ft^2)
ar	Aspect ratio of layout
θ	Orientation of racks (º)
α	Curvature of racks (º)

The objective of the ROCP is to maximize expected marginal impulse profit (i.e., the difference between expected impulse profit and cost of floor space). To estimate expected impulse profit per product category, we use (i) visibility (i.e., the probability a shopper will see product category p at least once as they walk past a layout). (ii) impulse

purchase rate (i.e., probability a shopper will purchase a product from category *p* if seen), and (iii) unit profit (i.e., average expected profit across all products in that category considering quantity of products purchased). We assume that (ii) and (iii) are known by the retailer a priori based on historical sales, and so we focus on estimating (i), which is dependent on the variations in the rack layout (see Section 3.3 and 3.4 for details).

Constraint (1) estimates a product category's visibility (v_p) using the location assignments of each product category (z_{pl}) and the visibility of each location (v_l). Because v_l in Constraint (2) is based on the cumulative effect of a shopper walking past the rack layout, it is difficult to estimate this value in a closed-form, and so we use the approach suggested in Guthrie and Parikh (2018). The function $g(\Omega_H, \Omega_V)$ is the distribution of shopper angular head positions derived from a prior human subjects study; see Section 3.4. Constraints (3) and (4) derive the area of floor space and aspect ratio of the layout (from Guthrie and Parikh, 2018), where we restrict aspect ratio to a maximum aspect ratio of Ar_{MAX}. Finally, Constraints (5) and (6) indicate bounds on the decision variables.

3.3.3 Estimating the Probability, v_p

Recall that v_p is the probability of product *p* being seen at least once during the shopper's path. We define 'seen' as a fixation of the shopper's focal point on product category *p*, such that a discrete step *y* on a shopper's path corresponds to one possible fixation. To find v_p, we first estimate the probability of seeing a location *l* at step *y* (say, v_{ly}). The cumulative effect of v_{ly} across all shopper steps *Y* during the entire shopper path will allow the estimation of v_l; the probability of seeing a location *l* along the travel path. We can then estimate v_p using v_l and the assignment information, z_{pl}. We now present details of how we estimate these probabilities; v_{ly}, v_l, and v_p.

Consider a shopper walking past the layout at a speed of ω ft/s, where they make ρ eye fixations per second (fps). If we let x be the number of times the shopper's focal point falls on location l throughout the path, then x follows a Poisson Binomial distribution with independent success probabilities v_{ly} for y = 1, 2, …, Y steps. Note that if v_{ly} are all identical, then x would follow a Binomial distribution. But these probabilities are not necessarily the same, as discussed in Section 3.4. Per the Poisson Binomial distribution, the probability of 'not' seeing location l, P(x=0) = $\prod_{y=1}^{Y}(1 - v_{ly})$. Subsequently, the probability of seeing location l at least once, $v_l = P(x > 0) = \left(1 - \prod_{y=1}^{Y}(1 - v_{ly})\right)$.

Finally, to estimate v_p, we again use the Poisson Binomial distribution and let x_p equal the number of times the shopper sees a location l that contains product category p. We let s_p and e_p represent the minimum and maximum values of consecutive locations where product category p is located; these are derived from product category location decisions z_{pl}. Accordingly, $v_p = P(x > 0) = (1 - \prod_{l=s_p}^{e_p}(1 - v_l))$. That is, v_p is dependent on the total shelf locations allocated to product category p (i.e., F_p), and *where* on the rack these locations l exist. Figure 4 illustrates an example placement of product categories A-G on Face B (inside face facing a shopper) of a rack (assuming each location is 1ft × 1ft in size). We also illustrate how we derive s_p and e_p from z_{pl}. Red shaded locations indicate higher values of v_l for Figure 24 (a) and higher values of v_p for Figure 24 (b). We now present details of how we estimate v_{ly}.

$z_{Al} = 1 \; for \; l \in [1,35] \Rightarrow s_A = 1$ and $e_A = 35$

(a)

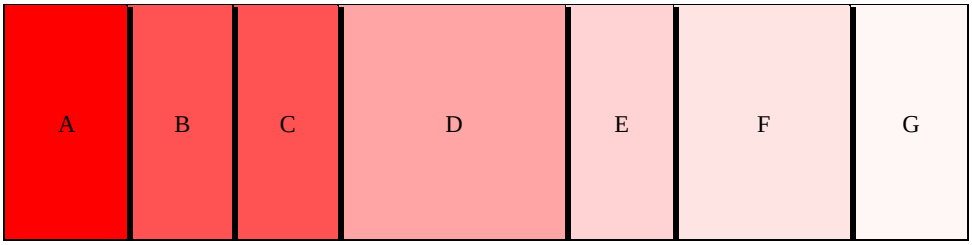

$v_A = (1 - \prod_{l=1}^{35}(1 - v_l))$ and $v_B = (1 - \prod_{l=36}^{70}(1 - v_l))$

(b)

Figure 24. (a) v_l for locations; (b) v_p for products

3.3.4 Procedure for Deriving v_{ly}

We derive v_{ly} by (i) calculating the angular coordinates (horizontal and vertical) of each corner point corresponding to each location l to determine the effective (i.e., angular) area visible to the shopper, (ii) deriving the probability of the shopper's focal point falling within this effective area using data from a prior human subjects study, and (iii) overlaying the distribution from (ii) over the effective area for each location l. For (i), first let S_x, S_y, and S_E represent the Cartesian coordinates for the shopper location, x_{li}, y_{li}, and z_{li} represent the Cartesian coordinates for the four vertices of location l, where i=1,2,3,4 are indicators for each vertex. Also, let Ψ_{li} and Γ_{li} represent the horizontal and vertical angles from the shopper's eye to each of the four vertices for location l. For a given shopper height, S_E, we

can calculate $\Psi_{li} = \sin^{-1}\left(\frac{x_{li}-x_s}{B_{li}^{S_E}}\right)$ and $\Gamma_{li} = \sin^{-1}\left(\frac{|z_l-S_E|*Lh}{B_{li}}\right)$, where $B_{li}^{S_E}=\sqrt{(y_{li}-y_s)^2+(x_{li}-x_s)^2}$ and $B_{li}=\sqrt{\left(B_{li}^{S_E}\right)^2+(|z_l-S_E|*Lh)^2}$. $B_{li}^{S_E}$ represents the Euclidean distance (in 2 dimensions) between the shopper's eye and the point on the rack at eye-height directly below the vertex of location *l* denoted by indicator *i*. B_{li} meanwhile is the Euclidean distance (in 3 dimensions) between the shopper's eye and the vertex of location l denoted by *i*. See Figure 25 for an illustration of how the angular coordinates $\Psi_{l=1,i=1}$ and $\Gamma_{l=1,i=1}$ are found at a step *y* assuming an eye height (S_E) of 5 ft. This process is repeated at each step *y* as the shopper's angle and distance to location *l* will change with every step.

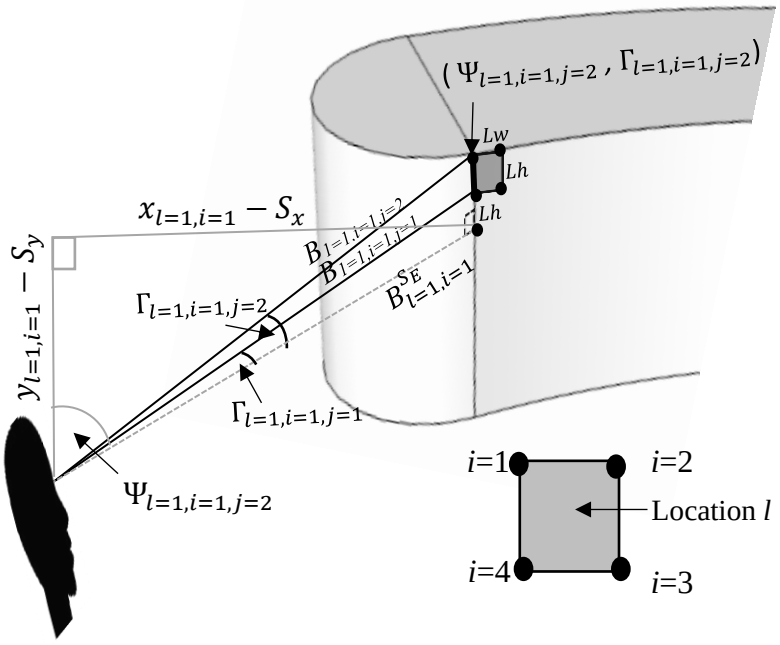

Figure 25. Determining angles for vertices of location *l*

For (ii), we derive the probability distribution for the angular position of the shopper focal point at any given step using data obtained from a prior human subjects study (Guthrie et. al., 2018). Essentially, we designed a virtual environment to simulate a retail store with 10 racks on each side. We placed a total of 12 red-colored squares (1″×1″ in size)

on these racks, strategically placed on the front (B) and back (D) faces at distinct rows (i.e., heights) and columns (i.e., distance from main aisle). We then recruited 18 participants to locate these targets in this virtual store section. We simulated walking by moving the environment past the stationary participant at the speed of 3.33 ft/s. We recorded the head position, using a head tracker, both horizontal (Ω_H) and vertical (Ω_v) angular coordinates at a refresh rate of 60 Hz (once every 0.016 seconds).

We then compiled the head tracker data for each of the 18 participants who evaluated a layout with straight racks (α=0˚) oriented at 90˚ and discretized the horizontal and vertical head positions (across the entire path) into 0.25˚ range bins. We further added 15˚ in both horizontal and vertical directions to account for potential eye movements and recorded the corresponding frequency (F_{Ω_H,Ω_V}) of head positions aggregated across all steps *y*. These frequencies were then converted to a probability distribution $g(\Omega_H, \Omega_V)$ associated with a shopper's focal point falling in the direction (Ω_H, Ω_V); $\Xi_{\Omega_H,\Omega_V} \sim g(\Omega_H, \Omega_V)$ and $\mathrm{p}(\Xi_{\Omega_H,\Omega_V}) = \frac{\mathrm{F}_{\Omega_H,\Omega_V}}{\sum \mathrm{F}_{\Omega_H,\Omega_V}}$. Figure 26 shows the resulting probability distribution, where darker shades indicate higher probabilities, while lighter shades indicate lower probabilities.

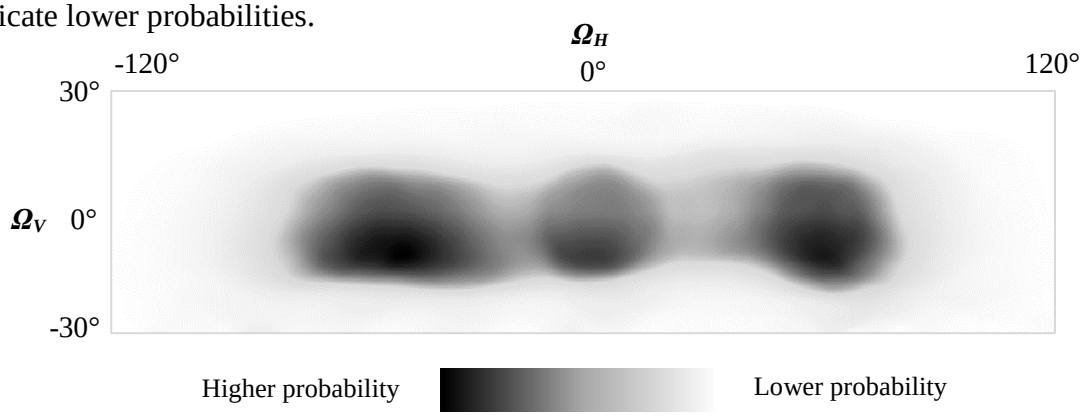

Figure 26. Probability distribution of shopper focal point direction; Ω_H =0° and Ω_V =0° indicate a shopper looking straight ahead.

Finally, for (iii) – the probability of a shopper's focal point falling on each location *l* at each step *y* (v_{ly}) – we aggregate the probabilities of a shopper's focal point falling on to the effective area of a location. Specifically, we sum the probabilities of all the discrete intervals in the distribution set that fall within the rectangular boundaries dictated by the four angular coordinates of each location *l*. However, not all locations with non-zero probabilities will be exposed at a step *y*. In other words, a location may be obstructed (i.e., blocked by another rack) or outside the shopper depth of vision (i.e., too far away to be clearly seen). Thus, we define E_{ly} as a binary indicator of whether location *l* is exposed at step *y* (based on the approach presented in Guthrie and Parikh (2018)). Consequently, $v_{ly} = E_{ly} * \sum_{\Omega_H,\Omega_V}(\Xi_{\Omega_H,\Omega_V})$ such that $\min\{\Psi_{h,i}, \Psi_{h+1,i}\} \leq \Omega_H \leq \max\{\Psi_{h,i+1}, \Psi_{h+1,i+1}\}$ and $\min\{\Gamma_{h,i}, \Gamma_{h,i+1}\} \leq \Omega_V \leq \max\{\Gamma_{h+1,i}, \Gamma_{h+1,i+1}\}$. Note that the shopper's focal point may not always fall on the rack location as the head may be pointing in directions with no rack locations (e.g., straight forward or in between two racks); i.e., for each step *y*, $\sum_l v_{ly} \leq 1$. Figure 27 illustrates how we overlay the distribution of shopper's focal point on the effective area of a location. The resulting v_l for each location on a rack (i.e., $1 - \prod_{y=1}^{Y}(1 - v_{ly})$) across the entire layout is illustrated in Figure 28.

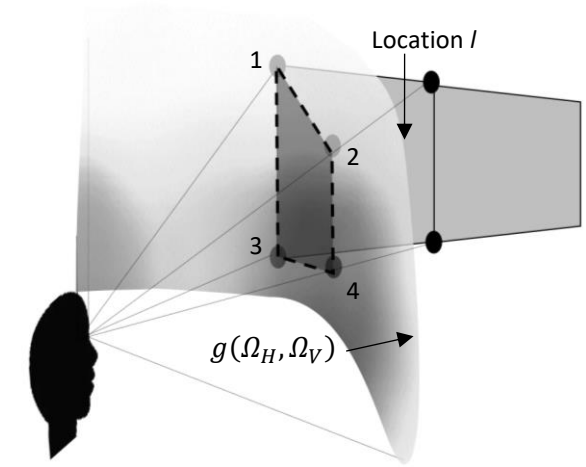

1: ($\Psi_{l,i=1,h=2}$, $\Gamma_{l,i=1,h=2}$) 2: ($\Psi_{l,i=2,h=2}$, $\Gamma_{l,i=2,h=2}$)
3: ($\Psi_{l,i=1,h=1}$, $\Gamma_{l,i=1,h=1}$) 4: ($\Psi_{l,i=2,h=1}$, $\Gamma_{l,i=2,h=1,}$)

Figure 27. Overlaying shopper head position distribution with location *l*

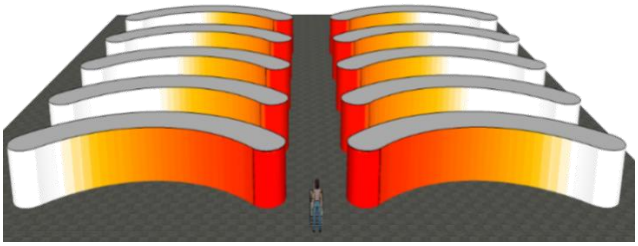

Figure 28. Probability $\boldsymbol{v_l}$ of layout with θ=90°, α=90°;. Red areas indicate locations with higher values of $\boldsymbol{v_l}$.

3.4 A Particle Swarm Optimization Algorithm for the ROCP

It is evident by now that commercial solvers would not be viable to solve the mathematical model for the ROCP given the non-closed form nature of Constraints (1) and (2). We, therefore, propose a metaheuristic approach based on particle swarm optimization (PSO).

3.4.1 PSO Description

PSO was introduced by Kennedy and Eberhart (1995) as a population-based stochastic optimization technique. The key benefits of using PSO are that it can search within a continuous space, is simple and easy to implement, and provides a good balance between solution speed and quality (Shi & Eberhart, 1998, Bansal et al., 2011; Jolai et al., 2012). PSO employs a finite number of particles, each carrying knowledge of its own solution history, searching through the solution space until convergence. Below is an outline of our proposed PSO algorithm:

Initialize population of particles with random positions and velocities
Do
For each particle:
Evaluate feasibility (i.e., max aspect ratio) of the encoded solution (*Layout Design* subroutine)
If Feasible:
Estimate v_l (*Location Visibility* subroutine)
Place products on rack per location rule (*Product Category Placement* subroutine)
Estimate v_p (*Product Category Visibility* subroutine)
Evaluate fitness function
If fitness value is greater than global best:
Set current solution as global best
If fitness value is greater than neighborhood best:
Set current solution as neighborhood best
If fitness value is greater than particle best:
Set current solution as particle best
Else: Reject solution
End
For each particle:
Update particle velocity
Update particle position
End
Until termination criterion is met

3.4.2 Solution Representation

We use a swarm of 10 particles, with each particle representing a candidate layout determined by the two decisions variables, $\{\theta, \alpha\}$. At each iteration, for each particle (i.e., candidate layout), the *Layout Design* subroutine creates a rack layout for the specific combination of θ and α; the resulting area of floor space and aspect ratio is also calculated. If the aspect ratio of this layout is within the maximum limit (Ar_{MAX}), then the particle is considered feasible and three additional subroutines are called. First, the *Location Visibility* subroutine estimates v_l (the probability that location l is seen at least once by the shopper) for all locations. Second, the *Product Category Placement* subroutine then assigns product categories to rack locations l for a given location policy (see Section 5.2 for details).

Finally, the *Product Category Visibility* subroutine estimates v_p (the probability that product category *p* is seen at least once by the shopper) for all product categories. Finally, the objective function is computed for this particle as $S(\sum_p^P P_p T_p v_p) - C*al$.

The resulting expected marginal impulse profit is compared to the particle's best solution, the neighborhood's best solution, and the global best solution. The particle's best solution is the best solution of that particle found across all iterations. The neighborhood best solution is the best solution found among a finite set of particles, where each particle communicates information of its best solution to all particles in its neighborhood. We use a nearest neighbor topology of 3 particles, where each particle *i* shares a neighborhood with particles *i*+1 and *i*-1 (Kennedy, 2007). This strategy dissuades particles from immediately swarming to the first good solution that is found (Kennedy, 2007; Yapicioglu et al., 2007). The global best solution, meanwhile, is the best solution found among all particles across all iterations.

3.4.3 Solution Updating

The particles in our proposed PSO explore the search space while utilizing information of their personal history (i.e., particle best) and the history of particles in their neighborhood (i.e., neighborhood best). At each iteration *t*, the dimension *d* of particle *i* has a position x_{id}^t. This position is based on the particle's previous position (x_{id}^{t-1}) and its velocity (v_{id}^t), where $x_{id}^t = x_{id}^{t-1} + v_{id}^t$. The velocity is computed using the following information across all particles: previous velocity (v_{id}^{t-1}), previous position (x_{id}^{t-1}), personal best solution (p_{id}), and neighborhood best solution (g_{id}), as $v_{id}^t = K(v_{id}^{t-1} + c_1 r_1(p_{id} - x_{id}^{t-1}) + c_2 r_2(g_{id} - x_{id}^{t-1})$. The variables r_1 and r_2 are random numbers, uniformly distributed [0,1]. We further let *K* represent the construction coefficient (Clerc,

1999), which assists particles to converge faster. We let c_1 and c_2 be the acceleration constants. Per Clerc and Kennedy (2002), we set $c_1 = c_2 = 2.05$ and $K = 0.7298$. We additionally incorporate limits on velocity for both orientation (V_{max}^{θ}) and curvature (V_{max}^{α}), where -180º $\leq V_{max}^{\theta} \leq$ 180º and -180º $\leq V_{max}^{\alpha} \leq$ 180º. These limits are created based on the range of feasible values for both θ and α, and are included to prevent the particle's velocity increasing (decreasing) to infinity (negative infinity). In our experiments, the PSO is considered 'converged' if the global solution does not improve for 10 successive iterations.

3.5 Experimental Study

Having presented our approach to model and solve the ROCP problem, we present details of our input data and location policies, followed by an experimental study using our PSO.

3.5.1 Data

Demand data over a 1-month period was acquired from a U.S. grocery store across 11,807 products, along with product dimensions (LxWxH), number of assigned shelf facings, and designated aisle. The grocer preassigned each product to an appropriate product category. Using available price and cost data for 670 of these products, for each product category (84 in total) we derived an average cost and price. Average profit for each product category was calculated by subtracting average cost from average price. Impulse purchase rates for product categories, meanwhile, are based on estimates used in Flamand et al., (2016). A table containing attributes for each product category can be found in Appendix F. We note that while we use product categories to derive insights in our

experimental study, applying our model on a product level would be possible given the necessary data.

3.5.2 Product Category Location Policies

Our PSO algorithm accepts an assignment of product categories to an aisle and the number of 1 ft x 1ft locations on the rack. Splitting of product categories within aisles is not allowed. To assign product categories to specific locations (within their respective aisle), we developed four location policies based on a location rule (i.e., how attractive is each location) and an ordering rule (i.e., in what order should product categories be placed into the most attractive locations). The specifics of each location policy are in Table 6.

Table 6. Location policies.

Location Policy	*Location Rule*	*Ordering Rule*	*Description*
Distance-Demand	Distance	Demand	Products categories in order of decreasing demand (within each aisle) are assigned to locations closest to the main aisle
Distance-Impulse	Distance	Impulse	The product of impulse purchase rate and average unit profit (i.e., impulse potential) is found for each product category, and product categories are assigned in decreasing order to locations closest to the main aisle
Visibility-Demand	Visibility	Demand	Products categories in order of decreasing demand (within each aisle) are assigned to locations with the highest visibilities (v_l)
Visibility-Impulse	Visibility	Impulse	The product of impulse purchase rate and average unit profit (i.e., impulse potential) is found for each product category, and product categories are assigned in decreasing order to locations with the highest visibilities (v_l)

Demand is widely utilized by both retailers and researchers as an ordering metric to place products (or product categories) on shelves; providing shoppers the opportunity to easily find the products they are looking for can positively impact shopping experience (Richins, 1997). Impulse purchase rate and profit have also been discussed as measures to rank products for location decisions (Flamand et al., 2016). We use these two approaches as the ordering rules. Evaluating rack locations by distance to the main aisle is the general

rule-of-thumb in retail literature (Samli et al., 2005). In contrast, evaluating locations by visibility is directly uses our v_l measure and is our proposed improvement over the distance ordering rule. We, therefore, use both distance and visibility as the location rules.

We illustrate how our location policies are used through the following example. Consider an assortment of products that are grouped into product categories A, B, …, AE (see Table 7). Each product category has a preassigned aisle, where an aisle is represented by two rack faces (Face D of preceding rack and Face B of the succeeding rack). If there is only one rack, we continue to call it an aisle for ease of exposition. Each product category is sorted within each aisle based on its total monthly demand (i.e., product category A has the highest demand in aisle 1, B has the second highest, and so on). Figure 29 shows how these product categories are assigned across the aisles for a given layout based on ordering product categories by demand (from here on, the Demand Ordering Rule). Notice how in Figure 29 (a) when evaluating locations by distance (from here on, the Distance Location Rule), categories with higher demand are placed closer to main aisle. However, moving to Figure 29 (b), when evaluating locations by visibility (from here on, the Visibility Location Rule) categories with higher demands are placed on Face A (near endcap) and Face B (front); these locations have higher visibility than those on Faces C (far endcap) and D (back). If ordering product categories by impulse (from here on, the Impulse Ordering Rule), this would simply require categories to be sorted based on their impulse potential (i.e., $P_p * T_p$) instead of demand.

Table 7. Example product category assignments.

Aisle	Rack	Assignment using Distance Rule	Assignment using Visibility Rule
1	1	A,B,C,D,E,F	A,B,C,D,E,F
2	1	I,K,M	K,L,M,N
2	2	G,H,J,L,N	G,H,I,J
3	2	S,U,W,Y	V,W,X,Y
3	3	O,P,Q,R,T,V,X,Z	O,P,Q,R,S,T,U
4	3	AA,AB,AC,AD,AE	AA,AB,AC,AD,AE

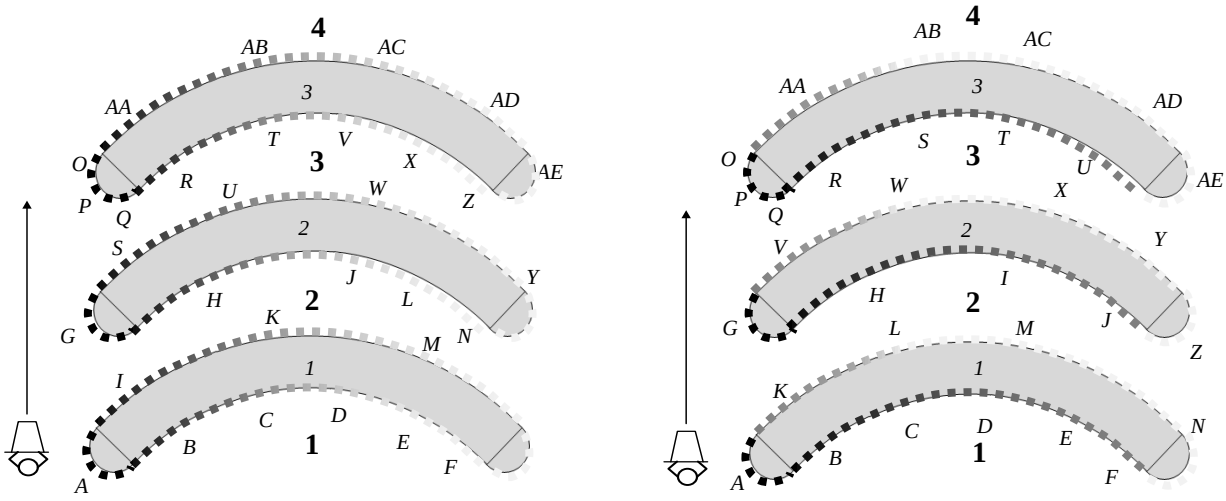

(a) Product placement based on distance location rule (i.e., Distance Rule)

(b) Product placement based on visibility location rule (i.e., Visibility Rule)

Figure 29. Illustration of location policies.
Darker shaded squares represent more attractive locations based on the respective location

3.5.3 PSO Evaluation

For our experiments, we consider a store section with realistic parameters summarized in Table 8. Using these, we first evaluated the performance of our proposed PSO approach against a Grid Search approach across each product category

Table 8. Baseline (realistic) parameters of a store section

Notation	Definition	Value
N	Number of full length racks (right	3
Ac and Aw	Width of cross aisle and main aisle	8 ft and 10 ft
Am	Shopper distance to racks	5 ft
M,W, and	Rack perimeter, width, and height	110 ft, 5 ft, and
DOV	Depth of focused vision	50 ft
S_E	Shopper eye height	5 ft
ρ	Eye fixations per second	3.33 fps
ω	Shopper walking speed	3.33 ft/s
$Lh \times Lw$	Size of the rack location	1 ft × 1 ft

location policy for both uni-directional and bi-directional traffic (total of 8 configurations). For Grid Search, we evaluated combinations of θ and α both in increments of 10º and present the best solution. We then used our proposed PSO, and similarly present its best-found solution.

We assumed shopper volume (S) to be 5,000 shoppers per day, store is operational 365 days a year, annual floor space cost (C) is \$50/ft^2, and the maximum aspect ratio is set to 2. We also set ρ to 3.33 fixations per second, which is between 2-4 as suggested by Yarbus (1967). With walking speed set at 3.33 ft/s, this works out to a shopper being able to have one fixation every 1 ft, allowing us to evaluate v_{ly} every 1 ft.

Columns A – C outline the 8 combinations, by traffic direction, location rule, and ordering rule. Column D indicates the solution approach. Column E presents the best layout found (combination of θ and α) using each approach, while Column F lists the marginal profit associated with the best layout. For values obtained from our PSO, we include the % increase from the best solution found by the Grid search approach. Column G lists the

Table 9. Best solutions from PSO and Grid Search.

A	B	C	D	E		F	G	H
Traffic Direction	**Location Rule**	**Ordering Rule**	**Solution Approach**	**Best layout**		**Marginal Profit (Objective)**	**% Diff from {90°,0°}**	**Time (min)**
				θ	α			
Uni-directional	Distance	Demand	Grid Search	20.0°	-180.0°	\$14,013,546	205%	3942
			PSO	23.3°	0.0°	\$15,283,451 (9.1%)	233%	1154
		Impulse	Grid Search	30.0°	70.0°	\$24,825,046	55%	3942
			PSO	27.4°	60.5°	\$25,116,899 (1.2%)	57%	2385
	Visibility	Demand	Grid Search	20.0°	-180.0°	\$14,453,179	162%	3430
			PSO	17.7°	-180.0°	\$15,002,593 (3.8%)	172%	998
		Impulse	Grid Search	30.0°	80.0°	\$26,324,982	67%	3430
			PSO	27.8°	77.5°	\$26,703,069 (1.4%)	70%	1087
Bi-directional	Distance	Demand	Grid Search	160.0°	180.0°	\$16,275,450	106%	4071
			PSO	**27.8°**	**73.8°**	\$16,718,756 (2.7%)	112%	468
		Impulse	Grid Search	160.0°	180.0°	\$24,954,502	22%	4071
			PSO	**162.3°**	**180.0°**	\$25,021,508 (0.3%)	23%	461
	Visibility	Demand	Grid Search	160.0°	180.0°	\$16,365,303	112%	3565
			PSO	162.2°	180.0°	\$16,807,371 (2.7%)	118%	2337
		Impulse	Grid Search	30.0°	60.0°	\$25,751,308	29%	3565
			PSO	**25.4°**	**23.3°**	\$26,121,297 (1.4%)	31%	1980

relative increase in marginal profit from a {90°,0°} layout for that particular combination of traffic direction, location rule, and ordering rule. Finally, Column H contains the time for each solution approach.

It is clear from Column F that our proposed PSO approach was able to achieve solutions that out-performed the Grid Search in substantially less time (in column H). A closer look at the values of best $\{\theta,\alpha\}$ from both these solution approaches (Column E) suggests that while the PSO is able to obtain the best values close to the Grid Search values, there are instances where the best layouts between them are substantially different. For instance, for bi-directional traffic, considering the Distance-Demand policy, the best layouts were {160°,180°} and {27.8°,73.8°} for the Grid Search and PSO approaches, respectively. We attribute these differences to the coarseness of the grid (i.e., 10°×10°) and the structure of the solution space. As we discuss later, marginal profit tends to increase as θ tends away from 90° towards both acute (until 0°) and obtuse (until 180°) orientations; so there exist nearly supplementary values of orientation (θ) with similar objective values. For the results in this table, we used a maximum aspect ratio of 2, which removed extremely acute (θ<17.7º) and obtuse (θ>162.3º) orientations; aspect ratio is also dependent on curvature however, so the cutoff point is slightly closer to 90° for smaller values of α. So in the instance called out above, the {160°,180°} layout was the only layout from our grid search with θ=160º that had an aspect ratio under 2 (i.e., 1.95). If we had set Ar_{MAX} to say, 1.9, then the new best layout from our grid search for this instance would be {30°, 70°}, much closer to the best solution from the PSO (i.e., {27.8°,73.8°}).

Further, we note that some PSO solutions had alternative solutions within 1% marginal impulse profit from the best solution that had nearly supplementary values of θ;

the values of θ and α are bolded in Table 9 for these instances. For our study, it is intuitive that these instances all occurred for bi-directional traffic, where layouts had to tailor to a shopper's field of regard in *both* directions. Uni-directional cases however all exhibit acute orientations as best solutions; this is consistent with prior literature that suggests acute orientations are more align with a shopper's field of regard.

Given the ability of our proposed PSO to achieve better solutions in quick time, we use it in all subsequent experiments as our primary solution approach. We do utilize the Grid Search approach to provide visual evidence of specific observations in Section 6.6.

5.4 Sensitivity of Ordering Rules and Location Rules

Considering the solutions in Table 9 derived from our PSO, we now discuss key observations related to the four location policies:

Obs 1: When using the Impulse Ordering Rule, the most appealing layouts have a relatively large percentage of locations with <u>high</u> v_l; however when using the Demand Ordering Rule, layouts with a relatively large percentage <u>moderate</u> v_l locations are more appealing.

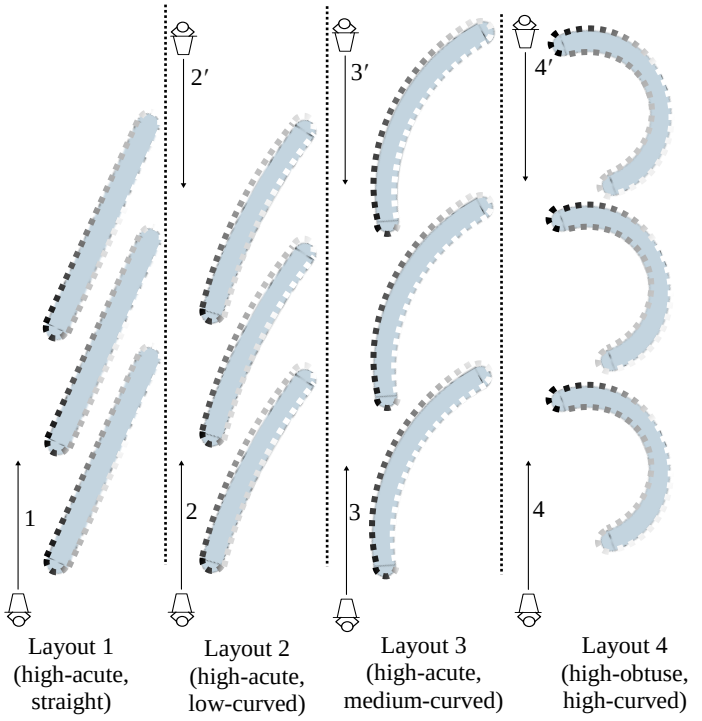

Figure 30. Top performing layouts from PSO. Darker squares indicate higher values of v_l.

We make our case for this observation by first introducing four general layouts noticed from Table 9, and subsequently presenting each layout's unique distribution of

visibilities (i.e., v_l). Utilizing these details, we will then connect each ordering rule to the type of layout that best suits it.

The four general layouts exhibited in Table 9 (from the PSO solutions) are illustrated in Figure 30, where shoppers are labeled to represent either uni- or bi-directional traffic; i.e., the combination of shoppers 2 and 2′ represent bi-directional traffic for layout 2, whereas 2 and 2′ *individually* represent uni-directional traffic. Layout descriptions are labeled with respect to shoppers 1-4. For instance, layout 4 is labeled as high-obtuse, high-curved considering shopper 4, while it is also high-acute, high-curved (negative) for shopper 4′. We define high-acute and high-obtuse racks as those with θ values in the range [1°,35°] and [145°,179°], respectively. Values of α, meanwhile, are classified by straight: α=0°, low: α=[1°,30°], medium: α=[31°,90°], and high: α=[91°,180°].

After identifying the general layouts from Table 9, we examined each layout's distribution of v_l values, as these values ultimately determine impulse profit (i.e., recall that v_p used in the objective function is derived from v_l). Table 10 outlines the distribution for each of the layout types introduced above, in addition to a straight and orthogonal (i.e., {90°,0°}) layout for comparison purposes. For each layout, we list the percentage of 1ft×1ft locations that fall within the specified range of v_l. Gray scale is specific by range and by traffic direction along each row. Darker shades have a different meaning for the dotted and solid cells that indicate v_l; for rows with solid lines, darker refers to higher % of visible locations (preferred), while for rows with dotted lines, darker shade indicates lower % of locations with low visibility (also preferred). For instance, layouts with a higher percentage of locations with $v_l < 1\%$ is *less* preferred (considering impulse profit) than layouts with a lower percentage.

Table 10. Comparing the distribution of v_l of top performing layouts against {90°,0°}.

Traffic Direction	Uni-directional				Bi-directional			
Layout Type (Shopper)	*N/A*	*1(1)*	*3(3)*	*4(4')*	*N/A*	*2*	*3*	*4*
Orientation	*Orthogonal*	*High-Acute*	*High-Acute*	*High-Acute*	*Orthogonal*	*High-Acute*	*High-Acute*	*High-Obtuse*
Curvature	*Straight*	*Straight*	*Medium*	*High (negative)*	*Straight*	*Low*	*Medium*	*High*
$v_l > 0.20$	0.10%	0.10%	1.20%	0.20%	0.00%	0.10%	1.50%	0.00%
$0.15 < v_l < 0.20$	0.60%	0.40%	2.00%	0.80%	0.30%	0.70%	0.80%	0.30%
$0.10 < v_l < 0.15$	0.80%	1.10%	2.30%	1.20%	1.00%	2.00%	3.80%	0.90%
$0.05 < v_l < 0.10$	2.40%	3.50%	4.10%	2.80%	1.70%	6.40%	5.60%	2.50%
$0.01 < v_l < 0.05$	10.60%	26.20%	15.90%	27.00%	11.50%	19.80%	15.90%	40.70%
$v_l < 0.01$	85.50%	68.60%	74.40%	68.00%	85.50%	70.90%	72.40%	55.60%

Darker shades indicate *higher* % values (i.e., preferred)

Darker shades indicate *lower* % values (i.e., preferred)

From Table 10, we find layouts 2 and 3 offer a (relatively) large percentage of locations with high visibility (i.e., $v_l > 0.05$), while layouts 1 and 4 offer a (relatively) large percentage of locations with moderate visibility (i.e., $0.01 < v_l < 0.05$). For instance, 9.6% of locations in layout 3 (shopper 3) have high visibility, compared to 5.1% in layout 1 (shopper 1). Meanwhile, layout 1 (shopper 1) exhibits 26.2% of locations with moderate visibility compared to 15.9% for layout 3 (shopper 3). Orthogonal and straight racks (i.e., {90°,0°}), in comparison, have a relatively small percentage of locations with either high or moderate visibility; 85.50% of locations for this layout (both traffic types) have low visibility (i.e., $v_l < 0.01$).

Now going back to Table 9, we find that combinations using the Impulse Ordering Rule generally result in layouts 2 or 3 (i.e., relatively large percentage of locations with high visibility) as the best solution. Although the combination of the Distance-Impulse policy with bi-directional traffic resulted in layout 4 as the best solution from PSO, a layout 3 solution exists that is within 1% (as noted by the bold font). On the other hand, combinations using the Demand Ordering Rule generally result in layouts 1 or 4 (i.e.,

relatively large percentage of locations with moderate visibility) as the best solution from PSO. Similarly, while the best solution for the combination of the Distance-Demand policy with bi-directional traffic is layout 3, a layout 4 solution exists that is within 1% (i.e., bold font).

We attribute these pairings (i.e., Impulse Ordering Rule → layouts 2 & 3 and Demand Ordering Rule → layouts 1 & 4) to how each rule locates product categories with high impulse potential (i.e., $P_p * T_p$). For the Impulse Ordering Rule, these categories are assigned to the most attractive locations (i.e., high v_p or closer to the main aisle). Because the expression for expected impulse profit per shopper (i.e., $\sum_p^P P_p T_p v_p$) directly uses v_p (which is derived from v_l), it is intuitive that having a large percentage of locations with high visibility to accommodate categories with high impulse potential will benefit impulse profit. When using the Demand Ordering Rule, however, layouts with a large percentage of locations with moderate visibility are appealing because this rule assigns *high demand* items to the most attractive locations. So if the demand and impulse potential among product categories are uncorrelated (or negatively correlated), as observed in the data we collected (correlation=-0.2), then a substantial portion of product categories with high impulse potential will most likely be placed in less attractive locations per the Demand Ordering Rule. What we observed is that if these locations have moderate visibility (i.e., $0.01 < v_l < 0.05$) to expose these product categories with high impulse potential to the shopper, then a relatively high impulse profit can be sustained. For instance, a product category that takes up, say, 21 1x1 locations each with v_l=0.03 will have a v_p=0.47 (derived from the Poisson binomial distribution) probability of being seen by the shopper at least once throughout the path.

Obs 2: In absolute terms, the Impulse Rule results in the highest marginal impulse profit; however, in relative terms, the Demand Rule results in the highest percentage increase in profit (from {90°,0°}).

From Column F in Table 9, on average (across all 4 combinations), the Impulse Ordering Rule resulted in an (*absolute*) marginal impulse profit of $25,740,693; this was 61% greater than the Demand Ordering Rule at $15,953,043. Considering the *relative* increase in marginal profit (from a {90°,0°} layout), the Demand Rule averaged a 159% increase (maximum 233%), while the Impulse Rule was only at 45% (maximum 70%).

Our finding considering *absolute* marginal impulse profit is consistent with existing literature (e.g., Flamand, 2016) that suggests there are benefits for assigning product categories with high impulse potential to the most attractive locations, as matching these categories to locations with high v_l with benefit the objective function. In fact, considering only {90°,0°} layouts, the Impulse Ordering Rule produced marginal impulse profits 188% (on average across both location rules and traffic directions) higher than the Demand Ordering Rule. Placing product categories with high impulse potential in *less* attractive locations (as in the Demand Rule) significantly reduces their visibility (i.e., v_p), in some cases to 0. While retailers may prefer to place high demand product categories in more visible locations to allow shoppers to easily find *planned* purchases, this is not an attractive option considering the negative impact on impulse profit.

For *relative* marginal profit, the Demand Ordering Rule outperformed the Impulse Ordering Rule due to the substantial increases in v_p for product categories with high impulse potential gained from varying θ and α from {90°,0°}. Recall, categories with high impulse potential are often placed in less attractive locations when using the Demand Ordering Rule;

these are usually farther from the main aisle and/or on the back side of racks for a {90°,0°} layout. Since less than 15% of locations have v_l above 0.01 for a {90°,0°} layout (from Table 10), categories with high impulse potential generally have a low, if not zero probability of being seen by shoppers. When varying θ and α, however, these same locations can become much more visible (because of greater effective area of the product facing visible to the shopper and extended duration of exposure), thereby substantially increasing the impulse profit gained from these product categories and *overall* marginal impulse profit. Both policies using the Impulse Ordering Rule, on the other hand, realize less benefits from variations in θ and α because these policies already place potentially profitable product categories in attractive locations for a {90°,0°} layout; although manipulating θ and α increases marginal profit, it is not as high as the Demand Ordering Rule (45% vs. 159%).

Observation 3. The Distance Location Rule can be limiting compared to the Visibility Location Rule.

While it is true for a {90°,0°} layout that locations closer to the main aisle have higher visibility than those farther away, this rule-of-thumb is often violated in layouts with high-curved and high-acute racks or straight and high-obtuse racks. For such layouts, there are locations that are farther from the main aisle with higher visibilities than locations closer to the main aisle. Further, it is often the case (e.g., {90°,0°}) where all visibilities on the front face (i.e., Face B) of racks are higher than those on the back (i.e., Face D). In both scenarios, using the Distance Location Rule will not always assign product categories (using either ordering rule) to locations with the highest visibilities. This limitation becomes prominent when using the Impulse Ordering Rule, as the Visibility Location Rule can *directly*

assign product categories with the highest impulse potential to locations with the highest visibilities (*independent* of distance to the main aisle). This ultimately resulted in the best solutions from Visibility Location Rule to perform, on average across both traffic directions, 5% (6% uni-directional, 4% bi-directional) better than those using the Distance Location Rule.

3.5.5 Aspect Ratio Sensitivity

We acknowledge that some retailers may require a smaller aspect ratio (*ar*= length/width or *Le*/*Wi*) of the store section considering overall store dimensions, location of adjacent store sections, customer travel paths, and replenishment policies. We, therefore, evaluated the sensitivity of the PSO solutions to allowable Ar_{MAX} (maximum aspect ratio) by varying it between 0.27 to 2.0 in increments of 0.25; in our experiments, *ar*=L/W=31/114=0.27 for the {90°,0°} layout. Figure 31 displays the best values corresponding to these intervals for each location policy and traffic direction. We let *S*=5,000 shopper/day and *C* = \$50/ft^2. We also depict the relative increase in marginal profit with respect to {90°,0°} through the size of each bubble.

Based on the findings in Figure 31, we make the following observation:

Obs 3: As the allowable aspect ratio (Ar_{MAX}) increases, the best layouts generally tend towards (i) either high-acute or high-obtuse orientations and (ii) large curvatures.

Since the {90°,0°} layout provides the minimum aspect ratio, any variation in either curvature or orientation will result in a higher aspect ratio. However, increasing curvature has a much smaller effect on aspect ratio than varying the orientation from 90°. For instance, the layout {90°,180°} has an aspect ratio of 0.84, while {30°,0°} has an aspect ratio of 1.46; i.e., a change of curvature from 0° to 180° (when θ=90°) increases aspect

ratio by 0.57, while varying orientation by 60° (i.e., from 90° to 30° when α=0°) increases aspect ratio by 1.19. This phenomenon ultimately results in high-acute (and obtuse) orientations becoming *infeasible* for tighter constraints on aspect ratio, while high-curved racks oriented closer to 90° continue to remain feasible.

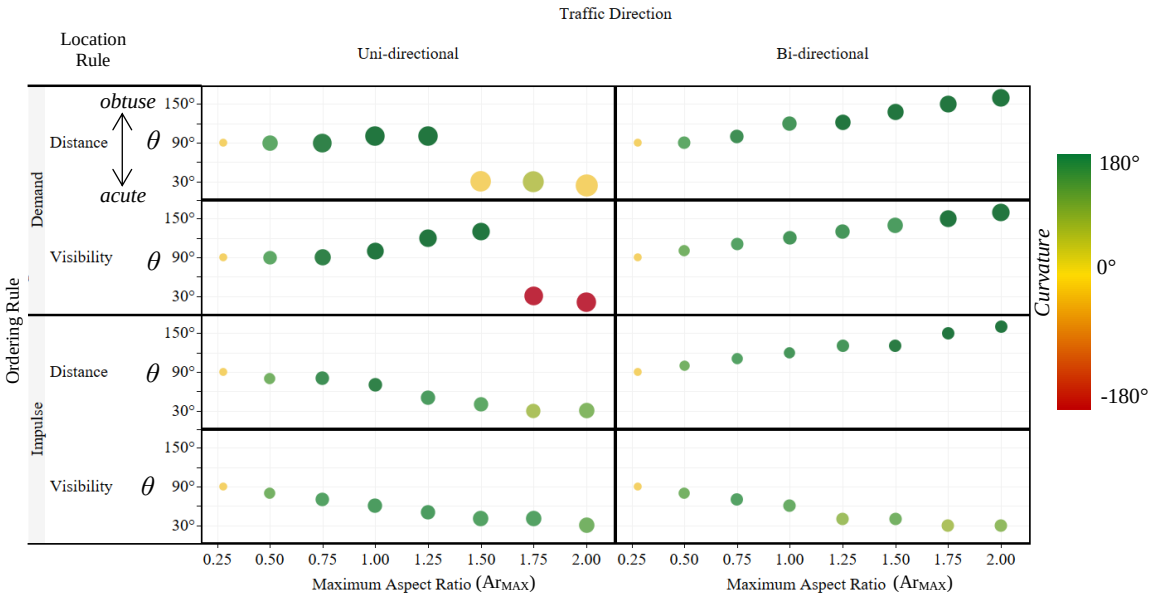

Figure 31. Sensitivity of the solutions to the Ar_{MAX} constraint.
Larger circles indicate higher relative increase in marginal profit from {θ=90°, α=0°}.

That being said, initially as Ar_{MAX} increases from 0.27, we notice the best values of θ *slowly* begin to deviate from 90°, while the best values of α *rapidly* increase from 0°; i.e., at Ar_{MAX} = 0.75, the best values of α are considered high-curved for all scenarios in Figure 11, while the best values of θ are within 20° of 90°. As Ar_{MAX} approaches 2, however, the best values of α vary (some decrease, others approach 180°) and values of θ continue to move away from 90°. If we relax the aspect ratio constraint (i.e., $Ar_{MAX}\rightarrow\infty$), then θ would approach either 0° or 180°. We attribute these convergence patterns to the longer shopping paths associated with such long, skinny, layouts; longer paths result in overall higher visibility of layouts. A real-world example would be the serpentine layout implemented by

retailers such as IKEA. Thus, given the option, it might be beneficial to the retailer (in terms of impulse profit) if they were to implement a layout design that allows a longer window of visibility to the shoppers to view products. However, there is indeed a tradeoff with considerations such as shopper walking distance (i.e., shoppers prefer not to walk too far for products) and product replenishment (i.e., replenishment is more efficient with compact layouts). It is, thus, critical for the retailer to determine an appropriate value for allowable Ar_{MAX} while balancing the above considerations aspects against marginal profit.

3.5.6 Sensitivity to Space Cost and Shopper Volume

Incorporated into our objective function is the annual volume of shoppers and the annual cost of floor space. It is intuitive that higher shopper volume will *increase* marginal impulse profit and higher floor space costs will *decrease* marginal impulse profit. In this section, however, we explore the effect of these two parameters on the best values of θ and α, and the resulting relative change in marginal impulse profit (from {90°,0°}). Figures 32 and 13 display results for uni-directional and bi-directional traffic across two shopper volumes of 500/day and 5,000/day, and two floor space costs of \$50/ft^2 and \$200/ft^2. The values of S used are based on the average daily foot traffic across drug, grocery, convenience, and grocery stores (Walmart, 2018; DistribuTech, 2014); we use 500 and 5000 to provide a reasonable range. Floor space costs, meanwhile, are based off of estimates for suburban and high-end urban areas. The best layouts for each combination derived using the PSO are indicated (with a black star) along the spectrum of solutions derived using the Grid Search. The Ar_{MAX} constraint was set to 2. Only results for the Visibility-Impulse location policy are shown.

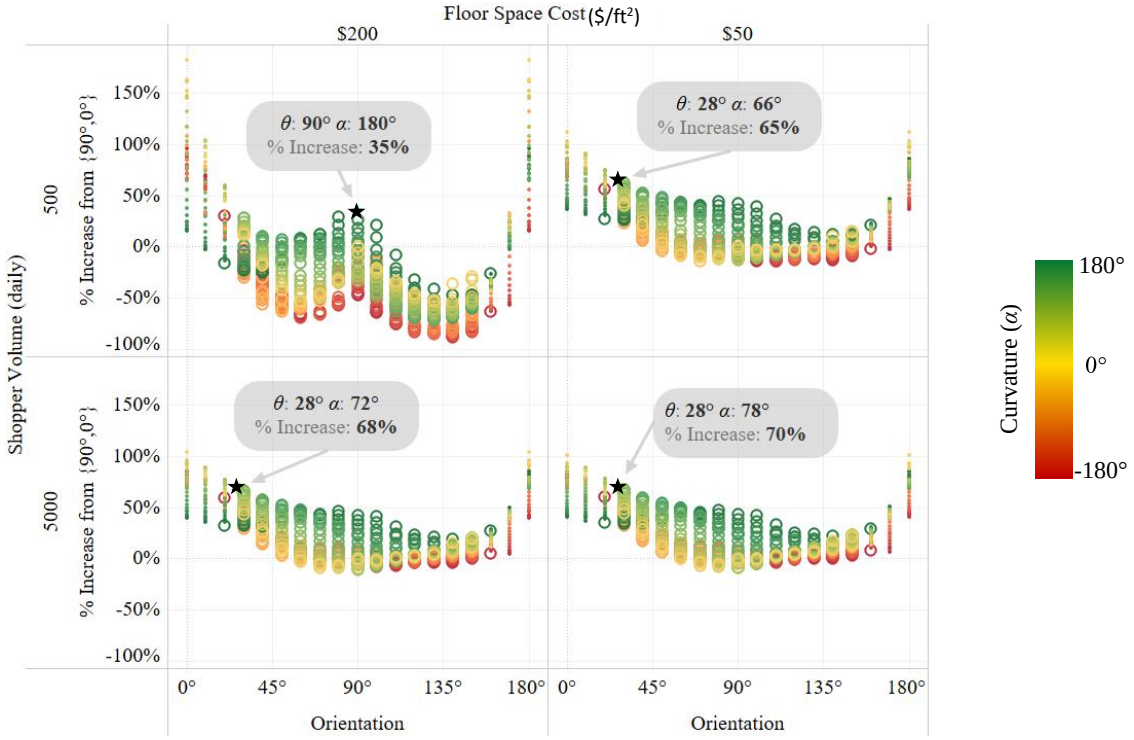

Figure 32. Sensitivity of floor space cost and shopper volume (uni-directional traffic).
Large markers indicate layouts within the aspect ratio limit (2). Black stars are best solution from PSO.

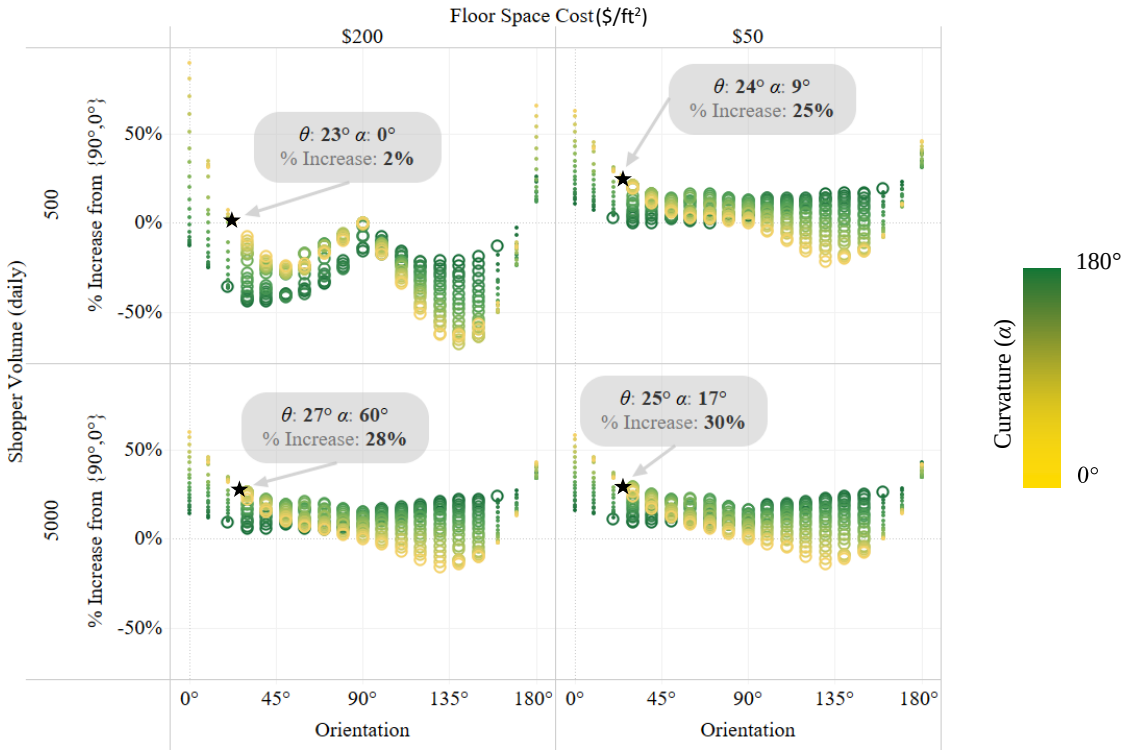

Figure 33. Sensitivity of floor space cost and shopper volume (bi-directional traffic).
Large markers indicate layouts within the aspect ratio limit (2). Black stars are best solution from PSO.

The following can be observed from these results.

Obs 4: As shopper volume increases and floor space cost decreases, orienting (θ) and curving (α) racks lead to increased benefits over a {90°,0°} *layout.*

Our results show that the relative increase in marginal profit (from {90°,0°}) with uni-directional traffic increased from 35% to 70% as shopper volume increases and floor space cost decreases (Figure 32); the increase for bi-directional traffic was from 2% to 30% (Figure 33). We attribute this to the impact of a layout's floor space on the objective function. Recall in Observation 1 where we discussed how high-acute and straight-to-medium-curved racks allowed for either relatively high quantities of premium locations (i.e., $v_l > 0.10$) or moderately appealing locations (i.e., $0.01 < v_l < 0.05$); these layouts resulted in the highest marginal impulse profits *even though* they have higher floor space requirements (e.g., {28º,78º} has a 116% higher floor space requirement than {90º,0º}). As S decreases and C increases from S=5000 shoppers/day and C=\$50/ft^2 (used in our experiments for Observation 1), these layouts continue to remain attractive (though to a lesser extent) because of the dominance of impulse profit in the objective function. In other words, these layouts provide such a high gain in impulse profit (from allowing shoppers the ability to view product categories with high impulse potential for extended durations of their path) that the higher costs associated with increased floor space are offset.

Only under circumstances when S is low and C is high does the floor space cost component of the objective function begin to notably impact the objective function, as the layout with the least space requirement (i.e., {90º,0º}) becomes moderately attractive. Even under this scenario (i.e., low shopper volume, high floor space cost), however, a high-acute straight rack layout (i.e., {23°,0°}) is still attractive (but only by 2%) than the {90°,0°}

layout for bi-directional traffic; a tighter allowable aspect ratio (say, Ar=1.75 compared to Ar=2.0)) would result in {90°,0°} becoming the best layout. A similar situation arises for uni-directional traffic for which the best solution (when S=500 and C=\$200/ft^2) is a layout with {90°,180°} racks. Observing the Grid Search solutions for this shopper volume/floor space cost combination in Figure 32, however, we found that there were several high-acute rack layouts with similar relative marginal profit values.

3.6 Conclusions

A wide variety of new rack designs are being implemented in retail stores. However, to date no study has quantitatively evaluated their impact on impulse profit. Our research proposed the Rack Orientation and Curvature Problem (ROCP) and a corresponding optimization model to identify the best rack layout (i.e., orientation and curvature) that maximizes marginal impulse profit (discounting floor space cost) from a fixed assortment of product categories. To derive impulse profit, we modeled the dynamics of a shopper walking down the main aisle past a layout of racks to estimate a probabilistic visibility measure for product categories. We considered the effective area of product category facings, a distribution of head positions from a human study, and a binary exposure estimate. To place product categories on rack locations, we used four different product category location policies, as a combination of a location rule (e.g., distance and visibility) and an ordering rule (e.g., demand and impulse).

The key finding from this Chapter is that orienting and curving racks (from common orthogonal and straight racks) can result in increased marginal profit; our experiments suggested at maximum 70-233% depending on the location policy used to place product categories. The values of orientation (θ) and curvature (α) that resulted in the

best marginal impulse profits were either high-acute and straight-to-medium-curved, or high-obtuse and high-curved. These layouts either contained a relatively large percentage of highly visible locations (ideal when using the Impulse Ordering Rule), or racks with a relatively large percentage of moderately visible (ideal when using the Demand Ordering Rule).

We propose the models presented in this Chapter will benefit retailers substantially as they can quantitatively evaluate new rack designs and layouts, avoiding expensive trial-and-errors. Further, we advocate our insights considering sensitivity of location policy, traffic direction, shopper volume, maximum aspect ratio, and floor space cost will serve as guidelines retailers and researchers can refer to for future research.

4 Conclusions and Future Research

Product exposure is an important element in a retail store, as shoppers only buy (or consider buying) what they see. Designing a layout of racks that better aligns with (and even utilizes) the scanning tendencies of shoppers is key to maximizing shopper satisfaction and a retailer's revenue. Our research analyzed how varying several rack design parameters affected exposure and impulse profit; these designs were motivated by layouts we have seen in nearby retailers and online. Researchers can use our models as a foundation to formulate larger, more detailed models to address additional decision variables such as height, product location, and number of product facings. Practitioners can use our insights as a guideline for exploring and evaluating new rack layouts and product locations policies. Below we summarize the contributions of this research.

4.1 Summary of Contribution 1

We proposed a quantitative approach, which combined analytical (dynamically evolving geometrical relationships) and numerical methods (e.g., Reimann Sum, approximation algorithms) to estimate exposure (continuous area) in 3D as a shopper walked down the main aisle past a layout of racks. Further, at discrete shopper steps, we evaluated if each discrete rack location was exposed (binary); thus, we were able to derive the number of steps (or time) of exposure for each location (i.e., intensity). We also conducted an experimental study where we analyzed how 3 key design parameters (i.e., orientation, curvature, and height) affected exposure and intensity. The experimental results revealed the following:

- When the racks are required to be oriented orthogonally to the shopper travel (i.e., θ=90°), use of curved racks in the layout could increase exposure (by 3-121%) over straight racks (α=0°).
- If such curved racks can be placed at any orientation, then there exist layouts that would further increase exposure (by 18-321%) over straight racks at 90º. If curved racks are not viable, then there exist orientations with straight racks that allow achieving nearly this same increase in exposure.
- If the rack height (H) can be changed, then it dominates both orientation (θ) and curvature (α) in impacting exposure; rack heights just below eye-height appear to maximize exposure when the top of the rack is allowed for product allocation (and thus considered as exposed).
- The increase in exposure comes with a floor space tradeoff. Depending on the system parameters, it is possible to achieve nearly 530% increase in exposure with 18% floor space increase; 48% increase in exposure with a modest increase in space (<5%).

4.2 Summary of Contribution 2

We proposed the Rack Orientation and Curvature Problem (ROCP) and a corresponding optimization model to maximize marginal impulse profit by determining (near) optimal values of rack orientation and curvature. Marginal impulse profit was derived by subtracting the cost of floor space from the impulse profit obtained from shoppers as they walked past a layout of racks. Included in the ROCP is a novel probabilistic visibility measure that is derived from the effective area of rack locations, a distribution of real shopper head movements, and binary exposure estimates from Contribution 1. Due to the complexities in solving this model optimally, we developed a

particle swarm optimization approach (PSO) and demonstrated its performance against the Grid Search method. Using the PSO, we conducted an experimental study and evaluated the sensitivity of the optimal solution to product category location policy, maximum aspect ratio, shopper volume, direction of travel, and floor space cost. Below are the key insights from this study:

- Varying rack orientation (θ) and curvature (α) from orthogonal and straight racks can improve marginal impulse profit by 70-233% depending on the location policy for product categories.
- The values of orientation (θ) and curvature (α) that resulted in the best marginal impulse profits were either high-acute and straight-to-medium-curved, or high-obtuse and high-curved. These layouts either contained a relatively large percentage of highly visible locations (ideal when using the Impulse Ordering Rule), or racks with a relatively large percentage of moderately visible (ideal when using the Demand Ordering Rule).
- The Impulse Rule generally leads to higher absolute marginal profit, while the Demand Rule demonstrated a higher relative increase in marginal profit compared to a layout with orthogonal and straight racks.
- The best values of θ trend toward either high-acute or high-obtuse as the tolerable aspect ratio increases; this increases the time a shopper can see locations on racks. The best values of α meanwhile generally increase.
- As shopper volume increases and floor space cost decreases, orienting (θ) and curving (α) racks lead to increased benefits over a {90°,0°} layout.

4.3 Future Research

There are many future extensions this research could lead to. While we only derived a distribution of head position for a {90,0} layout, it would potentially be beneficial to derive more distributions for varying values of θ and α. In a human subjects study, Guthrie et al., (2018) found that shopper scanning patterns were dependent on the layout (e.g., more obtuse layouts resulted in larger head movements). Thus, using a more realistic distribution of head positions for varying layouts (from {90°,0°}) would allow for more precise results. However, since these studies are time consuming, methods of interpolation and extrapolation between values of θ and α would need to be considered.

Investigating optimal human scanning patterns would also be an interesting domain. We noticed during the human subjects study that nearly every participant adapted to alternative layouts by modifying their head movement (scanning pattern). That is, what they preferred for a {90°,0°} layout was quite different from what they preferred for {45°,0°} or {135°,30°}. While understanding the characteristics of the best scanning pattern among these participants can lead to interesting findings, identifying an optimal scanning pattern for a given layout and benchmarking them against participant data could reveal novel insights.

Considering extensions to our ROCP, a logical next step would be to incorporate the location of product categories as a decision variable to jointly optimize it with rack orientation and curvature. The resulting increase in complexity will require more sophisticated heuristic approaches. While including product assortment and shelf space allocation as decision variables would be viable, it will further increase the complexity within the model and the solution approach. If an efficient solution approach can be

developed building upon our work, then it would further tie together retail layout and category planning domains, essentially incorporating retail layout decisions into already well-studied category planning models.

Further, in the ROCP, we assumed the height of racks to be a fixed parameter; i.e., 7 ft (2 ft above eye-height) for our experimental study. In reality, retailers have a wide variety of heights in their fixture assortment. In some cases, rack heights are even staggered (in increasing heights) in a single section of a layout. Introducing height (as either a varying parameter or a decision variable) could lead to interesting questions: *Which rack heights are the best (in terms of impulse profit) considering an average shopper height? Should rack heights be staggered in a layout? If placing products on the top surfaces of racks is feasible, which products should be placed there?* Addressing these, and similar questions, would be an interesting path to pursue.

References

1. Abratt, R., & Goodey, S. D. (1990). Unplanned buying and in-store stimuli in supermarkets. *Managerial and decision economics*, *11*(2), 111-121.
2. Applebaum, W. (1951). Studying customer behavior in retail stores. *Journal of Marketing*, *16*(2), 172-178.
3. Bai, R., Van Woensel, T., Kendall, G., & Burke, E. K. (2013). A new model and a hyper-heuristic approach for two-dimensional shelf space allocation. *4OR*, *11*(1), 31-55.
4. Bartie, P., Reitsma, F., Kingham, S., & Mills, S. (2010). Advancing visibility modelling algorithms for urban environments. *Computers, Environment and Urban Systems*, *34*(6), 518-531
5. Bitner, M. J. (1992). Servicescapes: The impact of physical surroundings on customers and employees. Journal of Marketing, 56, 57-71..
6. Bloomberg News. (2018, January 30). What Drew Amazon and Alibaba to Bricks-and-Mortar: Q&A. Retrieved August 9, 2018, from https://www.bloomberg.com/news/articles/2018-01-30/what-drew-amazon-and-alibaba-to-brick-and-mortar-quicktake-q-a?utm_source=Sailthru&utm_medium=email&utm_campaign=Issue: 2018-01-31 Retail Dive: Marketing [issue:13854]&utm_term=Retail Dive: Marketing
7. Botsali, A. R., and Peters, B. A. (2005). *A network based layout design model for retail stores.* Industrial Engineering Research Conference, Atlanta, GA.

8. Burke, R. (2006). The Third Wave of Marketing Intelligence. In M. Krafft & M. Mantrala (Eds.), Retailing in the 21st Century: Current and Future Trends (pp. 413). Berlin: Springer.
9. Cairns, J. P. (1962). Suppliers, retailers, and shelf space. *J of Marketing*, 34-36.
10. Chandon, P., Hutchinson, J. W., Bradlow, E. T., & Young, S. H. (2006) Measuring the Value of Point-of-Purchase Marketing with Commercial Eye-Tracking Data. *Marketing and Consumer Psychology Series*, 225.
11. Chen, Y. X., Hess, J. D., Wilcox, R. T., and Zhang, Z. J. (1999). Accounting profits versus marketing profits: A Relevant Metric for Category Management. *Marketing Science, 18*(3), 208-229.
12. Curhan, R. C. (1972). The relationship between shelf space and unit sales in supermarkets. *Journal of Marketing Research*, 406-412.
13. Daamen, W. (2004). *Modelling passenger flows in public transport facilities* (doctoral dissertation). Netherlands Research School for Transport, Infrastructure.
14. Desmet, P., & Renaudin, V. (1998). Estimation of product category sales responsiveness to allocated shelf space. *International Journal of Research in Marketing*, *15*(5), 443-457.
15. DistribuTech. (2014). Demograohics*. Retrieved August 12, 2018, from http://distribtech.net/Demographics.aspx
16. Dreze, X., Hoch, S. J., and Purk, M. E. (1994). Shelf management and space elasticity. *Journal of Retailing, 70*(4), 301-326.
17. Dunne, P. M., Lusch, R. F., and Gable, M. (1995). *Retailing* (2nd ed.). Cincinnati, Ohio: South-Western College Pub.

18. Ebster, C., & Garaus, M. (2015). Store Design and Visual Merchandising: Creating Store Space That Encourages Buying (2nd ed.). New York, NY: Business Expert Press.
19. Fisher-Gewirtzman, D. (2016). Integrating 'weighted views' to quantitative 3D visibility analysis as a predictive tool for perception of space. *Environment and Planning B: Planning and Design*, 45(2), 345-366.
20. Flamand, T., Ghoniem, A., & Maddah, B. (2016). Promoting impulse buying by allocating retail shelf space to grouped product categories. *Journal of the Operational Research Society*, *67*(7), 953-969.
21. Geismar, H. N., Dawande, M., Murthi, B. P. S., & Sriskandarajah, C. (2015). Maximizing Revenue Through Two-Dimensional Shelf-Space Allocation. *Production and Operations Management*, *24*(7), 1148-1163.
22. Gladwell, M. (1996). The science of shopping. *The New Yorker*, *4*(11), 66-75.
23. Granbois, D. H. (1968). Improving the study of customer in-store behavior. *J of Marketing*, 28-33.
24. Guthrie, B. and Parikh, P. J. (2018), "Evaluating Exposure of a Retail Rack Layout based on Human Vision in 3D," in review.
25. Guthrie, B., Parikh, P. J., Witlock, T., Glines, M., Wischgoll, T., Flach, J., and Watamaniuk, S. (2018), "Comparing and Enhancing the Analytical Model for Exposure of a Retail Facility Layout with Human Performance," *Proceedings of Industrial and Systems Engineering Research Conference*, May 19-22, Orlando, FL.
26. Hendrickson, K., & Ailawadi, K. L. (2014). Six lessons for in-store marketing from six years of mobile eye-tracking research. In *Shopper Marketing and the Role of In-Store Marketing* (pp. 57-74). Emerald Group Publishing Limited.

27. Hübner, A. H., & Kuhn, H. (2012). Retail category management: State-of-the-art review of quantitative research and software applications in assortment and shelf space management. *Omega, 40*(2), 199-209.
28. Hui, S. K., Fader, P. S., & Bradlow, E. T. (2009). The traveling salesman goes shopping: The systematic deviations of grocery paths from TSP optimality. *Marketing Science*, *28*(3), 566-572.
29. Hui, S. K., Inman, J. J., Huang, Y., & Suher, J. (2013). The effect of in-store travel distance on unplanned spending: Applications to mobile promotion strategies. *Journal of Marketing*, *77*(2), 1-16.
30. Iyer, E. S. (1989). Unplanned Purchasing: Knowledge of shopping environment and. *Journal of retailing*, *65*(1), 40.
31. Janiszewski, C. (1998). The influence of display characteristics on visual exploratory search behavior. *Journal of Consumer Research*, *25*(3), 290-301.
32. Kim, Y., & Jung, S. K. (2014). Distance-weighted isovist area: An isovist index representing spatial proximity. *Automation in Construction*, *43*, 92-97.
33. Kizer, R., & Bender, G. (2007). Everything You Need to Know About the Science of Store Design. Retrieved from http://www.vdta.com/Magazines/AUG07/fc-art-of-the-layout.html
34. Knox, G., Bell, D. R., & Corsten, D. (2011). Situational determinants of unplanned buying in emerging and developed markets. *Marketing Science Institute Working Paper Series, Marketing Science Institute, Cambridge, Massachusetts*.
35. Koltsova, A., Tunçer, B., & Schmitt, G. (2013). Visibility analysis for 3D urban environments. In *eCAADe 2013: Computation and Performance–Proceedings of the*

31st International Conference on Education and research in Computer Aided Architectural Design in Europe, Delft, The Netherlands.

36. Leadem, R. (2017, December 30). 67 Fascinating Facts About Ecommerce vs. Brick and Mortar (Infographic). Retrieved August 6, 2018, from https://www.entrepreneur.com/article/306678
37. Lee, G. (2017, October 17). Why 90 percent of sales still happen in brick and mortar stores. Retrieved August 8, 2018, from https://www.retailtechnologyreview.com/articles/2017/10/17/why-90-percent-of-sales-still-happen-in-brick-and-mortar-stores/
38. Li, C. (2011). *A facility layout design methodology for retail environments* (Doctoral dissertation, University of Pittsburgh).
39. Monty, R. A. and Senders, J. W. (1976). *Eye movements and psychological processes*. Hillsdale, N.J.: Lawrence Erlbaum Associates.
40. Mowrey, C., Parikh, P. J., and Gue, K. R. (2017), "The Impact of Rack Layout on Visual Experience in an Retail Store," in press, INFOR: Information Systems and Operational Research.
41. Mowrey, C., Parikh, P. J., and Gue, K. R. (2018), "A Model for the Retail Rack Layout Problem," in press, *European Journal of Operational Research*.
42. Ozgormus, E. (2015). *Optimization of Block Layout for Grocery Stores* (Doctoral dissertation).
43. Parker Jr, J. F., & West, V. R. (1972). *Bioastronautics Data Book*. Biotechnology Inc. Falls Church VA.

44. Peck, J., & Childers, T. L. (2006). If I touch it I have to have it: Individual and environmental influences on impulse purchasing. *Journal of business research*, *59*(6), 765-769.
45. Peters, B. A., Klutke, G.-A., and Botsali, A. R. (2004). Research issues in retail facility layout design. In R. D. Meller, M. K. Ogle, B. A. Peters, G. D. Taylor and J. S. Usher (Eds.), *Progress in Material Handling Research: 2004* (pp. 399-414).
46. Phillips, H. (1993). How customers actually shop: customer interaction with the point of sale. *Journal of the Market Research Society*, *35*(1), 51-63.
47. Pieters, R., & Warlop, L. (1999). Visual attention during brand choice: The impact of time pressure and task motivation. *International Journal of Research in Marketing*, *16*(1), 1-16.
48. Sorensen, H. (2009). *Inside the mind of the shopper: The science of retailing*. Upper Saddle River, N.J.: Wharton School Pub.
49. Sorensen, H., Bogomolova, S., Anderson, K., Trinh, G., Sharp, A., Kennedy, R., Page, B., and Wright, M. (2017). Fundamental patterns of in-store shopper behavior. *Journal of Retailing and Consumer Services*, 37, 182-194.
50. Spies, K., Hesse, F., & Loesch, K. (1997). Store atmosphere, mood and purchasing behavior. *International Journal of Research in Marketing*, *14*(1), 1-17.
51. Suher, J., & Sorensen, H. (2010). The power of atlas: Why in-store shopping behavior matters. Journal of Advertising Research, 50(1), 21-29.
52. Suleiman, W., Joliveau, T., & Favier, E. (2011). 3D urban visibility analysis with vector GIS data. *GISRUK 2011*, 27-29.

53. Underhill, P. (1999). Why we buy : the science of shopping: New York : Simon & Schuster, 1999.

54. U.S. Bureau of Economic Analysis, "Value Added By Industry," https://www.bea.gov/iTable/iTable.cfm?ReqID=51&step=1#reqid=51&step=51&isuri=1&5114=a&5102=1 (accessed August 6, 2018).

55. US Census Bureau. (2016). Latest Annual Retail Trade Report. Retrieved December 6, 2016, from https://www.census.gov/retail/index.html.

56. Wang, L. C., & Hsiao, D. F. (2012). Antecedents of Flow in Retail Store Shopping. Journal of Retailing and Consumer Services, 19(4), 381-389.

57. Ware, C. (2004). *Information Visualization Perception for Design* (2nd ed.). San Francisco, CA: Morgan Kaufman Publishers.

58. Wedel, M., & Pieters, R. (2008). A review of eye-tracking research in marketing. In *Review of marketing research* (pp. 123-147). Emerald Group Publishing Limited.

59. Wickens, C. D., and Hollands, J. G. (2000). *Engineering Psychology and Human Performance* (3rd ed.). Upper Saddle River, NJ: Prentice Hall.

60. Wischgoll, T., Glines, M., Whitlock, T., Guthrie, B., Mowrey, C., Parikh, P. J., and Flach, J. (2017), *Display infrastructure for virtual environments (DIVE)*, in press, Journal of Imaging Science and Technology.

61. Yapicioglu, H., and Smith, A. E. (2012). Retail space design considering revenue and adjacencies using a racetrack aisle network. *IIE Transactions*, *44*(6), 446-458.

62. Yarbus, A. L. (1967). Eye movements during perception of complex objects. In *Eye movements and vision* (pp. 171-211). Springer, Boston, MA.

Appendices

Appendix A. Determining the Distance l_r

Recall that before we estimate exposure and intensity, we need to design the layout of curved racks with appropriate aisle spaces. Recall that we use a_c as the minimum cross-aisle distance between the racks and that we introduce l_r as the linear distance between endcap midpoints on subsequent racks (n and n+1) measured in the direction of shopper travel (y-direction). To determine l_r, we need to first find which face on racks n and n+1 will produce the minimum distance; i.e., the minimum distance between racks n and n+1 will occur between face f_n and f_{n+1}. These faces will change based on values of θ and α.

Including faces A-D, the number of possible combinations of faces would be 16 (i.e., all combinations of 4 faces on racks n and n+1). However, we can immediately eliminate all combinations that include face B (since this face curves inward, and thus geometrically cannot be the closest face to a subsequent rack), as well as combinations that include like endcap faces (e.g., face A of rack n cannot be paired with face A of rack n+1). These eliminations leave us with 7 possible combinations where the minimum distance (a_c) may occur. Figure A1(a) illustrates all 7 combinations, where line segments are drawn between the center of curvatures of each respective face; if a feasible a_c were to occur between any two faces, it would fall on a connecting line segment.

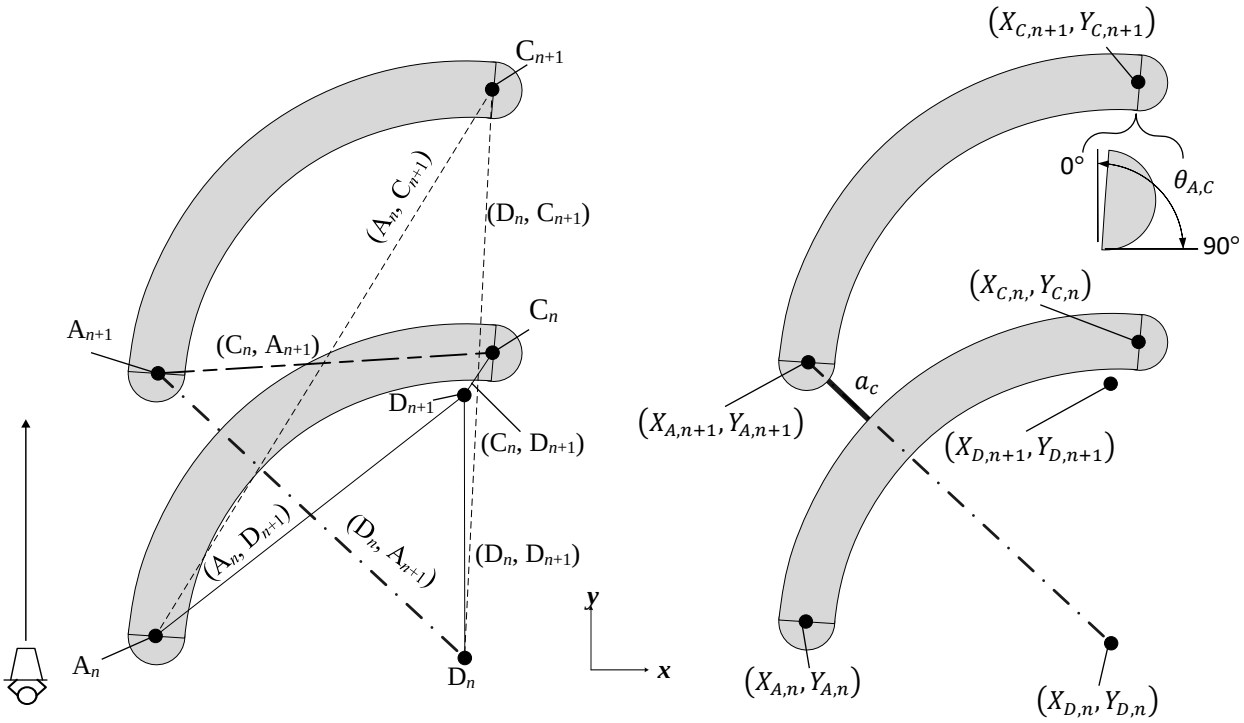

Figure A1. Determining combination that produces minimum distance between racks (a) 7 possible combinations (b) feasible combination for this example

We also derived the following 4 rules that eliminate other infeasible combinations of faces on racks *n* and *n*+1 to consider:

1. For either faces A_n and C_n to be feasible, they must be facing 'upward' (i.e., $-90° \leq \theta_{A,C} \leq 90°$), and $Y_{A(C),n} \geq Y_{C(A),n}$
2. For either faces A_{n+1} and C_{n+1} to be feasible, they must be facing 'downward' (i.e., $90° \leq \theta_{A,C}$ *or* $\theta_{A,C} \leq -90°$) and $(Y_{A(C),n+1}) \leq (Y_{C(A),n+1})$.
3. For face D_n to be feasible, $0° \leq \alpha \leq 180°$.
4. For face D_{n+1} to be feasible, $-180° \leq \alpha \leq 0°$.

To illustrate the above approach, consider Figure A1(a). Since face A_n is facing 'downward,' combinations (A_n, C_{n+1}) and (A_n, D_{n+1}) are infeasible. Similarly, face D_{n+1} is

infeasible as $\alpha > 0$, and so combinations (C_n, D_{n+1}) and (D_n, D_{n+1}) are infeasible. Face C_n is also facing 'downward,' and thus (C_n, A_{n+1}) is eliminated. Finally, combination (D_n, C_{n+1}) is eliminated as $(Y_{C,n+1}) \geq (Y_{A,n+1})$. Combination ($D_n$, A_{n+1}) is, therefore, the only feasible combination. Figure A1(b) illustrates the line segment connecting the center of curvatures of this combination, with the bold portion representing the feasible a_c.

We note that there may be specific combinations of θ and α that result in more than one combination being feasible following the above procedure. In these cases, we perform addition feasibility checks to see if the line segments connecting pairs of center of curvatures pass through the physical part of another face, or a non-physical part of a self-face. We explain these checks using Figure A2. Here, both combinations (C_n, A_{n+1}) and (D_n, A_{n+1}) are feasible after the above procedure. However, the line segment connecting the center of curvatures of C_n and A_{n+1} passes though both the physical part of face D_n and the non-physical part of face C_n (i.e., through the imaginary part of the face C circle, which is actually part of face D). In other words, the distance between these two racks from the line segment is actually between faces D_n and A_{n+1}. The other combination, (D_n, A_{n+1}) meanwhile, passes these two checks.

Once the feasible combination of face f_n and $f_{n+1,}$ is found we can calculate the corresponding value of l_r that determines the distance along the y-axis between two subsequent endcap midpoints. Figure A3 illustrates the parameters to be used in the equation to find l_r (combination (D_n, A_{n+1})). Table A1 summarizes equations for all 7 potential combinations, which are used when the corresponding face combination becomes feasible in certain layouts.

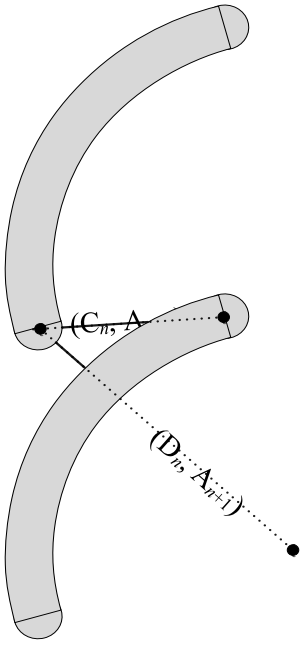

Figure A2. Layout with additional feasibility checks to determine l_r

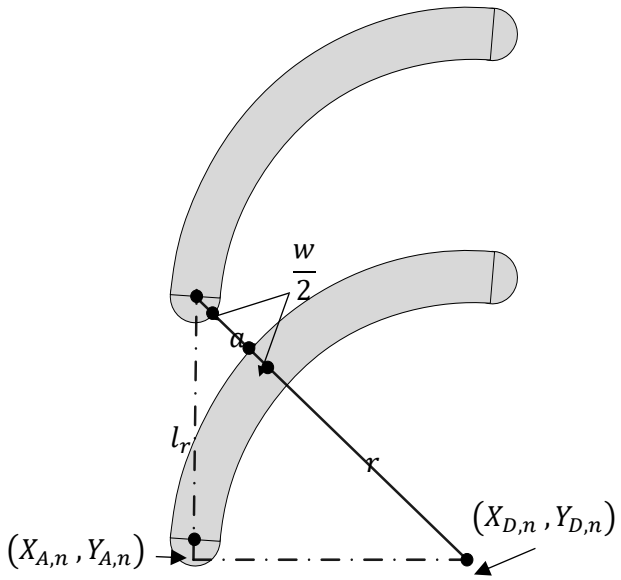

Figure A3. Illustration of parameters to determine l_r for combination (D_n, A_{n+1})

Table A1. Expressions to calculate l_r

Face Combination	**Expression to calculate l_r**
(D_n, D_{n+1})	$\sqrt{4\left(\mathrm{r}+\frac{w}{2}\right)^2+4a_c\left(\mathrm{r}+\frac{w}{2}\right)+{a_c}^2}$
(A_n, D_{n+1})	$\sqrt{\left(\mathrm{r}+\frac{w}{2}\right)^2+2\left(\mathrm{r}+\frac{w}{2}\right)\left(\frac{w}{2}\right)+2\,a_c\left(\mathrm{r}+\frac{w}{2}\right)+\left(\frac{w}{2}\right)^2+2\,a_c\left(\frac{w}{2}\right)+{a_c}^2 -(X_{A,n})^2-(X_{D,n})^2+2(X_{A,n})(X_{D,n})+(Y_{A,n})-(Y_{D,n})}$
(C_n, D_{n+1})	$\sqrt{\left(\mathrm{r}+\frac{w}{2}\right)^2+2\left(\mathrm{r}+\frac{w}{2}\right)\left(\frac{w}{2}\right)+2a_c\left(\mathrm{r}+\frac{w}{2}\right)+\left(\frac{w}{2}\right)^2+2\,a_c\left(\frac{w}{2}\right)+{a_c}^2 -(X_{C,n})^2-(X_{D,n})^2+2(X_{C,n})(X_{D,n})+(Y_{C,n})-(Y_{D,n})}$
(D_n, A_{n+1})	$\sqrt{\left(\mathrm{r}+\frac{w}{2}\right)^2+2\left(\mathrm{r}+\frac{w}{2}\right)\left(\frac{w}{2}\right)+2\,a_c\left(\mathrm{r}+\frac{w}{2}\right)+\left(\frac{w}{2}\right)^2+2\,a_c\left(\frac{w}{2}\right)+{a_c}^2 -(X_{A,n})^2-(X_{D,n})^2+2(X_{A,n})(X_{D,n})-(Y_{A,n})+(Y_{D,n})}$
(C_n, A_{n+1})	$\sqrt{4\left(\frac{w}{2}\right)^2+4a_c\left(\frac{w}{2}\right)+{a_c}^2-(X_{A,n})^2 -(X_{C,n})^2+2(X_{A,n})(X_{C,n})+(Y_{C,n})-(Y_{A,n})}$
(D_n, C_{n+1})	$\sqrt{\left(\mathrm{r}+\frac{w}{2}\right)^2+2\left(\mathrm{r}+\frac{w}{2}\right)\left(\frac{w}{2}\right)+2a_c\left(\mathrm{r}+\frac{w}{2}\right)+\left(\frac{w}{2}\right)^2+2a_c\left(\frac{w}{2}\right)+{a_c}^2 -(X_{C,n})^2-(X_{D,n})^2+2(X_{C,n})(X_{D,n})-(Y_{C,CoC})+(Y_{D,n})}$
(A_n, C_{n+1})	$\sqrt{4\left(\frac{w}{2}\right)^2+4a_c\left(\frac{w}{2}\right)+{a_c}^2-(X_{A,n})^2 -(X_{C,n})^2+2(X_{A,n})(X_{C,n})-(Y_{C,n})+(Y_{A,n})}$

Appendix B. Estimating 3D Exposure of Top Faces.

To estimate exposed area on the top faces of racks (E, F, and G), we propose a procedure that first discretizes the top face of the rack (with width *w*) into *s* arcs $\left(0 \leq s \leq \frac{w}{\gamma_d}\right)$ such that distance between successive arcs is fixed at γ_d, and then aggregate the area between these exposed arcs (E_{nfs}^{2D}) using the Riemann Sum and Trapezoidal Rule approximations; see the discretization of face F in Figure B1.

At each arc *s* (beginning with *s*=1), we calculate the area of the sector (i.e., SA_1) formed by arc length E_{nfs}^{2D} and radius (r-$\frac{w}{2}$+$(s-1)\gamma_d$), and the area of the sector (i.e., SA_2) formed by arc length E_{nfs}^{2D}, and radius (r-$\frac{w}{2}$+$s\gamma_d$) . The difference in area between these two sectors (SA_2 - SA_1) forms the left Riemann Sum ($E_{nfs,Left}^{3D}$), or in the case of Figure B2, the 'underestimate.' Figure B3 contains calculation steps to derive $E_{nfs,Left}^{3D}$. Similarly, the right Riemann Sum, or the 'overestimate,' is the difference in area between the sector formed by arc length E_{nfs-1}^{2D} and radius (r - $\frac{w}{2}$+$(s-1)\gamma_d$), and the area of the sector formed by arc length E_{nfs-1}^{2D}, and radius (r - $\frac{w}{2}$+$s\gamma_d$). These Right and Left Riemann Sums are then averaged to obtain the Trapezoidal Rule approximation. This procedure with calculations for estimating exposure on face F are shown in Figure B4. The below equations show the calculations for face F. Calculations for faces E and G are derived similarly, and thus not shown.

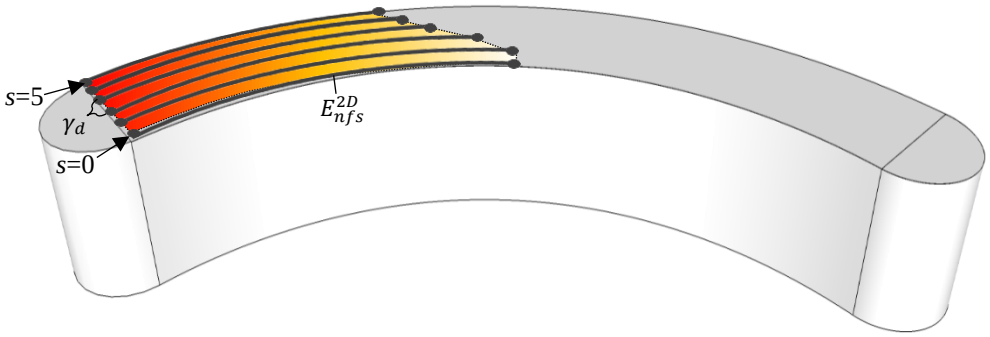

Figure B1. Approximated exposed area on face F

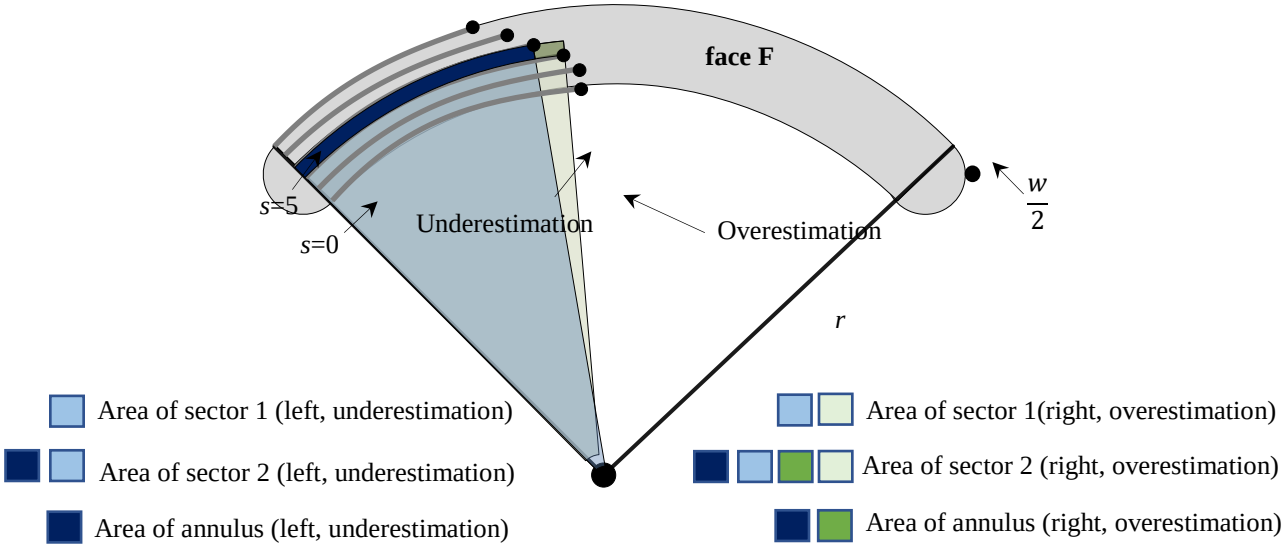

Figure B2. Reimann Sum approximation of exposure of face F

(1) $SA_1 = \frac{\alpha\pi}{360}(r_{s-1})^2 = \frac{\alpha\pi}{360}\left(r - \frac{w}{2} + (s-1)\gamma_d\right)^2$

(2) $SA_2 = \frac{\alpha\pi}{360}(r_s)^2 = \frac{\alpha\pi}{360}\left(r - \frac{w}{2} + s\gamma_d\right)^2$

(3) $\alpha = \frac{180E_{nfs}^{2D}}{\left(r-\frac{w}{2}+s\gamma_d\right)\pi}$

(4) $SA_1 = \frac{180\pi E_{nfs}^{2D}}{\left(\left(r-\frac{w}{2}+s\gamma_d\right)\pi\right)/360}\left(r - \frac{w}{2} + (s-1)\gamma_d\right)^2$

(5) $SA_2 = \frac{180\pi E_{nfs}^{2D}}{\left(\left(r-\frac{w}{2}+s\gamma_d\right)\pi\right)/360}\left(r - \frac{w}{2} + s\gamma_d\right)^2$

(6) $E_{nfs,Left}^{3D} = SA_2 - SA_1 = \frac{180\pi E_{nfs}^{2D}}{\left(\left(r-\frac{w}{2}+s\gamma_d\right)\pi\right)/360}\left(r - \frac{w}{2} + s\gamma_d\right)^2 - \frac{180\pi E_{nfs}^{2D}}{\left(\left(r-\frac{w}{2}+s\gamma_d\right)\pi\right)/360}\left(r - \frac{w}{2} + (s-1)\gamma_d\right)^2$

(7) $$E^{3D}_{nfs,Left} = 0.5E^{2D}_{nfa_t+s}\left(\left(\left(r\text{-}\frac{w}{2}\right)+(s)\gamma_d\right) - \frac{\left(\left(r\text{-}\frac{w}{2}\right)+(s\text{-}1)\gamma_d\right)^2}{\left(\left(r\text{-}\frac{w}{2}\right)+(s)\gamma_d\right)}\right)$$

Figure B3. Calculations steps to determine $\boldsymbol{E^{3D}_{nfs,Left}}$

(1) For rack (n)

(2) For $0 < s \leq \frac{w}{\gamma_d}$

(3) $$E^{3D}_{nfs,Right} = E^{2D}_{nf,s-1} * \left(\frac{\left(\left(r\text{-}\frac{w}{2}\right)+(s)\gamma_d\right)^2}{\left(\left(r\text{-}\frac{w}{2}\right)+(s\text{-}1)\gamma_d\right)} - \left(\left(r\text{-}\frac{w}{2}\right)+(s\text{-}1)\gamma_d\right)\right)$$

(4) $$E^{3D}_{nfs,Left} = .5 * E^{2D}_{nfs} * \left(\left(\left(r\text{-}\frac{w}{2}\right)+(s)\gamma_d\right) - \frac{\left(\left(r\text{-}\frac{w}{2}\right)+(s\text{-}1)\gamma_d\right)^2}{\left(\left(r\text{-}\frac{w}{2}\right)+(s)\gamma_d\right)}\right)$$

(5) $$E^{3D}_{nfs} = \frac{E^{3D}_{nfs,Right}+E^{3D}_{nfs,Left}}{2}$$

Figure B4. Procedure for approximating the exposure of face F

Appendix C: Estimating Exposure in 2D $\left(E_{nfyh}^{2D} \forall n, f\right)$

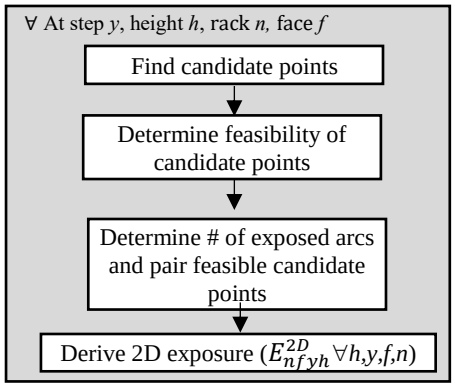

Figure C1. Estimating E_{nfyh}^{2D}

Figure C1 outlines our proposed 2D algorithm. Essentially, at each shopper step (*y*) and height (*h*), we first find *candidate* points – (*x*,*y*) points used to designate the potentially exposed arcs on a curved rack -- for each of the 4 rack faces (A-D) on each rack *n* separately. These points are found analytically and numerically (in Appendix C (Sections C.1 and C.2)). See Appendix C (Section C.3) for additional mathematical considerations for estimating 3D exposure in 2D slices. Further, we present a detailed example of estimating exposure at a point in Appendix C (Section C.4). We categorize each of these candidate points as shown below in Table C1. Because there are geometrical differences between each of the four faces (e.g., face B curves inward, eliminating tangent lines), there are some categories which apply to only a select number of faces.

Table C1. Candidate points to determine exposure.

Category #	Category Name	Applicable face
1	Face corners	All
2	Shopper FoR intersection points	All
3	Tangent line points	A,C,D
4	Horizontal tangent line points (from current rack)	A,B,C
5	Horizontal tangent line points (from preceding rack)	All
6	Horizontal tangent line points (from succeeding rack)	All
7	Dead zone curve intersection points	All
8	Vertical obstruction tangent line (from preceding rack)	All
9	Vertical tangent line (from succeeding rack)	All
10	Vertical obstruction tangent line (from current rack)	All

Once all candidate points are found for a 2D problem, we analytically evaluate the feasibility of these points. Table C2 lists each of these checks; they are carried out sequentially in the order presented.

Table C2. Feasibility checks for candidate points.

Category	Check
Existence	Does point exist?
	Is point on rack?
FoR	Is point within DOV?
	Is point within the horizontal angular limit ($\Phi_{HR(R)} + \Omega_{HR(R)}$)?
	Is point outside of Dead Zone?
Obstruction	Self-Obstruction?
	Succeeding Rack Obstruction?
	Preceding Rack Obstruction?

Existence: It is likely that the 2D geometric shapes (i.e., circles and lines) may not intersect. Consequently, the check "Does point exist?" will not hold true, making the candidate point infeasible. Even if an intersection point exists, it is possible that it may lie on the imaginary circle surrounding the center of curvature of a curved rack, but not on the *physical* part of this rack.

FoR: FoR checks ensure a point must be within a specified DOV and within the horizontal angular limits to be considered feasible. Essentially, we first calculate the Euclidean distance between a (*x*,*y*) coordinates of the shopper and the candidate point, and compare it to the DOV. Likewise, we compare the angle to a candidate point from the shopper (relative to the shopper's pathway) and compare it to the horizontal angular limit. Further, for levels below and above the shopper eye-height, points must be outside of the 'dead zone' which is formed from the vertical and horizontal eye and head movements of the shopper. This phenomenon is explained in Appendix C (Section C.2).

Obstruction: Finally, each candidate point on rack *n* is evaluated for obstruction by itself (self-obstruction), by previous racks *n*-*j* ($1 \leq j < n$) (preceding-obstruction), and by subsequent racks *n*+*j* ($1 \leq j < n$) (succeeding-obstruction). In other words, self-obstruction occurs when a rack *n* is obstructed by itself (Figure C2(a)). Preceding-obstruction occurs

when a rack *n* is obstructed by another rack *j* that lies *earlier* on the shopper's path (Figure C2(b)). Succeeding obstruction occurs when a rack *n* is obstructed by another rack *j* positioned *later* on the shopper's path (Figure C2(c)).

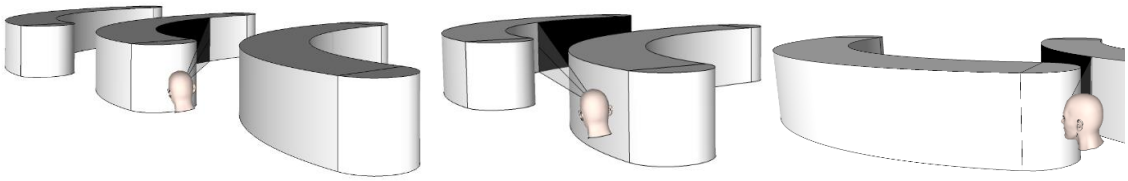

(a) Self-obstruction (b) Preceding-obstruction (c) Succeeding-obstruction

Figure C2. Classifications of obstruction where black shaded areas are obstructed

Figure C3 illustrates several examples of potential feasible and infeasible candidate points. These points are further explained in Table C3 (feasible points) and Table C4 (infeasible points). The light-shaded arcs represent exposed arcs to shopper step *y* and dark-shaded arcs represent exposed arcs to shopper step *y*+1. Note that some points may not necessarily be candidate points for each shopper step (i.e., point 15 is not considered as a candidate point for step *y*+1).

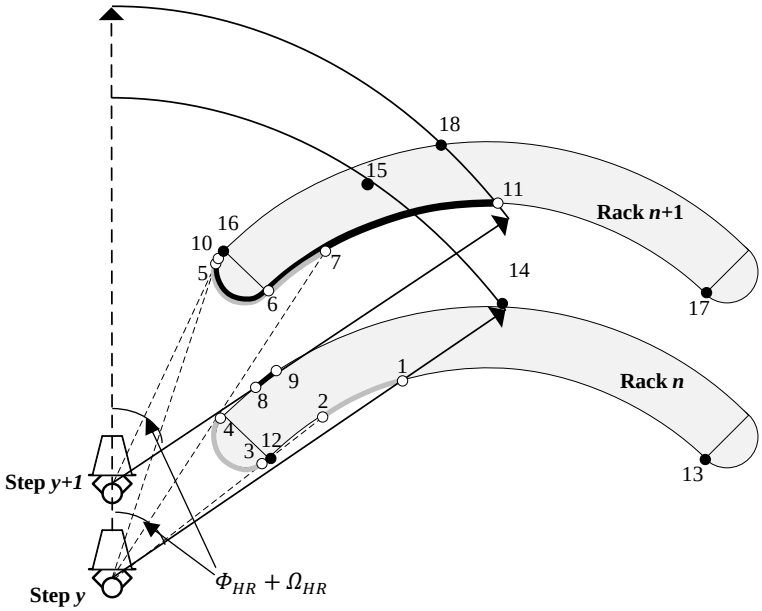

Figure C3. Illustration of example candidate points

Table C3. Explanation of example feasible candidate points

Point #	Category #	Shopper Step	Rack	face	Feasible Candidate Point
1	2	y	n	B	Horizontal angular limit line intersection point
2	4	y	n	B	Self-obstruction point from face A
3	3	y	n	A	Right tangent line point
4	3	y	n	A	Left tangent line point
5	3	y	n+1	A	Left tangent line point
6	1	y	n+1	A	face A/ B corner
6	1	y	n+1	B	face A/B corner
7	5	y	n+1	B	Preceding obstruction point from rack 1 face A
8	2	y+1	n	D	Horizontal angular limit line intersection point
9	3	y+1	n	D	Left tangent line point
10	3	y+1	n+1	A	Left tangent line point
6	1	y+1	n+1	A	face A/B corner
6	1	y+1	n+1	C	face A/B corner
11	2	y+1	n+1	C	DOV curve intersection point

Table C4. Explanation of example non-feasible candidate points

Point #	Shopper	Rack	Face	Infeasible Candidate Point	Failed Checks
12	y	N	A/B	face A/ B corner	Self-obstruction from face A
13	y	N	B/C	face B/C corner	Outside FoR
14	y	n	D	DOV curve intersection point	Self-obstruction from face B
15	y	n+1	B	DOV curve intersection point	Preceding obstruction from rack 1
16	y+1	n+1	D/A	face D/A corner	Self-obstruction from face A
17	y+1	n+1	B/C	face B/C corner	Outside FoR & preceding obstruction from rack 1
18	y+1	n+1	D	DOV curve intersection point	Self-obstruction from face B

Once all feasible candidate points are found, each feasible point (e.g., (x_a,y_a)) is paired with another feasible point (e.g., (x_b,y_b)) to form a feasible arc i. We know of circumstances with 2, 4, or even 6 different feasible points on a face f of a rack n at a given shopper step y, resulting in a maximum of 3 exposed arcs. For instance, see Figure C4 where points (x_b,y_b) and (x_c,y_c) form feasible arc 1, and points (x_d,y_d) and (x_e,y_e) form feasible arc 2 on face B for a curved rack (α=90º) placed at θ=130º. Points are paired together so that no overlapping arcs exist. To avoid pairing point (x_b,y_b) with (x_d,y_d) or point (x_c,y_c) with (x_e,y_e), we first calculate the Euclidean distance from each candidate point to a face corner. The points are then paired according to their respective distances (i.e., the two

points with the smallest distances would be paired together, and then the next two highest would be paired together).

Then, for each face, the length *L* of each exposed arc *i* is then calculated (using the radius of the respective face r_f); i.e., $L_i = 2\pi r_f \frac{\beta}{360}$, where the inside angle $\beta = \cos^{-1}\left(\frac{2r_f^2 - c^2)}{2r_f^2}\right)$ and the chord length (c) connecting feasible candidate point (x_{ia},y_{ia}) and (x_{ib},y_{ib}) is $c = \sqrt{(x_{ai} - x_{bi})^2 + (y_{ai} - y_{bi})^2}$. Finally, the 2D exposure (in ft) of face *f* on rack *n* at step *y* and height *h* can be estimated as $E_{nfhy}^{2D} = \sum_{i=1}^{N} L_i$.

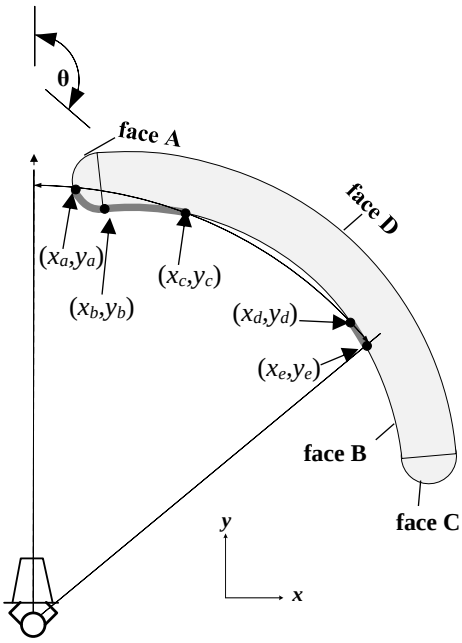

Figure C4. Pairing of feasible points

Recall that this 2D approach is repeated for each height *h* in the range [0, H_n] that falls within the 3D FoR. At each shopper step we find continuous exposed arcs (2D), and then derive intensity of discrete segments that falls within these arcs. Once a shopper path is completed, we derive both total exposure and intensity of a layout in 3D. In so doing, we are able to capture, via our proposed quantitative approach, the complex dynamics that ensues between a walking shopper's 3D FoR and a layout of static racks.

Appendix C.1: Approximation Algorithm for Vertical Tangent Curves

When we consider racks at varying heights both above and below the shopper's eye height, we must account for what the shopper can and cannot see *over* a rack. Thus, additional candidate points we derive are the intersection points (*x*,*y*) of vertical tangent curves (aggregation of tangent lines over the top of racks) with a height (*h*). Further, all other candidate points must lie *above* these curves in order to be considered feasible (these checks can be found analytically). We categorize these curves as either preceding, succeeding, or self, based upon the location of the obstructing rack compared to the rack of where the curve falls on. Figure C5 below illustrates each type of curve.

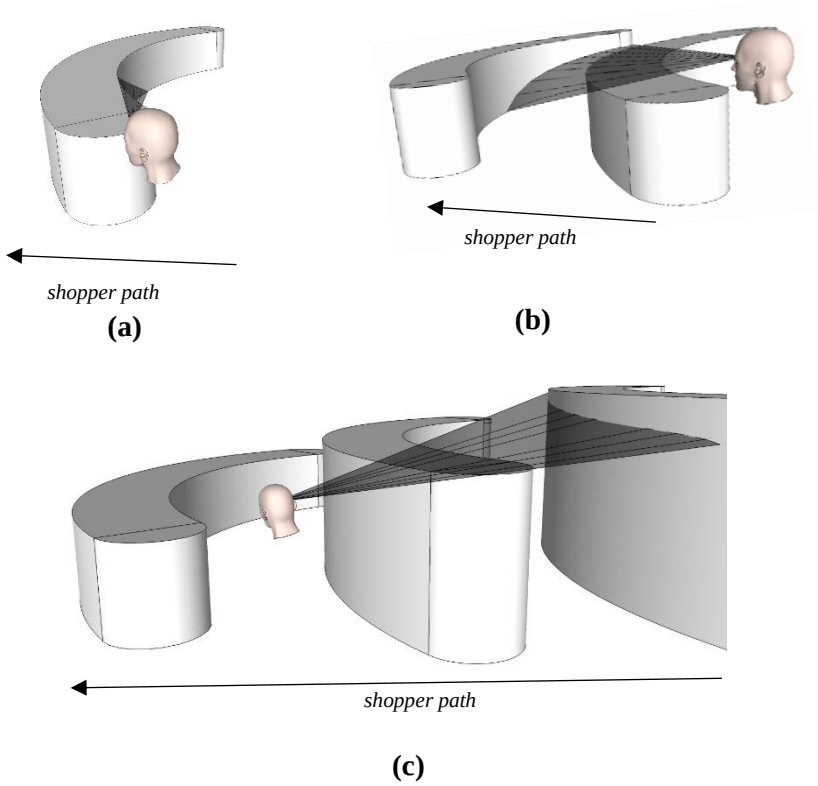

Figure C5. Vertical tangent curves. (a) Self, (b) Preceding, and (c) Succeeding.

To determine the extent to which a shopper can see over a rack onto another rack face *f*, we must find the intersection point (*x*, *y*) of the vertical tangent line that intersects face *f* at height *h*. To accomplish this, we propose a numerical/analytical approach shown in Procedure C1. Essentially, we increment an angular variable φ_1 by γ_1 degrees, in a range considering the minimum ($\varphi_{\min}$) and maximum ($\varphi_{\max}$) angles to face *f* (i.e., determined by the angles to tangent lines of face *f*; see Section 3.3.2 for examples of tangent lines to face *f*). At each increment, we project a vertical tangent line over the obstructing rack (e.g., self, preceding, succeeding) and find the height (V_H) that this projected line intersects face *f*. We project these lines until V_H crosses h (i.e., $V_H > h \; \forall \varphi_1 = [\varphi_{\min}, a]$, $V_H < h \; \forall \; \varphi_1 = [a + \gamma_1, \varphi_{max}]$ where a is any increment of φ_1). If a crossing in rank occurs between these two variables is found (i.e., one becomes larger than the other), then this entire process repeats for with progressively finer increment angles ($\gamma_2 > \gamma_3 > \gamma_4$) where the respective count variable ($\varphi_2, \varphi_3, \varphi_4$) is incremented (i.e., see line (8) for details of the second incremental stage). At the 4th incremental stage, we check at each increment if $V_H = h$. If so, the coordinates (X_I, Y_I) are found of that intersection point with face *f*, and saved as a candidate point (see illustrations in Figure C6 and equations (13) and (14) in Figure C7).

Procedure C1. Numerical algorithm to determine candidate points of vertical tangent curves.

(1) **For** face (f)
(2) **For** rack (*n*)
(3) **For** previous rack (*p*)
(4) **Compute** φ_{min} and φ_{max} based on tangent lines to face *f*
(5) **For** φ_1 **in** φ_{min} **to** φ_{max} **by** γ_1
(6) **Find** height (V_H) where tangent line from obstruction point to rack (*n-p*) intersects with face (*f*) on rack (*n*). See Figure C2 and Figure C3.
(7) **If** V_H crosses *h*
(8) **For** φ_2 **in** φ_1 - γ_1 **to** φ_1 **by** γ_2
(9) **Repeat** (6) – (7)
(10) **For** φ_3 **in** φ_2 - γ_2 **to** φ_2 **by** γ_3
(11) **Repeat** (6) – (7)
(12) **For** φ_4 **in** φ_3 - γ_3 **to** φ_3 **by** γ_4
(13) **If** $V_H = h$
(14) **If** there are no racks between the obstructing rack and the shopper that obstruct the tangent line
(15) **Save** X_I & Y_I coordinates of intersection point as a candidate point

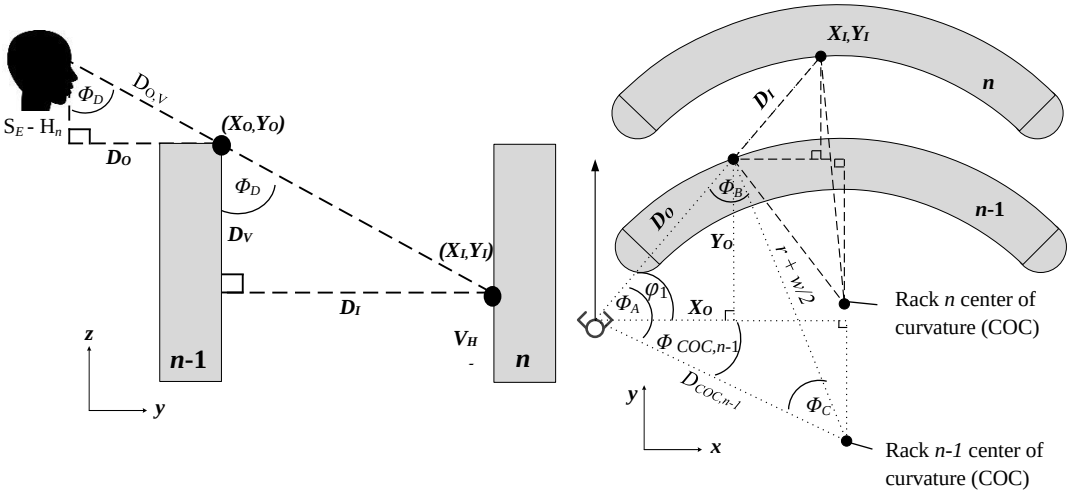

Figure C6. Illustration of vertical tangent lines

(1) $\Phi_A = (90 - \varphi_1) + \Phi_{COC,n-1}$

(2) $\Phi_B = \sin^{-1}\left(\frac{D_{COC,n-1} * \sin(\Phi_A)}{r+\frac{w}{2}}\right)$

(3) $\Phi_C = 180 - (\Phi_A + \Phi_B)$

(4) $D_O = \frac{(r+\frac{w}{2}) * \sin(\Phi_C)}{\sin(\Phi_A)}$

(5) $X_O = D_O * \sin(90 - \varphi_1)$

(6) $Y_O = D_O * \sin(\varphi_1)$

(7) $D_{O,V} = \sqrt{D_O{}^2 + (S_E - H_{n-1})^2}$

(8) $\Phi_D = \sin^{-1}\left(\frac{D_{O,V}}{D_O}\right)$

(9) $\Phi_{A'} = (90 - \varphi_1) + \Phi_{COC,n}$

(10) $\Phi_{B'} = \sin^{-1}\left(\frac{D_{COC,n} * \sin(\Phi_{A'})}{r+\frac{w}{2}}\right)$

(11) $\Phi_{C'} = 180 - (\Phi_{A'} + \Phi_{B'})$

(12) $D_I = \frac{(r+\frac{w}{2}) * \sin(\Phi_{C'})}{\sin(\Phi_{A'})}$

(13) $X_I = D_I * \sin(90 - \varphi_1)$

(14) $Y_I = D_I * \sin(\varphi_1)$

(15) $D_V = D_I * \frac{\sin(\Phi_D)}{\sin(90 - \Phi_D)}$

(16) $V_H = H_{n-1} - D_V$

Figure C7. Analytical expressions to determine vertical tangent lines

Appendix C.2: Approximation Algorithm for Dead Zone Curve

When determining exposure at heights above and below the shopper's eye height, we must also check if a candidate point falls within the "dead zone of vision" that exists due to the vertical angular limits (see Figure C8(c)). Points must lie beyond this zone to be considered feasible. Figure C8(a) displays an illustration of this curve on the X-Y plane at a height *h* (above or below eye-height), which is made up of two connecting curves (one for head movement (Ω_{HR}), the other for eye movement (Φ_{HR})).

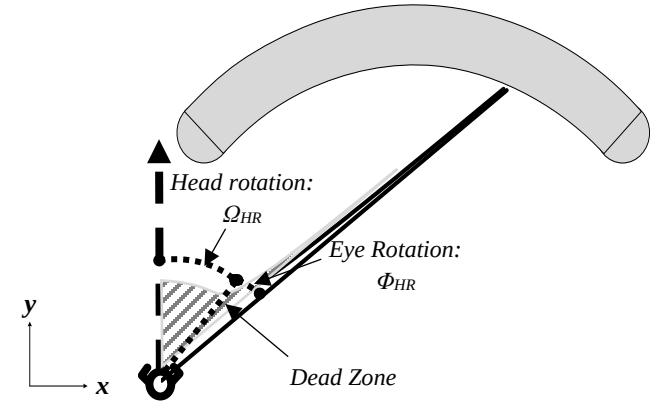

(a) Top view

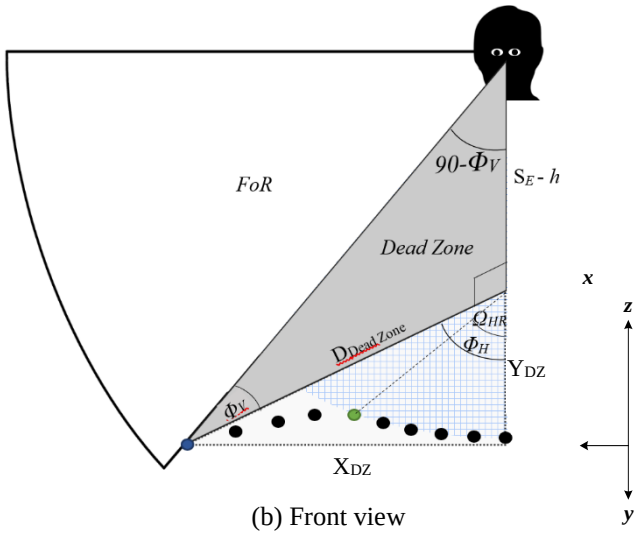

(b) Front view

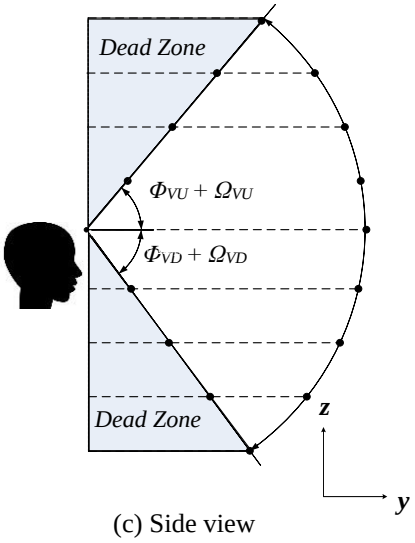

(c) Side view

Figure C8. Illustration of dead zone curve (a) top view (b) front view (c) side view

Figure C8(b) illustrates a front view of the shopper's head looking down onto an X-Y plane below their eye-height. The dead zone from this perspective is in the form of a right triangle at a specific angle Φ_H. We project this triangle at discrete values of Φ_H in the range [0, $\Omega_{HR} + \Phi_{HR}$] to approximate the dead zone curve at height h. Values of Φ_H from 0 to Ω_{HR} create the curve resulting from head rotation, and values of Φ_H from Ω_{HR} to $\Omega_{HR} + \Phi_{HR}$ create the curve resulting from the eye's curvature. A summary of the calculation steps to determine the coordinate points (X_{DZ}, Y_{DZ}) of the dead zone curve at a given value of Φ_H are shown in Procedure C2 below:

Procedure C2. Calculation steps to determine candidate points of dead zone intersection with rack.

(1) *If* $\Phi_H < \Omega_{HR}$
(2) $\Phi_V = \Phi_{VD}$
(3) *Else*
(4) $\Phi_V = \frac{\Phi_{VU}}{\Phi_{HR}} \sqrt{(\Phi_{HR})^2 - (\Phi_H)^2}$
(5) $D_{\text{Dead Zone}} = (S_E - h) * \frac{\sin(90 - \Phi_V)}{\sin(\Phi_V)}$
(6) $X_{DZ} = D_{\text{Dead Zone}} * \sin \Phi_H$
(7) $Y_{DZ} = D_{\text{Dead Zone}} * \sin(90 - \Phi_H)$

We propose a numerical algorithm to determine this curve's intersection with a face (f) on rack (n). An outline of this approach is as follows in Procedure C3.

Procedure C3. Numerical algorithm to determine candidate points of dead zone curve.

(1) **For** face (*f*)
(2) **For** rack (*n*)
(3) **Compute** φ_{min} and φ_{max} based on tangent lines to face *f*
(4) **For** φ_1 **in** φ_{min} **to** φ_{max} **by** γ_1
(5) **Compute** Distance from Shopper to Dead Zone Curve ($D_{Dead\ Zone}$)
(6) **Compute** Distance from shopper to intersection with rack circle (D_{fn})
(7) **If** rank changes (e.g., $D_{Dead\ Zone} > D_{fn}\ \forall\ [\varphi_{min}, \varphi_1]$, $D_{Dead\ Zone} < D_{fn}\ \forall\ [\varphi_1 + \gamma_1, \varphi_{max}]$)
(8) **For** φ_2 **in** $\varphi_1 - \gamma_1$ **to** φ_1 **by** γ_2
(9) **Repeat** 5**,** 6,7
(10) **For** φ_3 **in** $\varphi_2 - \gamma_2$ **to** φ_2 **by** γ_3
(11) **Repeat** 5**,** 6,7
(12) **For** φ_4 **in** $\varphi_3 - \gamma_3$ **to** φ_3 **by** γ_4
(13) **Compute** $X_{Dead\ Zone}$,$Y_{Dead\ Zone}$
(14) **Compute** X_{nf},Y_{nf}
(15) **If** $X_{Dead\ Zone} = X_{nf}$ & $Y_{Dead\ Zone} = Y_{nf}$
(16) **Save** $X_{Dead\ Zone}$ & $Y_{Dead\ Zone}$ coordinates of intersection point as a candidate point

The algorithm begins by determining angular bounds (φ_{min}, φ_{max}) where the intersection points could possibly exist (step 3). These bounds are based on the tangent lines to face *f* on rack *n* (i.e., see Section 3.3.2 for examples of tangent lines to face *f).* Once these are obtained, for angle φ_1 in increments of γ_1, the distance from the shopper to the dead zone curve ($D_{Dead\ Zone}$) and the Euclidean distance to face *f* on rack *n* (D_{fn}) are calculated (steps 4,5,6). Subsequently, a check is made to see if the rank of each distance changes from the previous increment (i.e., one distance suddenly becomes larger than the

other) (step 7). This indicates that there is an intersection point between the angle of the previous step (φ_1- γ_1) and the current step (φ_1); we subsequently return φ_1 to the previous step (φ_1- γ_1). In order for our approximation algorithm to be both fast and precise, we repeat steps 5, 6, and 7 two additional times using increasingly smaller increment sizes ($\gamma_1 < \gamma_2 < \gamma_3$) to pinpoint the location of the intersection point. We then include a fourth incremental stage ($\gamma_4 < \gamma_3$) where we find the angle (φ_4) where both the x and y coordinates of each intersection point are approximately equal (i.e., $X_{De}=X_{nf}$ and $Y_{DZ}=Y_{nf}$).

Appendix C.3: Additional Considerations for Estimating 3D Exposure

Since the *DOV* of a shopper's eye extends as a radius in a spherical form, the effective depth of vision will change based on the height at each height *h*. We define this effective depth of vision as DOV_h, which can be calculated analytically considering *DOV*, *h*, and S_E. Figure C9 below illustrates these calculations.

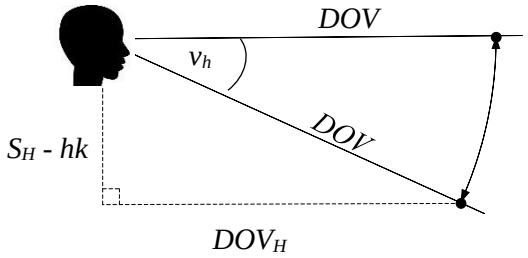

$$v_h = \sin^{-1}\left(\frac{S_H - h}{DOV}\right)$$

$$DOV_H = \sqrt{(DOV)^2 - (S_H - h)^2}$$

Figure C9. Changing DOV with changes in height

Further, the effective horizontal angular limit at height *h* $(\Phi_H + \Omega_H)_h$ will also change with respect to *h*. In other words, the maximum angular limits (left and right) for a human's eye occurs at eye-height; these limits will shrink when shifting the focal point up or down. To determine $(\Phi_H + \Omega_H)_h$, we first determine the vertical angle *v* associated with *h* and then utilize the equation of an ellipse (approximation of the 3D FoR) considering the horizontal and vertical angular limits. Figure C10 below illustrates this procedure.

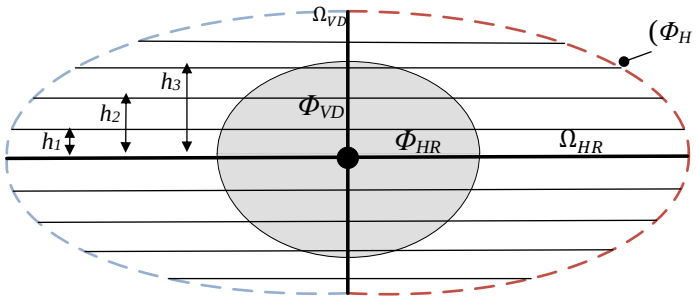

$$(\Phi_H + \Omega_H)_h = \frac{\Phi_{HR} + \Omega_{HR}}{\Phi_{VD} + \Omega_{VD}} \sqrt{(\Phi_{VD} + \Omega_{VD})^2 - v_h}$$

Figure C10. Changing angular limits with changes in height

Appendix C.4. An Example of Illustrating our Proposed Approach

We present in this appendix an example of how we estimate exposure in 3D at a shopper step *y*. In this example, we will present analytical expressions to derive select candidate points (at two different heights *h*), in addition to select feasibility checks. Figure C11 illustrates, in 3D, a few candidate points that fall within the shopper's FoR at that step *y*. These points are notated by their (x,y,z) coordinate points (i.e., X_{CP_1} and X_{CP_1} represent the x and y coordinates of candidate point 1; S_E is the known z coordinate). Green shaded points are feasible, while the red shaded points are infeasible; these points are determined based on the approach presented in the main body of the paper.

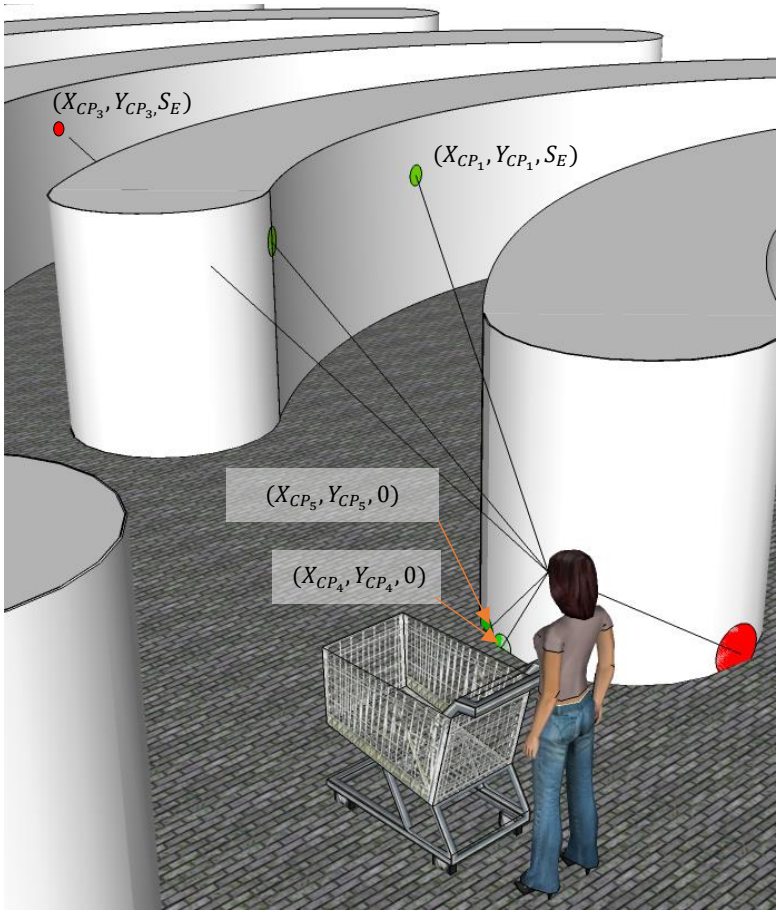

Figure C11. 3D view of select candidate points at shopper step *y*.

Candidate Points 1 and 2: We first present expressions to find candidate points 1 and 2. These points are illustrated as green circles on face B on rack $n + 1$ in Figure C12. Since both points are at height $h=S_E$, racks in Figure C12 are shown on a 2D x-y plane at this height. We denote the position of the shopper at step y through coordinates (X_s, Y_s). A non-candidate point that is utilized in expressions is denoted by (X_p, Y_p). Midpoints of rack endcaps are denoted as (X_M, Y_M). All line segments are denoted as D in units of feet, while all angles are φ, in units of degrees.

For these expressions, and all others in this appendix, we use the design values in Table C5 and Table C6.

Table C5. Design values for rack layout.

Name	Notation	Value
Rack height	H	7 ft
Rack width	w	5 ft
Orientation	θ	90°
Curvature	α	90°
Perimeter	p	110 ft
Min distance between racks	a_c	8 ft
Shopper distance to racks	a_m	5 ft
Main aisle width	a_w	10 ft
Depth of vision	DOV	40 ft
Radius	r	30.01 ft
Shopper eye-height	S_E	5 ft

Table C6. Eye and head movement parameters.

Eye Movements				*Head Movements*			
Φ_H	Φ_{HR}	Φ_{VU}	Φ_{VD}	Ω_{HL}	Ω_{HR}	Ω_{VU}	Ω_{VD}
15°	15°	15°	15°	75°	75°	25°	25°

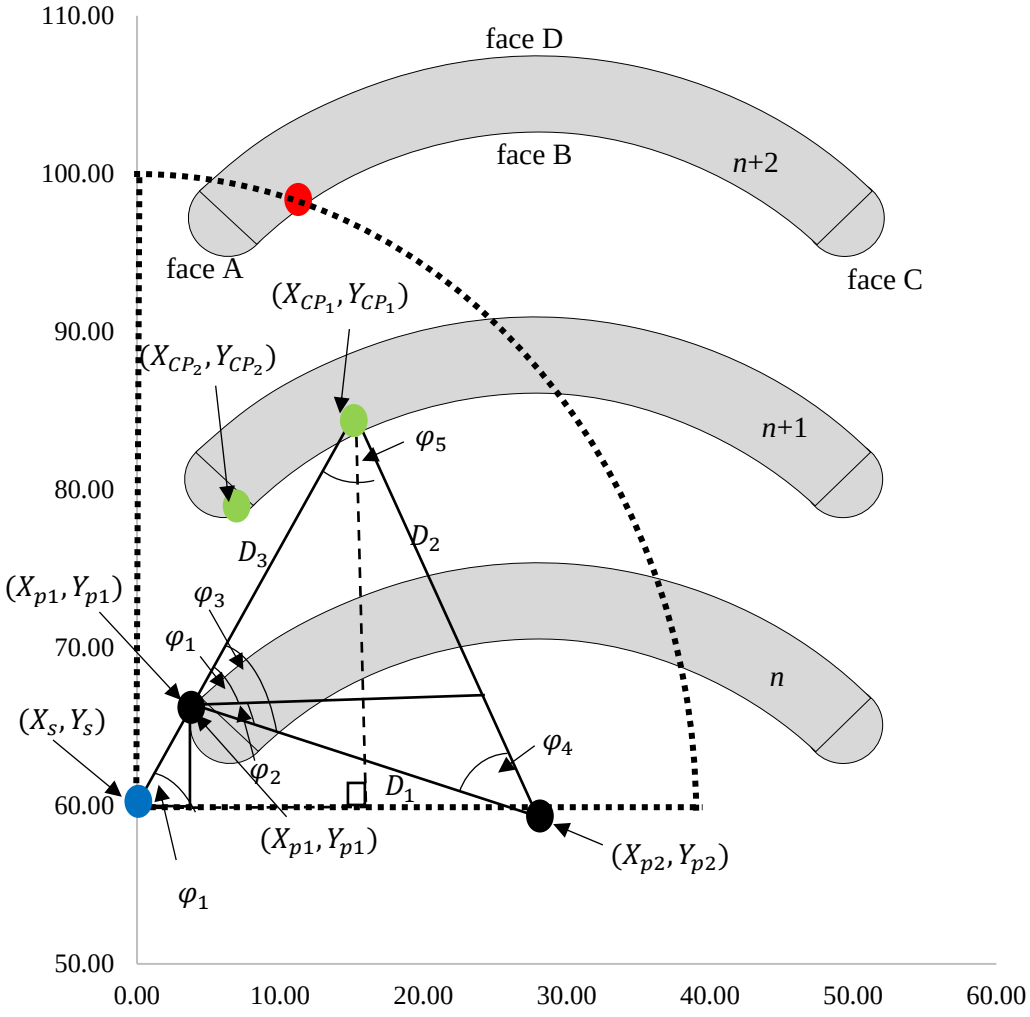

Figure C12. Finding candidate points 1 and 2 at height $h = S_E$.

$$\varphi_1 = \tan^{-1}\left(\frac{Y_{p1}-Y_S}{X_{p1}-X_S}\right) = \tan^{-1}\left(\frac{66.61-60}{5.59-0}\right) = 49.79 \quad (1)$$

$$D_1 = \sqrt{\left(X_{p2}-X_{p1}\right)^2 + \left(Y_{p2}-Y_{p1}\right)^2}$$

$$D_1 = \sqrt{(28.72-5.59)^2 + (59.97-66.61)^2} = 24.07 \quad (2)$$

$$D_2 = r - \frac{w}{2} = 30.01 - \frac{5}{2} = 27.51 \quad (3)$$

$$\varphi_2 = \tan^{-1}\left(\frac{Y_{p2}-Y_{p1}}{X_{p2}-X_{p1}}\right) = \tan^{-1}\left(\frac{59.97-66.61}{28.72-5.59}\right) = -16.03 \quad (4)$$

$\varphi_3 = \varphi_2 - \varphi_1 = -16.03 - 49.79 = -65.82$ (5)

$\varphi_4 = \sin^{-1}\left(\frac{D_1 * \sin(\varphi_3)}{D_2}\right) = \sin^{-1}\left(\frac{24.07 * \sin(-65.82)}{27.51}\right) = -52.94$ (6)

$\varphi_5 = 180 - (\varphi_4 + \varphi_3) = 180 - (-52.94 + -65.82) = 298.77$ (7)

$D_3 = \left(\frac{D_1 * \sin(\varphi_5)}{\sin(\varphi_4)}\right) = \left(\frac{24.07 * \sin(298.77)}{\sin(-52.94)}\right) = 26.44$ (8)

$X_{CP} = D_3 * \sin(90 - \varphi_1) + X_s = 26.44 * \sin(90 - 49.79) + 0 = 22.66$ (9)

$Y_{CP} = D_3 * \sin(\varphi_1) + Y_s = 26.44 * \sin(49.79) + 60 = 86.80$ (10)

Candidate Point 3: We now present expressions to find candidate point 3, which is the intersection of the shopper's FoR with face B on rack *n* + 2. Figure C13 illustrates how this point is derived.

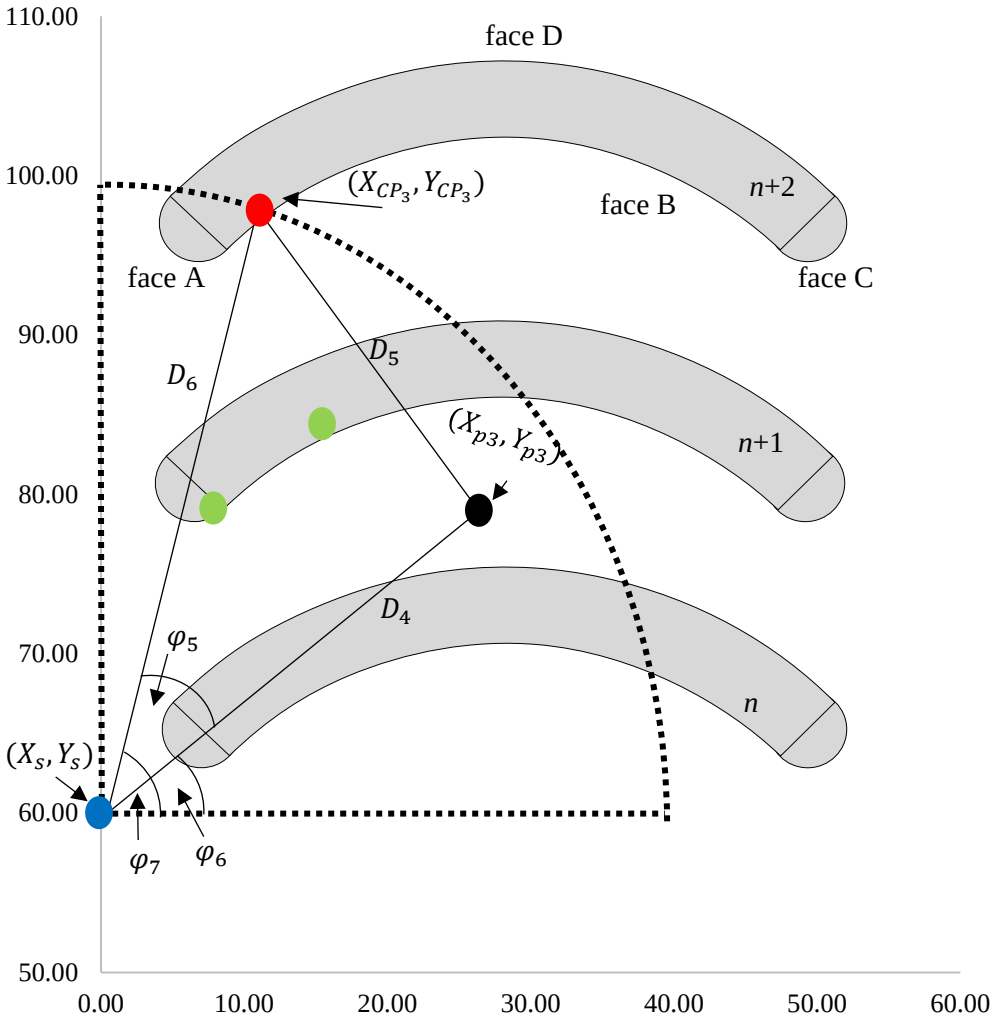

Figure C13. Finding candidate point 3 at height $h = S_E$.

$$D_4 = \sqrt{(Y_s - Y_{p3})^2 + (X_s - X_{p3})^2} = \sqrt{(60 - 76.16)^2 + (0 - 28.72)^2} = 32.96 \quad (11)$$

$$D_5 = r - \frac{w}{2} = 30.01 - \frac{5}{2} = 27.51 \quad (12)$$

$$D_6 = DOV = 40 \quad (13)$$

$$\varphi_5 = \cos^{-1}\left(\frac{(D_6)^2 - (D_5)^2 + (D_4)^2}{(2 * D_4 * D_6)}\right) = \cos^{-1}\left(\frac{40^2 - 27.51^2 + 32.96^2}{2 * 32.96 * 40}\right) = 43.29 \quad (14)$$

$$\varphi_6 = \tan^{-1}\left(\frac{(Y_{p3} - Y_s)}{(X_{p3} - X_s)}\right) = \tan^{-1}\left(\frac{(76.16 - 60)}{(28.72 - 0)}\right) = 29.36 \quad (15)$$

$$\varphi_7 = \varphi_5 + \varphi_6 = 43.29 + 29.36 = 72.65 \quad (16)$$

$$X_{CP_3} = D_6 * \sin(90 - \varphi_7) + X_s = 40 * \sin(90 - 72.65) = 11.84 \quad (17)$$

$$Y_{CP_3} = D_6 * \sin(\varphi_7) + Y_s = 40 * \sin(72.65) = 97.88 \quad (18)$$

As illustrated in Figure C14, candidate point 3 is infeasible. In fact, it is obstructed by both face A and face D of rack *n* + 1. We present below expressions to check obstruction from face D of rack *n* + 1. Figure C15 illustrates how this check is completed.

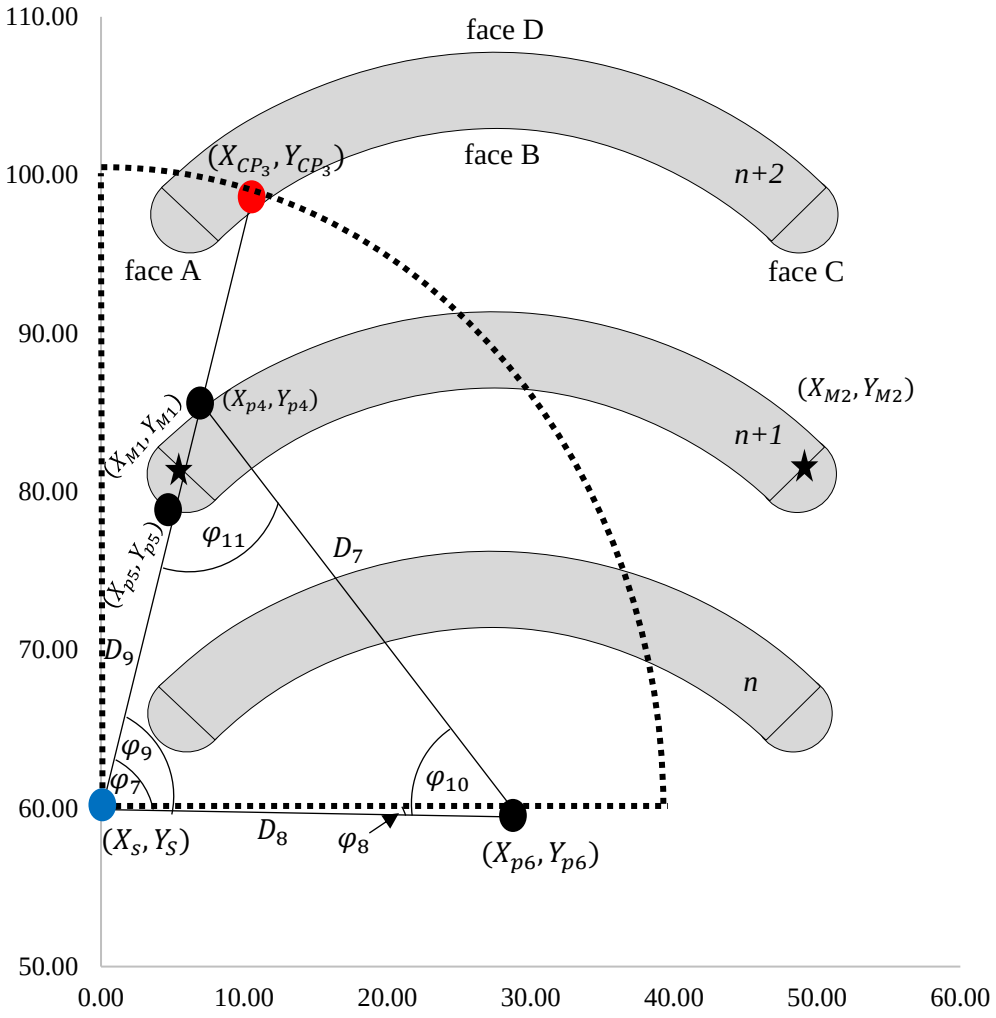

Figure C14. Finding obstruction points to candidate point 3.

$$D_7 = r + \frac{w}{2} = 30.01 + \frac{5}{2} = 32.51 \quad (19)$$

$$D_8 = \sqrt{\left(Y_s - Y_{p6}\right)^2 + \left(Y_s - Y_{p6}\right)^2} = \sqrt{(60 - 59.97)^2 + (0 - 28.72)^2} = 28.72 \quad (20)$$

$$\varphi_8 = \left(\tan^{-1}\left(\frac{(Y_{p6} - Y_s)}{(X_{p6} - Y_s)}\right)\right) = \tan^{-1}\left(\frac{59.97-60}{28.72-0}\right) = -.06 \quad (21)$$

$$\varphi_9 = \varphi_7 - \varphi_8 \ = 72.65 - -.06 = 72.71 \quad (22)$$

$$\varphi_{10} = \sin^{-1}\left(\frac{D_8 * \sin(\varphi_9)}{D_7}\right) = \sin^{-1}\left(\frac{28.72 * \sin(72.71)}{32.51}\right) = 57.51 \quad (23)$$

$$\varphi_{11} = 180 - (\varphi_9 + \varphi_{10}) = 180 - (72.71 + 57.51) = 49.78 \quad (24)$$

$$D_9 = \left(\frac{(D_7) * \sin(\varphi_{11})}{\sin(\varphi_9)}\right) = \left(\frac{32.51 * \sin(49.78)}{\sin(72.711)}\right) = 26.00 \quad (25)$$

$$X_{p4} = D_9 * \sin(90 - \varphi_7) + X_s = 26.00 * \sin(90 - 72.65) + 0 = 7.75 \quad (26)$$

$$Y_{p4} = D_9 * \sin(\varphi_7) + Y_s = 26.00 * \sin(72.65) + 60 = 84.82 \quad (27)$$

Once we know the location of this intersection point, we need to find out if this point is blocking the shopper's view of the candidate point. In other words, we want to find out if this point is on physical part (i.e., the face D) of the circle it resides on, and if this point is *between* shopper and candidate point.

If $Y_{M1} = Y_{M2}$ (81.19 = 81.19) and $X_{M1} < X_{M2}$ (7.5 < 49.95) then (28)

If $Y_{p4} > Y_{M1}$ (84.81 > 81.19) then (29)

If $D_9 < D_6$ (26.00 < 40) then (30)

Candidate Point 4 is infeasible (31)

Since both of these conditions are true in this case, candidate point 3 is obstructed from face D of rack n+1, and thus infeasible.

Candidate Points 4, 5, and 6 (at height *h*=0): We now consider a few candidate points at height *h*=0. These three points fall on rack *n*, face A. Candidate point 4 (feasible) represents the intersection of the dead zone curve with face A; the procedure to obtain these coordinates are found in Appendix C.2. Candidate point 5 (feasible) is the corner of face

A and face D. Candidate point 6 is the intersection of the tangent line from the shopper to face A. We now present expressions to obtain the coordinates of candidate point 6, and provide expressions for the feasibility check that makes this point infeasible. Figure C15 illustrates how these are derived.

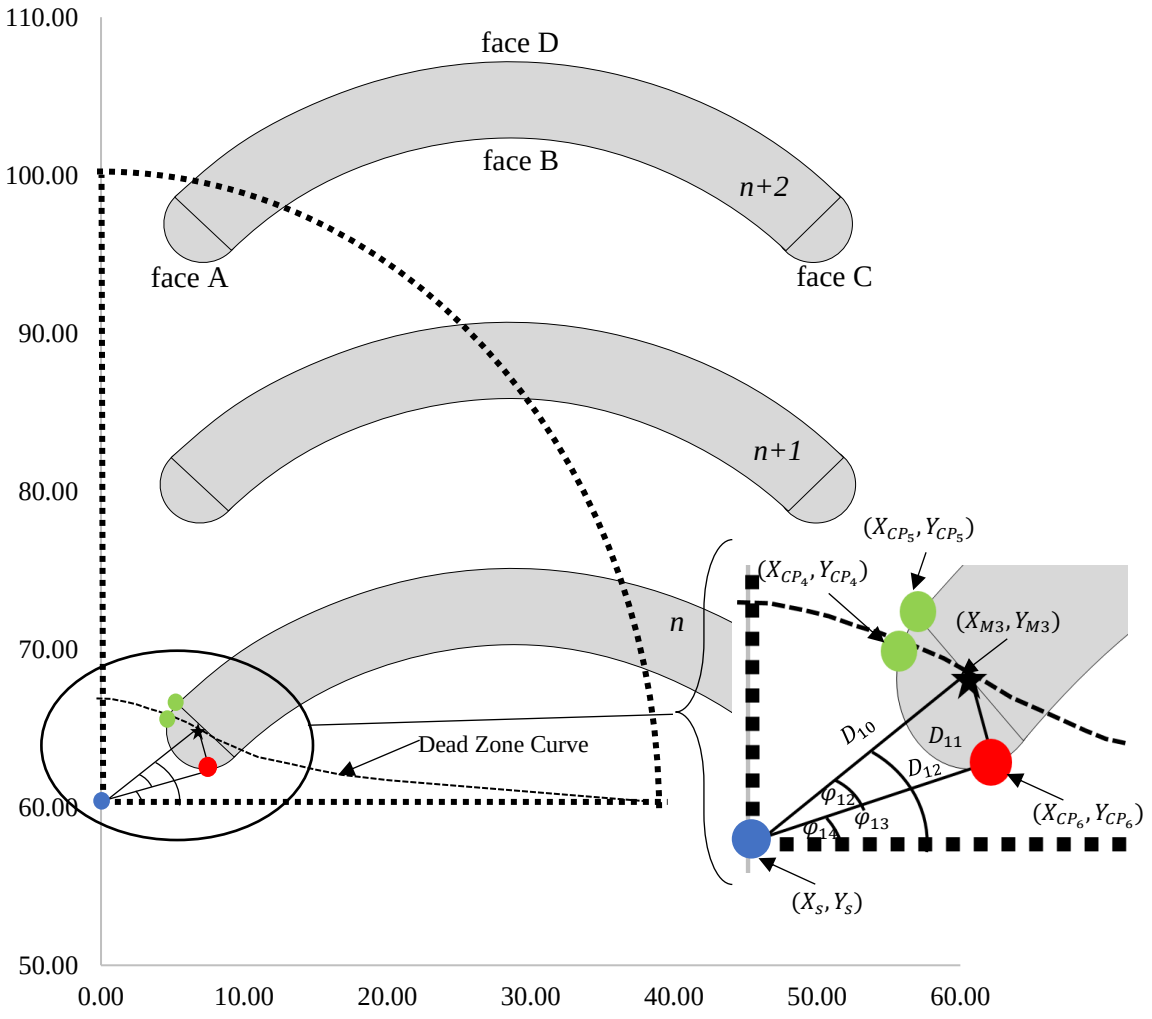

Figure C15. Finding candidate point 6 at height $h = 0$.

$$D_{10} = \sqrt{(X_{M3} - X_s)^2 + (Y_{M3} - Y_s)^2} = \sqrt{(7.5 - 0)^2 + (65 - 60)^2} = 9.01 \quad (32)$$

$$D_{11} = \frac{w}{2} = \frac{5}{2} = 2.5 \quad (33)$$

$$D_{12} = \sqrt{(D_{10})^2 - (D_{11})^2} = \sqrt{(9.01)^2 - (2.5)^2} = 8.66 \quad (34)$$

$$\varphi_{12} = \sin^{-1}\left(\frac{D_{11}}{D_{10}}\right) = \sin^{-1}\left(\frac{2.5}{9.01}\right) = 16.10 \quad (35)$$

$$\varphi_{13} = \sin^{-1}\left(\frac{Y_{M3} - Y_S}{D_{10}}\right) = \sin^{-1}\left(\frac{65}{9.01}\right) = 33.69 \quad (36)$$

$$\varphi_{14} = \varphi_{13} - \varphi_{12} = 33.69 - 16.10 = 17.59 \quad (37)$$

$$X_{CP_6} = D_{12} * \sin(90 - \varphi_{14}) + X_s = 8.66 * \sin(90 - 17.59) + 0 = 8.26 \quad (38)$$

$$Y_{CP_6} = D_{12} * \sin(\varphi_{14}) + Y_s = 8.66 * \sin(17.59) + 60 = 62.62 \quad (39)$$

We now present the expressions to check whether or not this candidate point falls within the dead zone. This dead zone is bounded by a curve at height *h* as shown in Figure C16.

$$\varphi_v = \frac{(\Omega_{VD} + \Phi_{VD})}{(\Omega_{HR} + \Phi_{HR})}\sqrt{(\Omega_{HR} + \Phi_{HR})^2 - (90 - \varphi_{14})^2}$$

$$\varphi_v = \frac{25+15}{75+15}\sqrt{(75 + 15)^2 - (90 - 17.59)^2} = 23.8 \quad (40)$$

$$D_{13} = (S_E - h) * \frac{\sin(90 - \varphi_v)}{\sin(\varphi_v)} = (5 - 0) * \frac{\sin(90 - 23.8)}{\sin(23.8)} = 11.36 \quad (41)$$

$$X_f = D_{13} * \sin(90 - \varphi_{14}) + X_s = 11.36 * \sin(90 - 17.59) + 0 = 10.83 \quad (42)$$

$$Y_f = D_{13} * \sin(\varphi_{14}) + Y_s = 11.36 * \sin(17.59) + 60 = 63.43 \quad (43)$$

If $D_{13} > D_{12}$ $(11.36 > 8.66)$ $Then$ (44)

Candidate point 6 is infeasible (45)

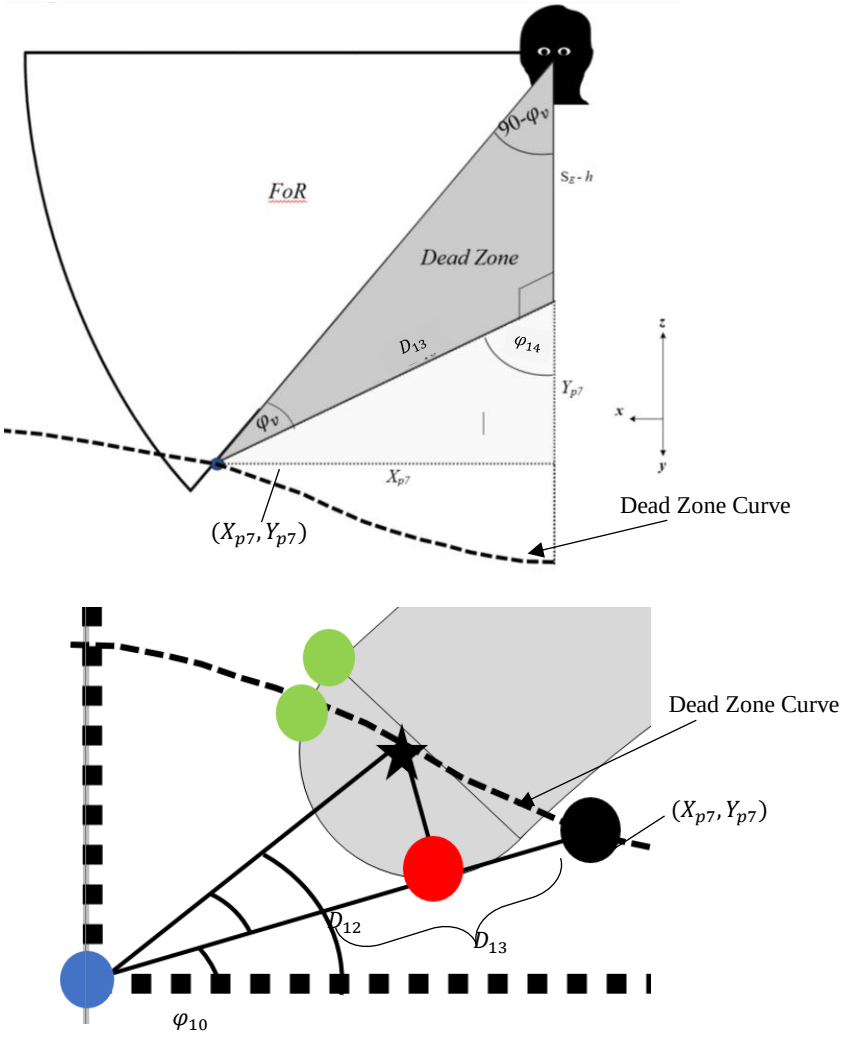

Figure C16. Determining if candidate point 6 is in dead zone.

Appendix D. Models for Space and Aspect Ratio

We estimate the floor space A of a given layout by the rectangular area that bounds the perimeter of the layout. Let L and W be the length and width of this rectangular bounded area. To find L and W, we must determine the left-most and right-most edges of this rectangle along the width (x-direction) and the length (y-direction). Let these be represented as (X_{min}, X_{max}) and (Y_{min}, Y_{max}), respectively, such that $W = X_{max} - X_{min}$ and $L = Y_{max} - Y_{min}$. Depending on the combination of θ and α for a specific layout, these extreme points may fall on Faces A, C, or D. We propose an exact procedure to determine L and W as illustrated in Figure D1. Subsequently, the floor space A ($A = L \times W$) and the aspect ratio R ($R = \frac{L}{W}$) can be estimated.

(1) **For** $n = 1$ or $n = N$

(2) **For** $f \in$ {A, C, D}

(3) **Compute** extreme points of face f in x and y directions

(4) $X_{max,n,A} = X_{midpoint,n,A} + r_f$

(5) $X_{min,n,A} = X_{midpoint,n,A} - r_f$

(6) $Y_{max,n,A} = Y_{midpoint,n,A} + r_f$

(7) $Y_{min,n,A} = Y_{midpoint,n,A} - r_f$

(8) **Determine** if points fall on the physical part of rack (per Table 2).

(9) **Compare** the feasible extreme points to determine X_{max}, X_{min}, Y_{max}, and Y_{min}

(10) $X_{max} = \max\{X_{max,n,f}; \forall f, n\}$

(11) $X_{min} = \min\{X_{min,n,f}; \forall f, n\}$

(12) $Y_{max} = \max\{Y_{max,n,f}; \forall f, n\}$

(13) $Y_{min} = \min\{Y_{min,n,f}; \forall f, n\}$

(14) **Compute** $L = Y_{max} - Y_{min}$ and $W = X_{max} - X_{min}$

Figure D1. Exact procedure to estimate L and W of the layout

Figure D2 illustrates 3 example layouts with their respective dimensions (L, W) and locations of values X_{max}, X_{min}, Y_{max}, and Y_{min}.

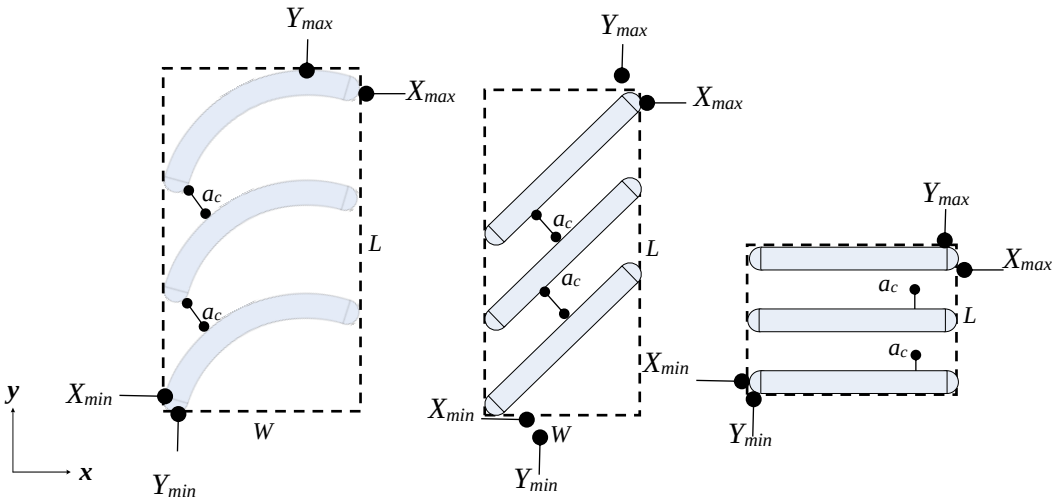

(a) θ = 60°, α = 90° (b) θ = 45°, α = 0° (c) θ = 90°, α = 0°

Figure D2. Dimensions of L and W for example layouts with N = 3

Using the above procedure, we can compute the floor space for any combination of θ and α. Figure D3 presents the floor space (right side only) for 133 combinations of θ and α with values of θ ranging from 0° to 180° in steps of 10° and values of α ranging from 0° to 180° in steps of 30°. Design parameters are identical to those in Table 5. For this specific configuration, the maximum floor space occurs at θ=40° and θ=140°, while minimum values occur at θ=0° and θ=180°. Further, among values of α, α=0° results in the minimum floor space across all values of θ. The value of α that results in the maximum floor space however varies across values of θ. For this specific configuration, at (θ=90°, θ=0°) and (θ=180°, α=150°) results in the maximum space value, while at θ=40° and θ=140°, α=90° results in the maximum space value. While it would seem intuitive that space would always increase as α increases from 0° to 180°, because our layouts maintain a fixed shelf-area for

any value of α, the chord length (i.e., aisle length) rapidly decreases as α approaches 180°. This reduced *W*, thereby, lowering the total floor space.

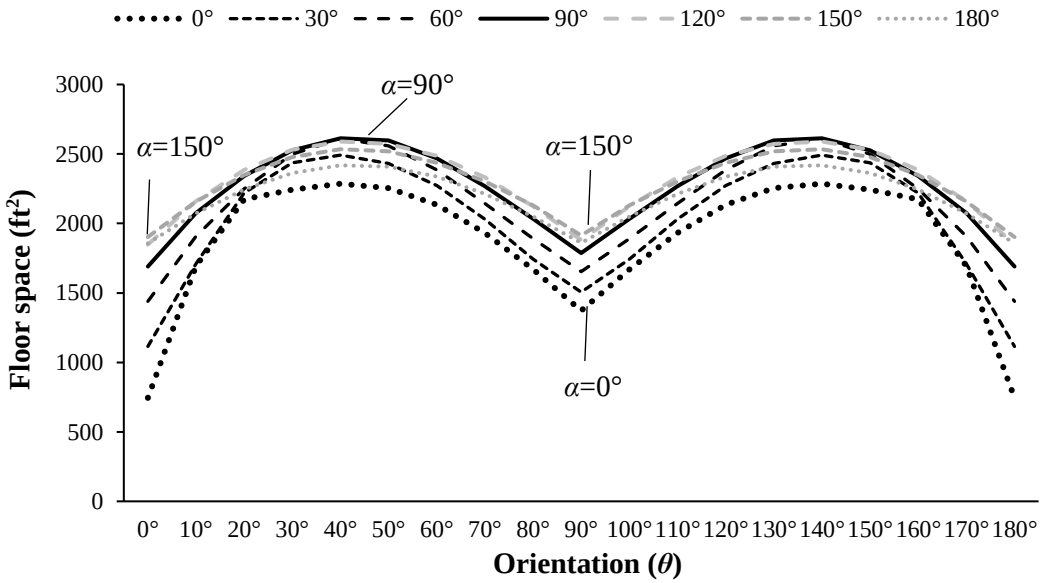

Figure D3. Change in floor space (ft^2) for various rack orientations and curvatures

Aspect ratio is illustrated in Figure D4. While the combination of $\theta = 0° = 180°$ and $\alpha = 0°$ resulted in in the lowest space, it provides for the highest aspect ratio (29.77); i.e., 'long and skinny'. The rack layout of $\theta = 90°$ and $\alpha = 0°$ provides the lowest (0.7); i.e., 'short and wide'. Notice here for θ values 0° and 10° (alternately, 180° and 170°) the aspect ratio *decreases* as α increases to 180°. This trend, however, steadily shifts to the aspect ratio *increasing* for an increasing α as θ approaches 90°. This phenomenon occurs due the nature of curved racks to increase either *W* or *L* values relative to α=0°. For θ values closer to 0° or 180°, the curved racks increase *W*, thereby lowering the aspect ratio as *L* is much higher. For θ values closer to 90°, the curved racks increase *L*, thereby increasing the aspect ratio as *W* is much higher in this case.

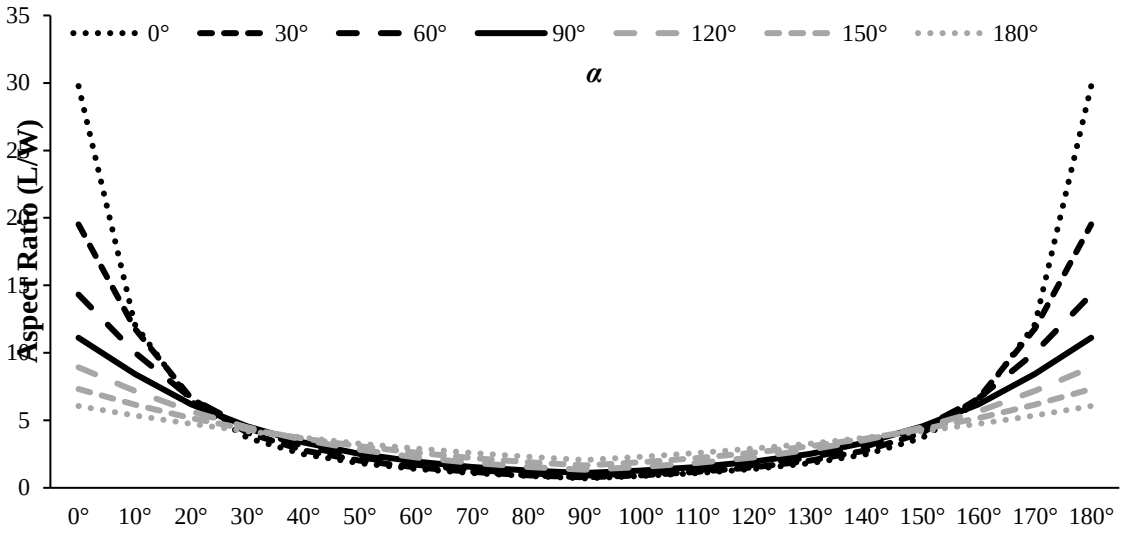

Figure D4. Change in Aspect Ratio with varying values of θ and α

Appendix E. Validation Study Conference Paper

Comparing and Enhancing the Analytical Model for Exposure of a Retail Facility Layout with Human Performance

Abstract ID: 1266

Bradley Guthrie, Pratik J. Parikh, Tyler Whitlock, Madison Glines, Thomas Wischgoll, John Flach, and Scott Watamaniuk
Wright State University
Dayton, OH 45435 USA

Abstract

Recent research in retail facility layout has focused on developing analytical models to *estimate* visibility measures of novel rack layouts based on assumptions about a shopper's field of view. However, because of the human element involved in the shopping experience, it is vital to compare these models relative to actual human performance. In this study, we evaluate the predictions of our previously developed analytical model (that estimates exposure of every location on a given rack layout assuming expected head movement) in a 3D Virtual Environment (VE). We conducted trials with 18 participants who were asked to find targets strategically placed on the racks for 9 unique layouts. A comparison of their performance with the analytical model suggested that our model performed well, but the performance varied across layouts. To enhance these exposure estimates from the analytical model, we combined it with parameters corresponding to human head movement collected from the VE study, along with layout and target location parameters, in a decision tree framework. Results indicate that combining analytical and empirical observations enhances the quality of estimates (test AUC = 0.9).

Keywords

Retail layout; exposure; human subjects; virtual environment

1. Retail Facility Layout

The facility layout in a retail setting plays an important role in the presentation of products to customers [1]. In fact, sales are a function of the number of people who are exposed (visually connected) to products [2]. As such, researchers have widely alluded to product exposure as a measure of importance for retail layout design [3]. Designing retail layouts catered to human visibility would potentially result in reduced search time for already planned purchases, as well as influence shoppers to make more unplanned purchases. Retail managers meanwhile would benefit by strategically placing their products in ‘hot spots' potentially increasing impulse purchases.

Our motivation for evaluating layouts based on exposure primarily stems from our personal visits to local retail stores, as well as discovery of up-and-coming retail layouts online (Figures 1-3). Racks placed at a more acute orientation could provide better alignment with human vision. Curved racks potentially allow shoppers to have a better view of products deep in the aisle, and can be visually more appealing. Many studies in the retail domain address or allude to human visibility, from both analytical [4,5] and empirical perspectives [6]. However, these studies do not consider the effect of layout (e.g., rack

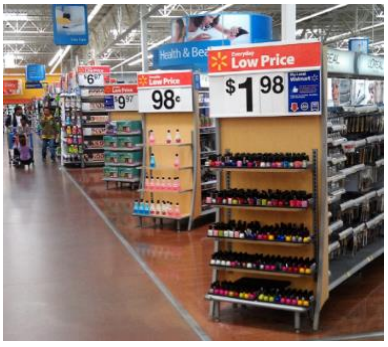

Figure 1. Racks oriented at 45°

Figure 2. Curved racks

Figure 3. Curved endcaps

orientation and curvature) on shopper visibility. The existing analytical approaches also lack comparisons of their models to human behavioral data.

The objective of this research is to compare our previously proposed analytical models with human performance through a study in a virtual store. That is, if our models suggested that orienting racks differently from a standard 90° would aid shoppers visually connect with more products, do actual shoppers experience that? What if the racks were curved as in Figure 2? Further, how would varying orientation and curvature affect the scanning pattern of shoppers? Would different layouts influence shoppers to make larger head rotations, or even increase the speed of their scanning? Using this information, we not only *compare* the performance of our analytical models with human performance, but also *enhance* the model's predictions with key human performance factors to increase the quality of prediction. The main goal is to use such a combined analytical-empirical model in optimizing the rack orientation and curvature to meet specific objectives; e.g., maximizing impulse purchases due to increased product exposure (for the retailer) and/or minimizing search time (for the shopper).

2. Existing Analytical Exposure Models with Human Vision

Mowrey et al. [7] recently proposed an analytical model and an algorithm to capture the dynamic interaction between a walking shopper's 2D field of regard (FoR) – the angular size of possible viewing angles for a fixation point – and a static layout of racks. They evaluated both exposure and intensity (time of exposure) of racks for varying orientations (θ).

Guthrie and Parikh [8] expand their work to model this interaction in 3D, while also considering both the curvature (α) and height of racks. Figure 4 illustrates how they model a shopper 3D FoR. They consider angular limits

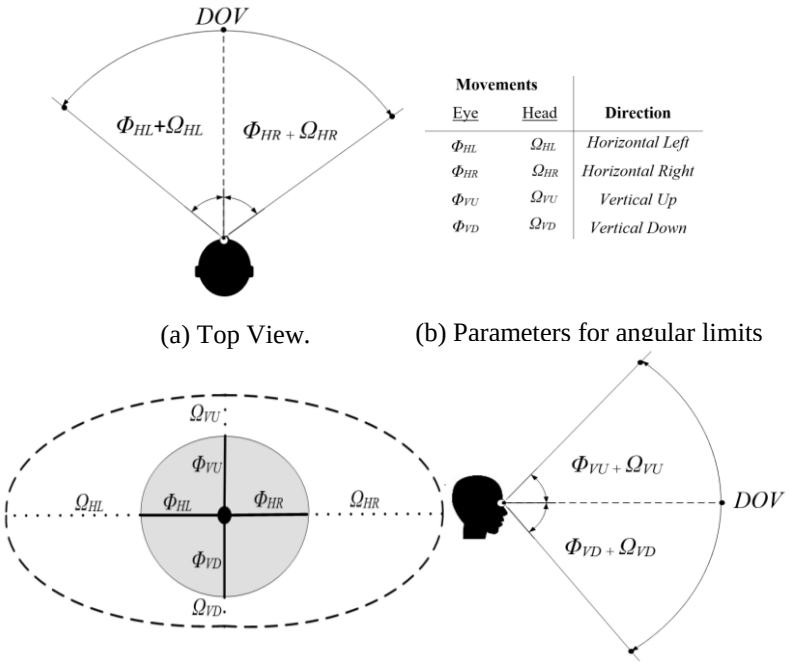

(a) Top View. (b) Parameters for angular limits

(c) Front view. (d) Side view.

Figure 4. Modeling a 3D FoR.

of vision in both horizontal and vertical dimensions (Figures 4(a) and (d)), along with the depth of vision (*DOV*). The combination of both horizontal and vertical limits is modeled as an elliptical sector of a sphere; see Figure 4(c), where they further break down these limits by head (Ω) and eye (Φ) rotations. To illustrate how this shopper FoR interacts with a layout of racks, Figure 5 contains two layouts (θ =orientation and α=curvature) with overlaid profiles of the intensity of exposure (red = longest exposed, yellow = shortest exposed, white = not exposed). Notice the different intensity levels starting from rack 2

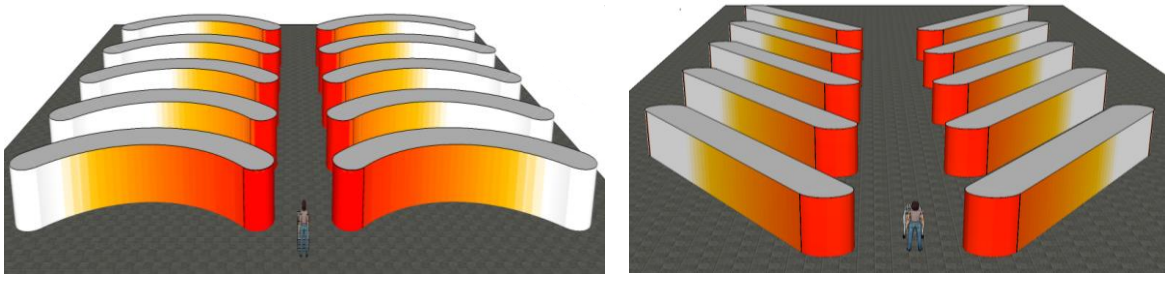

(a) Intensity of exposure for θ=90° and α=90° (b) Intensity of exposure for θ=30° and α=0°

Figure 5. Rack layout with overlaid intensity

between these figures, which occur due to the dynamic interaction of the shopper FoR with the curvature and orientation of the racks, and the resulting obstruction of the shopper FoR.

3. Virtual Environment for Comparing the Analytical Model with Human Performance

For this comparison, we evaluated human performance in a virtual environment (VE). This study was approved by Wright State University's Institutional Review Board (IRB).

3.1 VE Setup

The VE utilizes 27 LCD screens with LED backlight (each 55" in size) to create a three-walled CAVE-type immersive display to a height of 87 inches surrounding a 12x12 sq. ft. walkable area (see Figure 6). The optical tracking system composed of 11 cameras provided maximum redundancy and accuracy to track the user's head position. Based on that head position, the system recreates the user's perspective view on all 27 displays in such a way that the user feels completely immersed in the scenario. A head tracker captures both horizontal (x-axis) and vertical (z-axis) head movements made by the human participant. Additional details about the VE setup can be found in Wischgoll et al. [9].

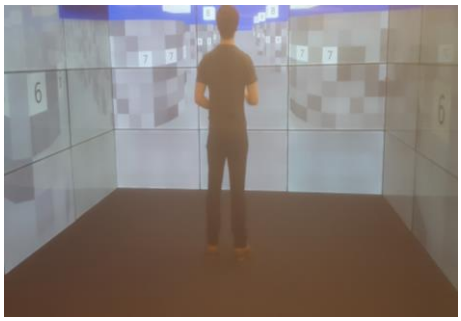

Figure 6. The VE set up; our co-author pictured

3.2 Study Design

We recruited 18 participants (of which 9 were female) between the ages of 19-26 years (avg=21.4) who had several years of prior shopping experience, and all were right-handed. Eleven participants had corrected vision and wore their glasses; all passed a visual acuity test. Each participant was informed through an IRB consent process before participating.

We limited our study to evaluating 9 rack layouts comprising all combinations of 3 values each of theta and alpha (θ = 45°, 90°, 135° and α = 0°, 30°, 90°). All racks were above the participant's eye height. Participants evaluated all 9 layouts over a 1-hour study period (including training). For each layout (containing 10 racks on either side), a participant was asked to search for targets (12 red colored squares, 1″x1″ in size) strategically placed on the front and back faces of the racks at distinct rows (i.e., heights) and columns (i.e., distance from walking aisle). The shopper's walking along the aisle was simulated by configuring the VE to move at a speed of 3.33 fps (similar to 3.41 fps in Daamen [10]) while the participant remained stationary. We simulated bidirectional travel by first letting the racks pass by the shopper in one direction and then reversing the environment to let the racks pass by in the reverse direction for the same layout. Participants were asked to push a button on a wireless device and call out the aisle number and side (left or right) when they saw a target. We conducted a total of 324 trials (18 trials x 18 participants) while recording their head movements.

4. Observed Human Behavior and Performance in the VE

Since we were able to record the actual head movements for each participant, we derived several measures to broadly analyze their scanning patterns. For this study, we focus on horizontal scanning patterns; vertical scans were relatively consistent with minimal variance and thus are not discussed. First, we calculated both the 'average head rotation' and the 'maximum head rotation' specific to each layout (in both forward and reverse directions). Figure 7 shows the time history for angular position (horizontal) for one participant in a layout with θ=135º and α=0º.

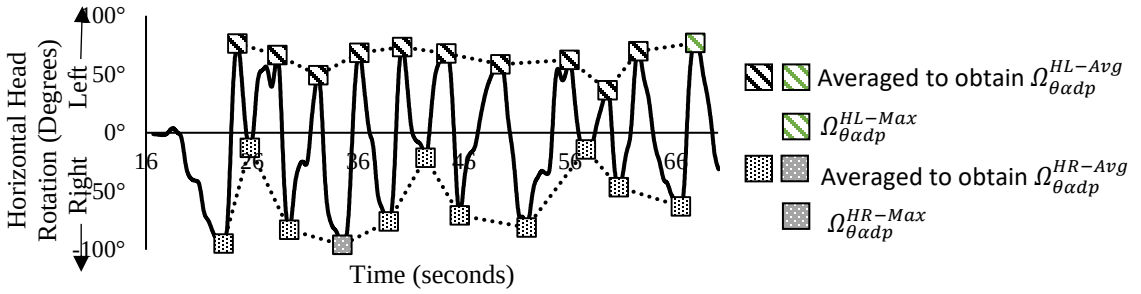

Figure 7. Head Rotation (horizontal) for single participant run

Each time the participant's head rotated across the center line of their pathway (0°), we recorded the maximum angle of the head turn. To derive an 'average head rotation' for each participant (*p*), we subsequently averaged these values (left and right, separately) across all orientations (θ), curvatures (α), and directions (*d*); these are notated as $\Omega_{\theta\alpha dp}^{HL-Avg}$ and $\Omega_{\theta\alpha dp}^{HR-Avg}$, respectively. Averaging across both directions and across all participants helps estimate the overall 'average head rotation,' $\Omega_{\theta\alpha d}^{H-Avg}$. Similarly, we derive the average 'maximum head rotation' across the two sides and all participants as $\Omega_{\theta\alpha d}^{H-Max}$.

Further, we derived the average angular speed (degrees/second or deg/s), average crossing speed (deg/s), number of center crosses, bias, and extreme head activity. Average angular speed was calculated by taking the average change in head position (over an increment of 0.001 sec) divided by the total run time. The number of center crosses was calculated as the number of times participants' heads rotated across the center point of the display (i.e., 0° line in Figure 7). Crossing speed is the average instantaneous velocity of a participant's head rotation for all crosses in a run. Bias was defined as the proportion of time a participant's head position was left of the center line, whereas 'absolute bias' represents the magnitude to which a participant favored either the right or left side. This is estimated as |0.5 – bias|. We define extreme head activity as the proportion of time where

speed of head position was above 100 deg/s or acceleration above 500 deg/s^2. This can be a factor in a participant not seeing a target due to such fast head movement.

Figure 8 depicts the normalized averages across 18 participants for each measure visualized as a star plot, for all 9 layouts. Values are normalized linearly on a 0-1 scale for each measure; 1 corresponds to the outer gridline, 0 is the center. Observing in Figure 8(a) the relatively high values of average angular speed, average head rotation, maximum head rotation, and extreme head activity for θ values of 135°, followed closely by 90°; these measures are close to 0 for θ = 45°. This is because rack orientations of 90° or greater required the shopper to use faster and larger head rotations to closely align their head rotation angle to the orientation of the racks given the constant forward translation. For racks oriented at 45°, however, much less head movement was required to see both rack faces.

Further, racks oriented at 90° resulted in participants being more biased toward one side verses the other, in addition to making a minimal number of crosses at relatively high speeds. These movements may be due to the relatively condensed space for these layouts (i.e., deviations of θ and α from 90° and 0° result in increased floor space and travel path – space models not included due to space limitations), exposing participants to view a relatively large quantity of rack area per unit of time along their path. For reverse travel in each of these layouts, similar, but opposite patterns were observed likely because the angles in the reverse direction are complementary to the forward travel. So for the same participant, the behavior for θ = 135° in the forward direction would closely resemble that for θ = 45°in the reverse direction (Figure 8(b)).

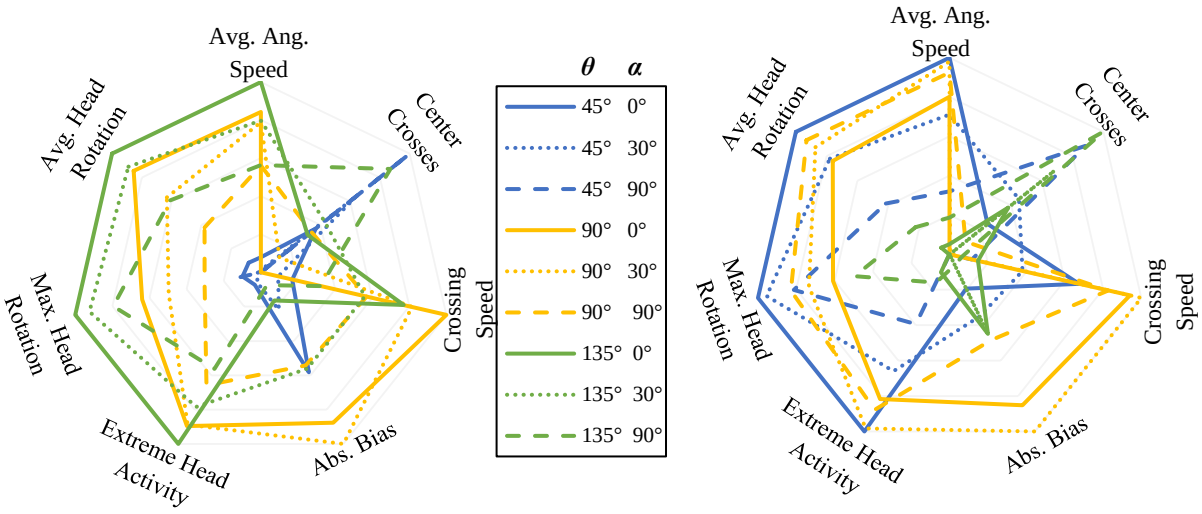

(a) Forward travel (b) Reverse travel

Figure 8. Normalized scanning pattern measures averaged across 18 participants

5. Comparison of the Exposure Models with Human Performance

We compare predictions from our analytical model (where estimated intensity≥1s meant shopper is exposed to the target) with human performance data. Based on whether a participant sees a target (i.e., a 'hit') or does not see it (i.e., a 'miss'), targets are classified as either *true positive* (TP or predicted hits; i.e., model predicts participant will see and participant actually sees), *false positive* (FP or unpredicted hits; i.e., model predicts participant will see, but participant does not see), *true negative* (TN or predicted misses; i.e., model predicts participant will not see and participant does not see) and *false negative* (FN or unpredicted misses; i.e., model predicts participant will not see, but participant sees). To then access the performance of our model, we calculated the positive prediction value (PPV), negative prediction value (NPV) and accuracy (ACC), where PPV=$\frac{TP}{TP+FP}$, NPV=$\frac{TN}{TN+FN}$, and ACC=$\frac{TN+TP}{TN+FN+TP+FP}$. The PPV measure fundamentally tells us, 'for targets our model predicted to be *seen*, what proportion were actually *seen*?' NPV contrarily answers 'for targets our model *did not* predict to been seen, what proportion were

actually *not seen*?' The ACC measure however represents (1 – total error rate), where the error rate accounts for both overestimates (FN) and underestimates (FP). Figure 9 contains average values (across all participants for each layout); global averages were PPV=0.82, NPV=0.72, and ACC=0.77. Layouts with NPV=0 contained no targets not predicted to be seen.

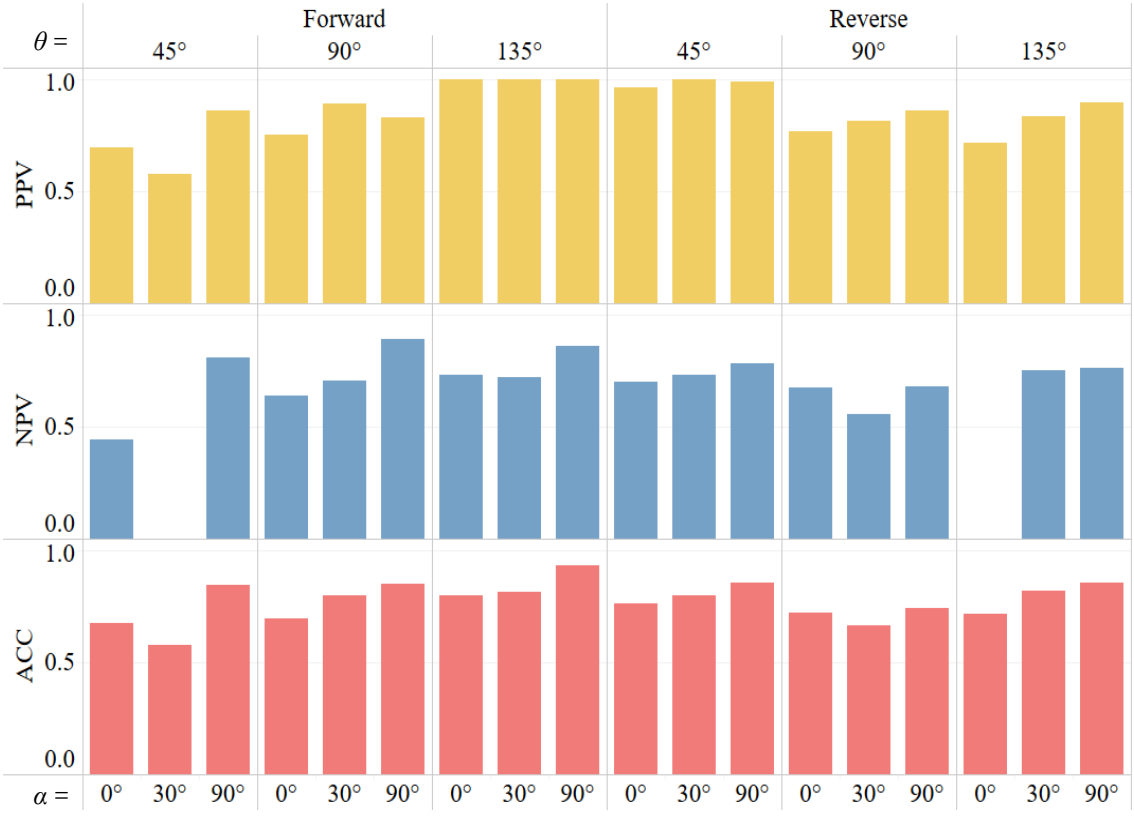

Figure 9. PPV, NPV, and ACC averaged across 18 participants

These results indicate that our analytical exposure models performed fairly well on certain layouts. For instance, for layouts with θ=135°, (forward travel) and θ=45° (reverse travel), the PPV was 1.0 and 0.98, respectively; ACC was acceptable too, 0.85 and 0.80, respectively. On the contrary, our models performed relatively weaker for layouts with θ=45°, (forward travel) and θ=90° (reverse travel); PPV=0.71 and 0.81 (ACC=0.70 and 0.71), respectively. One possible explanation for these differences may be the distribution

of intensity values for specific layouts. For instance, the average intensity value of targets predicted to be seen for layouts with θ=135°, (forward travel) and θ=45° (reverse travel) were 6.7 and 6.8 seconds respectively, whereas those for layouts with θ=45°, (forward travel) and θ=90° (reverse travel) were 3.9 and 4.2 seconds respectively. Participants were more likely to see targets with higher intensity values in the former instances, leading to a higher match with the predictions from the analytical model; recall, if the intensity is >1 second, the analytical model would mark it as likely seen.

6. Enhancing the Analytical Exposure Models with Human Behavior

Considering that the participants altered their scanning pattern based on the layout (whereas our analytical model assumed a single, fixed, FoR for all layouts), we sought to utilize these unique scanning patterns to enhance the quality of exposure predictions from the analytical models. As a first step, we combined both the analytical estimates and human behavior measures into a prediction model using decision trees. We chose this non-parametric approach for two reasons; first, the normality and relevant assumptions for use of ANOVA could not be verified, and second, the decision tree model aids in intuitive analysis via if-then rules. We built four decision tree models, each with an incremental addition of factors. Model 1 uses only the analytical model (AM) estimates (i.e., estimated intensity of exposure of a target in seconds). Model 2 included layout and target parameters (e.g., θ, α, direction, target location quantified as the row and column on a rack). Models 3 and 4 included human behavior factors (from Section 5); Model 3 was allowed limited number of splits, while

Table 1. The four enhanced exposure models based on decision trees

#	**Factors included in the Decision Trees**	**# of Splits**	**AUC**			**ACC**
			Train (60%)	*Validation* (20%)	*Test* (20%)	*Test* (20%)
1	Analytical Model (AM)	21	0.861	0.857	0.860	0.795
2	AM + layout + target	29	0.923	0.905	0.890	0.818
3	AM + layout + target + human (limited splits)	27	0.922	0.881	0.889	0.828
4	AM + layout + target + human	63	0.938	0.908	0.912	0.835

Model 4 was allowed to have unlimited splits. We used a train-validation-test approach (60:20:20 split of 324 data elements), where the validation data was used to stop model training to avoid overfitting.

Table 1 summarizes the performance of these models on AUC (area under the ROC curve) and test ACC. Notice that the Test AUC (measure of the model's performance on unseen data), is reasonably high just with the predictions from the AM (Model 1). The other models show the incremental benefits to the Test AUC.

Table 2: Parameter contributions

Parameter	**Splits**	**G^2**	**Parameter**	**Splits**	**G^2**
Model 1: Intensity			*Model 4: All parameters*		
AM-Intensity	21	1167.5	AM-Intensity	10	1139.2
Model 2: Intensity + layout + target			Face (front/back)	6	168.9
AM-Intensity	7	977.5	Target column	6	147.3
Face (front/back)	4	222.7	Orientation	9	134.3
Target column	7	201.8	Avg. head rotation	5	109.7
Curvature	5	88.0	Curvature	6	90.2
Orientation	4	76.3	Avg. angular speed	4	63.2
Direction	1	25.2	Abs. bias	3	34.9
Target row	1	23.1	Direction	4	30.3
Model 3: Intensity + layout + target + some human parameters			Avg. crossing speed	3	29.9
AM-Intensity	5	968.6	Center crosses	2	26.1
Face (front/back)	4	186.0	Saccade time	2	25.9
Target column	7	163.4	Max head rotation	2	25.0
Curvature	5	92.9	Target row	1	7.7
Orientation	3	66.7			
Avg. head rotation	1	51.4			
Avg. angular speed	1	51.1			
Direction	1	18.1			

Individual contributions of parameters for each model are shown in Table 2. The number of splits refers to the number of times a node is divided. G^2 is the likelihood ratio chi-square statistic (i.e., higher values indicate higher variation within a parameter with respect to the response). A deeper analysis of these decisions trees revealed that the root node (first split) in all the 4 models was always based on the intensity estimate from the AM. This is intuitive as the quality of prediction of the AM is already fairly high. After this, the next few splits were largely dependent on the location of the target (rack face, and target column) and the layout (orientation and curvature). Further, with the exception of average head rotation, the splits for human

parameters in Models 3 and 4 were generally located towards the bottom of the decision trees (farthest from the root node). In both models, average head rotation occurred as the 2nd split for lower intensity values. In other words, if intensity values were low, the odds of a participant seeing the target were highly dependent on the average extent to which they rotated their head. Overall, Models 2 and 3 appear to strike a good trade-off between the quality of exposure predictions for a layout and the model's complexity.

7. Conclusion and Next Steps

The objective of this study was to compare the findings from a recently proposed analytical model (for estimating exposure of racks in a 3D retail store) to human performance. To do this, we designed a virtual environment of a retail rack layout, where curved racks were placed at various orientations. We asked 18 participants to search for targets in 9 unique layouts. Our trials revealed substantial variation in the head movement of these participants. The analytical model, that assumed an expected horizontal head movement with a single scan at each shopper step, appeared to perform reasonably well. However, further enhancements to the exposure estimates are possible with the inclusion of target and layout parameters in a decision tree framework. The inclusion of human behavior parameters further increased the prediction quality, but only marginally. Essentially, both Models 2 and 3 seem to provide good tradeoff in terms of quality of estimates and complexity.

As next steps, we plan to use either Model 2 or 3 as exposure estimates in an optimization model to determine the optimal rack orientation and curvature that maximizes total exposure under space constraints. If possible, we will derive expected impulse

purchase (retailer) and improved experience (shopper) as functions of total exposure of a layout in subsequent optimization models.

Acknowledgements

This research was partially supported by the National Science Foundation grant CMMI #1548394.

References

1. Dunne, P. M., Lusch, R. F., and Gable, M. (1995). *Retailing*. Cincinnati, OH: South-Western College Pub.
2. Cairns, J. P. (1962). Suppliers, retailers, and shelf space. *Journal of Marketing*, 34-36.
3. Sorensen, H. (2009). *Inside the mind of the shopper: The science of retailing*. FT Press, NJ.
4. Peters, B. A., Klutke, G.-A., and Botsali, A. R. (2004). Research issues in retail facility layout design. In R. D. Meller, M. K. Ogle, B. A. Peters, G. D. Taylor and J. S. Usher (Eds.), *Progress in Material Handling Research: 2004* (pp. 399-414).
5. Yapicioglu, H., and Smith, A. E. (2012). Retail space design considering revenue and adjacencies using a racetrack aisle network. *IIE Transactions*, *44*(6), 446-458.
6. Phillips, H. (1993). How customers actually shop: Customer interaction with the point of sale. *Journal of the Market Research Society, 35*(1), 51-63.
7. Mowrey, C. H., Parikh, P. J., and Gue, K. R. (2017). The impact of rack layout on visual experience in a retail store. *INFOR: Information Systems and Operational Research*, 1-24.
8. Guthrie, B. and Parikh, P. J. (2017). Analyzing a shopper's visual experience in a retail store in 3D. In *IISE Annual Conference. Proceedings* (pp. 746-751), Pittsburgh, PA.

9. Wischgoll, T., Glines, M., Whitlock, T., Guthrie, B., Mowrey, C., Parikh, P. J., and Flach, J. (2017), *Display infrastructure for virtual environments (DIVE)*, in press, Journal of Imaging Science and Technology.
10. Daamen, W. (2004). *Modelling passenger flows in public transport facilities* (doctoral dissertation). Netherlands Research School for Transport, Infrastructure.

Appendix F. Product Category Assortment Data

Table F1. Data from U.S grocery store

Category	Product Category	Monthly Demand	Profit Category	Impulse Category	Impulse Rate	Allocated Area	1*1 Facings	Aisle	Side
1	Gravy Mix	6449	M	M	0.33	23.86	21	1	Right
2	Kraft Spreads	3644	M	M	0.29	20.08	14	1	Right
3	Italian Supplies	404	M	M	0.22	7.02	7	1	Right
4	Chili	8393	L	H	0.41	29.46	14	1	Right
5	Tuna	12379	L	M	0.30	37.94	35	1	Right
6	Pickles	5967	M	M	0.21	75.63	56	1	Right
7	Japanese Food	2698	L	M	0.24	41.82	42	1	Right
8	Croutons	2778	M	L	0.09	35.65	28	1	Right
9	Dressing	1823	L	M	0.17	23.70	7	1	Right
10	Condiments	10425	L	M	0.32	76.94	63	1	Right
11	Macaroni	11237	L	L	0.03	70.43	56	1	Right
12	Gatorade	5248	M	M	0.23	86.02	42	2	Right
13	Pizza Supplies	936	L	M	0.32	10.59	14	2	Right
14	Baking/Chocolate	4480	M	M	0.28	52.25	98	2	Right
15	Pasta Sauce	8821	L	M	0.30	73.26	84	2	Right
16	Jell-O	2775	L	M	0.27	25.42	14	2	Right
17	Canned Fruit	4607	L	H	0.47	27.66	21	2	Right
18	Tonic Water	7944	M	L	0.15	113.66	112	2	Right
19	Baking Supplies	946	L	M	0.32	10.76	7	2	Right
20	Rice	7519	M	L	0.07	58.67	56	2	Right
21	Oil	2158	L	L	0.08	24.56	7	2	Right
22	Seasonings	5267	M	L	0.04	25.67	21	2	Right
23	Seasonings/Spices	2145	L	L	0.07	5.22	7	2	Right
24	Brita Water	3291	M	L	0.03	25.34	14	2	Right
25	Beans	8456	L	M	0.31	40.83	35	2	Right
26	Canned Vegetables	14262	L	M	0.32	52.51	84	2	Right
27	Tomato Sauce	12676	L	L	0.08	18.87	14	2	Right
28	Sugar	3430	L	L	0.02	121.09	56	2	Right
29	Chocolate Syrup	1555	M	H	0.49	25.75	56	3	Right
30	Dried Fruit	2069	M	H	0.42	25.04	28	3	Right
31	Coffee	10344	L	M	0.25	104.36	126	3	Right
32	Peanut Butter	8931	M	L	0.15	54.21	56	3	Right
33	Health Bars	313	L	M	0.30	3.63	7	3	Right
34	Cereal	19257	L	M	0.30	260.00	252	3	Right
35	Cereal Bars	10049	L	M	0.29	51.03	84	3	Right
36	Oatmeal	3627	L	L	0.14	48.72	56	3	Right
37	Filter	628	L	L	0.02	10.19	7	3	Right
38	Tea Leaves	1739	L	L	0.01	27.95	14	3	Right
39	Nuts	7631	M	H	0.47	79.71	133	4	Right
40	Air fresheners	2834	M	H	0.46	32.48	21	4	Right
41	Pretzels/Chips	6426	L	H	0.49	41.24	133	4	Right
42	Popcorn	3757	L	H	0.50	132.76	56	4	Right
43	Cleaning Wipes	5555	M	M	0.28	80.66	56	1	Left
44	Seeds	74	H	L	0.10	1.39	14	1	Left
45	Dish Soap	4012	M	L	0.11	41.46	28	1	Left
46	Vinegar	1119	L	L	0.11	21.21	7	1	Left
47	Toilet Paper	5614	L	L	0.07	110.49	168	1	Left
48	Juice	12328	L	M	0.23	74.16	56	1	Left
49	Rice Snacks	1188	L	L	0.06	36.37	14	1	Left
50	Lotion	2187	H	M	0.32	45.63	56	2	Left
51	Bug Stuff	47	M	M	0.27	7.89	7	2	Left
52	Hardware	262	M	M	0.23	195.93	224	2	Left
53	Cat Supplies	1224	M	L	0.06	97.62	126	2	Left
54	Stain Remover	1423	M	L	0.05	35.74	21	2	Left
55	Laundry Soap	4793	M	L	0.05	109.79	126	2	Left
56	Plastic Utensils	687	L	L	0.12	2.03	7	2	Left
57	Napkins	1956	L	L	0.08	50.62	56	2	Left
58	Cups	291	M	L	0.01	14.59	7	2	Left
59	Dyer Sheet	1723	L	L	0.01	38.68	56	2	Left
60	Pet Food	3641	M	M	0.34	22.95	56	3	Left

61	Meal Replacement	713	H	L	0.14	21.91	7	3	Left
62	Dog Supplies	541	L	M	0.30	25.39	21	3	Left
63	Deodorant	3009	L	M	0.26	34.44	56	3	Left
64	Cat Food	9615	M	L	0.12	66.22	77	3	Left
65	Shaving Gel	1626	M	L	0.06	25.85	14	3	Left
66	Diapers	1153	L	L	0.10	176.13	196	3	Left
67	Baby Supplies	571	L	L	0.10	8.52	7	3	Left
68	Shampoo	320	M	L	0.05	10.23	21	3	Left
69	Dog Food	1426	M	L	0.04	113.06	168	3	Left
70	Hair Supplies	283	L	L	0.03	7.11	7	3	Left
71	Soap	6404	L	L	0.07	72.27	56	3	Left
72	Nutrition Bars	1204	H	M	0.28	21.45	14	4	Left
73	Vitamins	1938	H	M	0.26	17.06	14	4	Left
74	Toothpaste	7025	H	L	0.07	68.18	63	4	Left
75	Drugs	1192	H	L	0.07	15.58	14	4	Left
76	Eye Stuff	604	H	L	0.07	11.31	7	4	Left
77	Ointments	1462	M	L	0.09	25.38	21	4	Left
78	Personal Products	163	H	L	0.04	4.40	7	4	Left
79	Medicine	135	M	L	0.04	0.89	7	4	Left
80	Cough Drops	4162	H	L	0.02	27.60	21	4	Left
81	Antacid	1286	H	L	0.02	16.67	14	4	Left
82	Feminine Products	2865	L	L	0.04	131.48	105	4	Left
83	Pain Medication	2158	H	L	0.01	19.30	14	4	Left
84	Boost Drinks	639	H	L	0.01	40.60	42	4	Left